

The erosion of ultrafine WC-Co

Victoria Antonietta Pugsley

Thesis submitted to the Faculty of Engineering of the University of Cape Town in fulfilment of the requirements for the degree of Master of Science in Engineering

Department of Materials Engineering

University of Cape Town

November 1998

The University of Cape Town has been given the right to reproduce this thesis in whole or in part. Copyright is held by the author.

The copyright of this thesis vests in the author. No quotation from it or information derived from it is to be published without full acknowledgement of the source. The thesis is to be used for private study or non-commercial research purposes only.

Published by the University of Cape Town (UCT) in terms of the non-exclusive license granted to UCT by the author.

ABSTRACT

A series of four ultrafine WC-Co alloys of varying cobalt contents has been sintered from powder produced through the spray conversion process. The materials have been characterised and subjected to slurry erosion and cavitation erosion. A further twelve WC-Co alloys of varying grain sizes and cobalt contents have been produced through conventional processes and subjected to the same tests in order to provide data for comparison.

The erosion resistance of all the grades tested was found to increase with decreasing grain size, both under cavitation erosion and slurry erosion conditions. Furthermore, a transition from a localised material removal mechanism to a bulk material removal mechanism was observed in both erosive systems as the WC grain size of the material decreased below about $1\mu\text{m}$. The erosion resistance of sub-micron materials was found to be considerably more sensitive to bulk deformation parameters than that of coarser materials. As a result, ultrafine grades subjected to slurry erosion or cavitation erosion were found to exhibit lifetimes up to seven times greater than those of the best-performing materials with grain sizes above $1\mu\text{m}$. This increase in erosion resistance was achieved without any significant drop in fracture toughness.

Significant differences were observed between the response of WC-Co to the two erosive systems, particularly in those materials exhibiting a localised erosion response. Under slurry erosion conditions, these materials displayed increasing erosion resistance with decreasing cobalt content, and both the cobalt and WC phases responded to erosive attack. Under cavitation erosion conditions, however, the opposite trend was observed, and only the cobalt phase responded to erosive attack. Materials exhibiting a bulk erosion response responded in a similar fashion to both forms of erosive attack, although cavitation erosion produced damage to a greater depth. The effect of defects on material performance was found to depend critically on the erosive system.

ACKNOWLEDGEMENTS

I would like to thank the following people for their support during the time I was carrying out this work:

Professor Colin Allen, my supervisor, for his support and guidance.

Mr. I.T.Northrop, of Boart Longyear Research Centre, for his advice, enthusiasm, approachability, and for sharing his encyclopaedic knowledge of WC-Co with me.

George, Archie, Chris, John, Lourens and Tony, of Boart Longyear Research Centre, for assistance with specimen preparation.

Mr Glen Newins for his unfailing good humour and for producing a limitless supply of refaced drill tips for me.

Ms Julie Henry for dealing with all my administrative hassles and always having lots of petty cash for me.

Mr Adriaan Loedloff and Mr James Petersen for assistance with photography.

Mr Reggie Hendricks for being on hand to sort out major or minor disasters, and always having a plan for everything

Mr Dave Dean and Mr Nick Dreze for sorting out electrical and mechanical problems

Mrs Mira Topic for laboratory assistance.

Associate Professor Rob Knutsen, for assistance with microscopy and metallography.

Mrs Doreen Young for putting up with what was surely the messiest desk in the department

My officemates: Marcel, Natasha, Machio, Bernd and Paul (and Zheng), for their moral support

Miranda Waldron, Professor Trevor Sewell and Dane Gerneke, of the Electron Microscopy Unit (University of Cape Town) for invaluable advice and assistance with electron microscopy.

Professor S.Luyckx, of the University of Witswatersrand, for valuable discussions.

Ms Charlotte Hill for providing accommodation in London.

The financial support of the Department of Materials Engineering of the University of Cape Town and Boart Longyear Research Centre is gratefully acknowledged.

CONTENTS

Chapter 1	Introduction	1
Chapter 2	Literature review: WC-Co alloys	3
	2.1 Introduction	3
	2.2 Physical and mechanical properties	4
	2.3 Ultrafine WC-Co	13
Chapter 3	Literature review: Erosive wear	20
	3.1 Slurry erosion	21
	3.2 Cavitation erosion	30
Chapter 4	Literature review: The wear response of WC-Co	33
	4.1 Slurry erosion	33
	4.2 Cavitation erosion	38
	4.3 Erosion of ultrafine WC-Co	41
Chapter 5	Experimental materials	42
	5.1 Introduction	42
	5.2 Quality control	44
	5.3 Material characterisation	50
	5.4 Summary	56
Chapter 6	Experimental methods	57
	6.1 Slurry erosion	57
	6.2 Cavitation erosion	65
	6.3 Specimen preparation	71
	6.4 X-ray diffraction	75
Chapter 7	Results	76
	7.1 Slurry erosion	76
	7.2 Cavitation erosion	88
Chapter 8	Discussion	103
	8.1 Introduction	103
	8.2 Slurry erosion	103
	8.3 Cavitation erosion	109
	8.4 Ultrafine grades	114
	8.5 Comparison of the two erosion systems	116
Chapter 9	Conclusions and recommendations	118
	References	121

Chapter 1

INTRODUCTION

WC-Co combines the high hardness of tungsten carbide with the ductility of cobalt to produce a material of superior wear resistance, yet with sufficient strength for use in practical applications. It has therefore long been used in the manufacture of wear parts such as jet nozzles, valves and seal rings. The composite nature of the material allows a wide range of properties to be achieved through the close control of carbide grain size and cobalt binder content, and thus it is possible to tailor the material properties to meet the requirements of highly diverse applications.

The production of hardmetals with a controlled grain size has long been of especial technological interest, particularly since it is well-known that by decreasing the carbide grain size it is possible to produce materials of high hardness which retain adequate fracture toughness [1-3]. Interest in the control of carbide grain size has led to the successive development of fine and ultrafine hardmetals, with carbide grain sizes of 0.5-1 μ m and 0.1-0.5 μ m respectively [4]. Most recently, the limitations of conventional processing technology have been overcome in the production of nanostructured WC-Co powder (known as Nanocarb[®]) through the spray conversion process [5]. The full potential of this powder has yet to be exploited, as conventional sintering technologies are not sufficiently powerful to prevent grain growth during sintering. As a result, WC-Co sintered from Nanocarb powder has an ultrafine microstructure.

A full characterisation of the wear performance of WC-Co sintered from Nanocarb powder has yet to be carried out, and little is known about the microstructure/property trends operating at ultrafine grain sizes. Preliminary work has shown the performance of this new material to be highly promising: under abrasive wear conditions, its wear resistance has been shown to be between two and three times greater than that of the best-performing conventional material. These results are due in part to the fact that this material exhibits a much greater tendency to a ductile wear response [6].

This study represents an attempt to provide a fuller understanding of the wear performance of ultrafine WC-Co, by examining its response to two highly contrasting modes of erosion, namely slurry erosion and cavitation erosion.

A series of four ultrafine WC-Co grades of varying cobalt contents has been sintered from powder produced through the spray conversion process and subjected to slurry erosion and cavitation erosion. A further twelve conventional WC-Co alloys of varying grain size and cobalt content have also been subjected to the same tests, to provide data for comparison. The erosion performance of the materials has been evaluated through mass loss measurements and microscopic examination. A qualitative evaluation of the dependence of slurry erosion performance on impact angle has been carried out, and an attempt has been made to clarify the relationship between cavitation erosion performance and the phase transformation of the cobalt binder. The erosion performance of the materials has been related to their measured microstructural and mechanical parameters. The influence of material defects has also been considered in a qualitative manner.

Chapter 2

WC-Co ALLOYS

2.1 Introduction

WC-Co is a sintered two-phase composite material, in which the high hardness and wear resistance of tungsten carbide is harnessed for use in practical applications through the addition of between 6 and 20 wt% cobalt. The addition of a cobalt binder serves to reduce the sintering temperature of WC from 2000°C to a more industrially feasible value of 1500°C, while simultaneously reducing its porosity and increasing its strength to acceptable levels. This results in a material whose hardness, which can exceed 2000HV, is allied to fracture toughness levels of between 8 and 22 MPam^{1/2}, which are generally sufficient to ensure reliable in-service operation [7,8].

WC-Co is used in a wide range of applications which exploit its excellent strength and wear resistance: notably tools for metal cutting, metal forming and percussion mining, and wear parts such as jet nozzles, valves and seal rings [7]. Due to their composite nature, hardmetals display properties which may vary over a wide range, and which can easily be tailored, through close control of composition and processing parameters, to meet the requirements of highly diverse applications.

In common with all composite materials, the properties of WC-Co alloys depend upon

- the properties of the constituent materials
- microstructural parameters
- interactions between constituent materials
- post-production treatment

These will be discussed in turn in the following sections.

2.2 Physical and mechanical properties

2.2.1 Bulk properties of the constituent phases

Tungsten carbide

WC, tungsten monocarbide, has a simple hexagonal structure with one W and one C atom per unit cell. The two atoms occupy the (0,0,0) and (1/3,2/3,1/2) positions respectively. The bond state of the compound is a mixture of metallic and covalent bonding [9]. The former accounts for tungsten carbide's relatively high electrical and thermal conductivity and for its metallic lustre, while the latter is responsible for its high hardness and modulus of elasticity.

As a consequence of the WC crystal structure, many of the properties of individual WC grains, including hardness, are highly anisotropic. However, no anisotropy is evident in the sintered structure due to the random orientation of the grains. The room temperature hardness of WC grains varies from a minimum of 1000 kg/mm² (measured parallel to the c axis on the {10 $\bar{1}$ 0} planes) to a maximum of 2400 kg/mm² (measured along the basal plane) [10]. The operative slip systems have been shown to be {10 $\bar{1}$ 0}<11 $\bar{2}$ 3> [11,12]. Only four independent slip systems exist, which are insufficient for general shape change during deformation of polycrystalline WC: this has important consequences for the fracture behaviour of WC-Co [13,14].

Cobalt

Although cemented carbides have been produced using a range of metals and alloys of the iron group as binder materials, historically cobalt has dominated the market. This is due primarily to its superior performance during processing. Unlike other potential binder materials, cobalt is available in very fine powders, of the order of 1 μ m. This allows for highly efficient comminution during milling, resulting in a fine, homogenous distribution of the binder phase throughout the composite [15].

Furthermore, the electronic configuration of cobalt is considered to optimise the thermokinetic reactions occurring during sintering. In practice, this results in rapid levels of densification at

relatively low sintering temperatures, and almost perfect wetting of the carbide phase by the cobalt, which produces excellent adhesion in the solid state [16].

Cobalt has two further important characteristics. Firstly, it is ferromagnetic, with a magnetic saturation of 160emu/g [17]: this allows hardmetals to be characterised by two magnetic properties, namely specific magnetic saturation and coercivity. The measurement of these properties provides a means for rapid non-destructive evaluation of hardmetal specimens and is in fact one of the most widely used quality control tests in industry [7,18,19].

Secondly, cobalt is allotropic, the h.c.p. structure being stable below 690K, and the f.c.c. structure above this temperature [20].

2.2.2 Microstructural features

Tungsten carbide-cobalt consists of carbide grains in the form of truncated triangular prisms which are cemented by a cobalt binder. The microstructural features of the sintered product are determined by the grain size of the WC powder used, the amount of cobalt added and processing parameters such as sintering temperature and time. The microstructure is characterised by four interrelated parameters, namely WC grain size, cobalt content, binder mean free path and contiguity [21]. These are illustrated in Figure 2.1. In addition, as for all materials produced through the powder metallurgy route, a certain level of porosity is unavoidable.

WC grain size

The WC grain size is generally defined as the mean linear intercept of the WC phase, as illustrated in Figure 2.1. The WC grain size does not in itself have a strong influence on the mechanical properties of the material, although it can impact on the fracture properties of coarse grain materials, since the strength of WC grains varies inversely with their size [21].

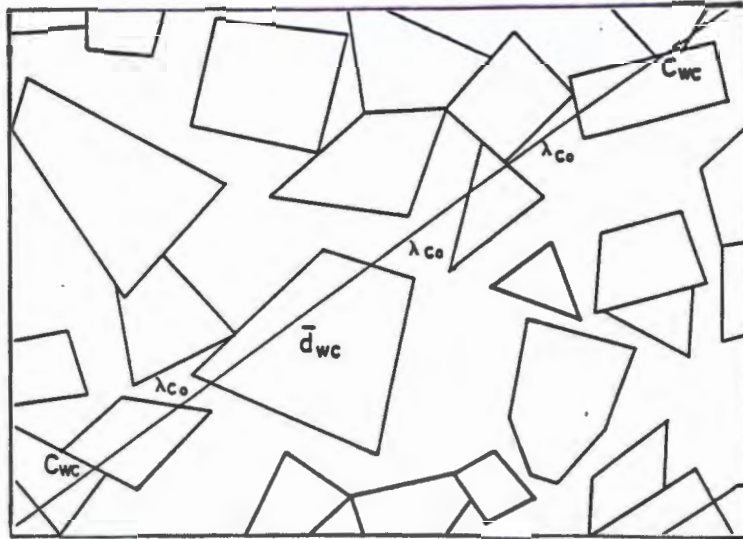


Figure 2.1: Schematic representation of a WC-Co alloy, illustrating the microstructural parameters λ (binder mean free path), C (contiguity), and d_{wc} (tungsten carbide grain size)

Binder mean free path

The binder mean free path is a measure of the thickness of the cobalt layers separating the WC grains and is defined as the mean linear intercept of the binder phase. It increases with both increasing cobalt content and increasing grain size.

The magnitude of the binder mean free path largely determines the constraint exercised on the binder by the adjacent carbide grains. This is considered to represent the most important contribution to the flow resistance of the binder phase. The binder mean free path therefore essentially determines the deformation characteristics of the binder and consequently has a strong influence on the bulk deformation properties of the material. It is in fact widely considered to be the single most important parameter characterising the microstructure [21].

Two examples of the dependence of bulk material properties on the binder mean free path are illustrated in Figure 2.2. From these graphs, it can be seen that both hardness and fracture toughness are closely, although not exclusively, dependent on the binder mean free path.

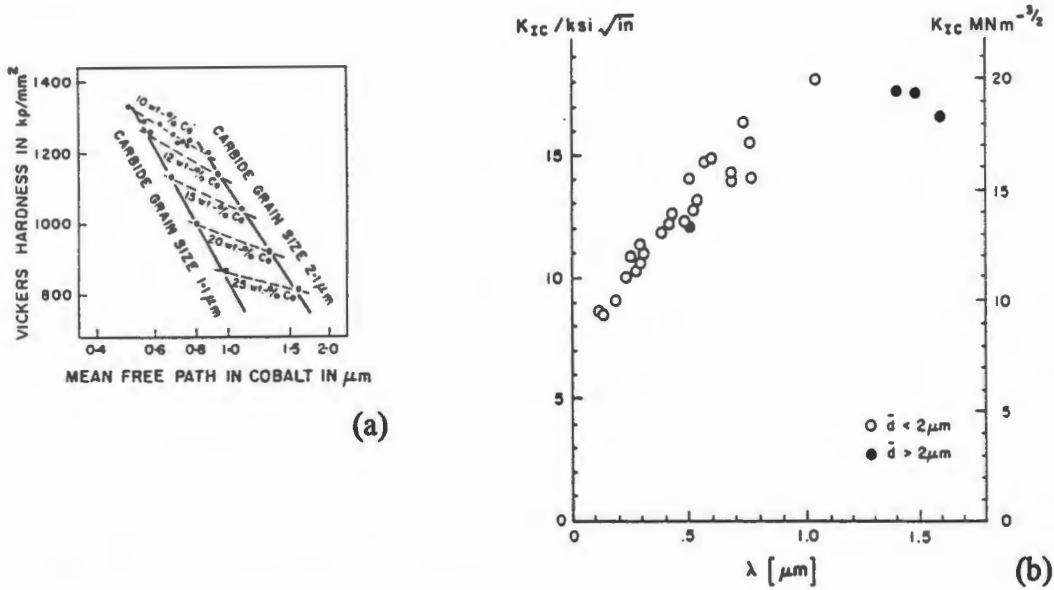


Figure 2.2: Dependence of a) hardness and b) fracture toughness on the binder mean free path [21,22]

Contiguity

The WC phase, in all hardmetals but those with the highest binder contents, is considered to exist in the form of a load-bearing carbide skeleton extending throughout the material. The existence of such a skeleton can be inferred from the observation of extensive slip lines in WC particles on the surface of deformed WC-Co composites: these indicate that deformation of a continuous carbide skeleton is required to accommodate bulk deformation of the material [1,23].

Contiguity is a measure of the degree of continuity of the carbide skeleton existing within a WC-Co alloy, and is defined as the fraction of the total WC grain boundary surface area that is taken up by the WC/WC interface [21]. It determines the deformation response of the carbide phase and consequently has a strong influence on the bulk deformation characteristics of the material.

The contiguity is difficult to determine accurately through microscopic examination, primarily due to the presence of layers of segregated cobalt at WC/WC interfaces [24]. However, it is known to be strongly dependent on and inversely related to the binder content of the material.

It also increases with increasing grain size and is dependent on processing parameters such as sintering time and temperature [21].

The effects of contiguity are difficult to isolate, but it appears that increases in contiguity will lead to increasing hardness and decreasing fracture toughness [21,25].

Porosity

Porosity results from the incomplete wetting of WC grains by the cobalt binder during sintering, which is generally due to insufficient milling or improper control of sintering time and temperature. It can have a deleterious effect on the transverse rupture strength and fracture toughness of components [26] and therefore has to be minimised in applications requiring high shock resistance, as well as applications where blemish-free mirror finishes are required. Near-zero porosity can be achieved using the hot isostatic pressing process [18].

2.2.2.1 Evaluation of microstructural parameters from magnetic measurements

The specific magnetic saturation value of a hardmetal is directly proportional to the amount of cobalt available for magnetisation, and may therefore be used to estimate the binder content of the material. However, the accuracy of this approach is limited by the fact that the magnetic saturation is also affected by the binder composition (as discussed in Section 2.2.3), and thus it is often necessary to consider additional data from density measurements.

The coercivity of WC-Co is related to the surface area of the WC grains, which is considered to represent the main imperfection inhibiting free movement of magnetic domain walls. The coercivity is therefore closely dependent on the microstructure of the material, and empirical equations relating it to the hardmetal grain size have been proposed. However, these must be used with caution since coercivity is also affected by the chemical composition of the binder phase and the presence of phase boundaries, stacking faults, and twins [27,28].

A full description of these techniques is given by Fang and Eason [19].

2.2.3 *In situ* properties of the constituent phases

The *in situ* properties of both the WC and Co phases differ from those of the parent material, due to the interaction of the two phases. These interactions may affect the chemical composition, stress state, crystal structure, and deformation behaviour of the phases. However, it is in the binder phase that these differences are most marked and have the most significant impact on the properties of the bulk material.

Chemical composition

While the *in situ* composition of WC grains is identical to that of the bulk material [29], it is more meaningful to regard the binder phase as being a Co-C-W alloy, due to the high solubility of WC in cobalt at the sintering temperature. Significant levels of tungsten are retained at room temperature in the interior of binder phase domains, due to the slow diffusion coefficient of tungsten [30]. The presence of tungsten in the binder phase serves to increase its strength [31-33] and corrosion resistance [34].

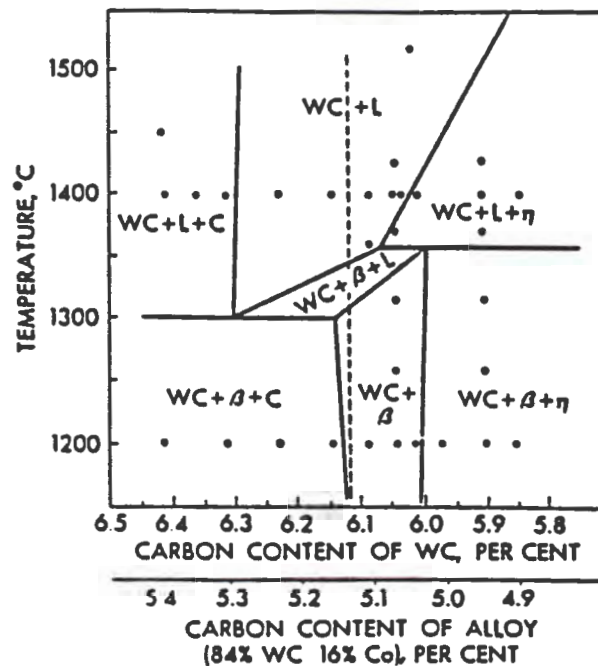


Figure 2.3: Vertical section through WC-Co-C ternary phase diagram at 16wt% Co, showing compositional range for WC [35]

As the phase diagram in Figure 2.3 shows, the range of carbon content over which the two-phase composition, WC + β (cobalt solid solution), exists is relatively narrow, and thus close control over the chemical composition of the material is required during processing to avoid the precipitation of a third phase. Carbon levels in excess of the stoichiometric value result in the formation of a finely dispersed free graphite phase, while carbon deficiency leads to the appearance of η phase, $\text{Co}_3\text{W}_3\text{C}$. The latter phase causes a significant drop in transverse rupture strength [36], due to its brittleness and the fact that it leaves the binder deficient in cobalt [21,37]. The presence of free graphite is much less detrimental, since its effect is similar to that of porosity. However, it may act as a stress raiser, with consequent adverse effects on transverse rupture strength [21].

The specific magnetic saturation of hardmetals varies inversely with the amount of tungsten in the binder [33] and may therefore be used to characterise the binder phase composition. It can also serve as a test for the possible presence of η phase: the formation of η phase reduces the amount of cobalt available for magnetisation and therefore leads to a significant reduction in magnetic saturation.

Low tungsten levels are associated with high carbon levels [32] and high magnetic saturation values are therefore an indication of the possible presence of free graphite.

Stress state

The thermal expansion coefficient of cobalt is about three times that of tungsten carbide. Differential contraction arising during cooling from the sintering temperature is therefore inevitable and results in the presence of residual stresses, which are tensile in the binder phase and compressive in the WC matrix [38].

Crystal structure

Although it is the h.c.p. form of cobalt which is stable at room temperature, in practice the majority of the binder phase in WC-Co consists of retained metastable f.c.c. cobalt [32]. This is due to the combination of two effects:

- the f.c.c. \rightarrow h.c.p. transformation in cobalt is martensitic and requires the motion of partial dislocations along the $\{111\}$ planes [39]. This mechanism is inhibited in the WC-Co binder both by the presence of WC grains and by the mechanical constraints resulting from differential thermal contraction during cooling
- W and C in solid solution are considered to produce an effective stabilisation of the f.c.c. phase [33]

The effects of cobalt crystal structure on the properties of WC-Co are difficult to isolate and hence unclear. However, partial transformation can be induced through deformation and this is considered to have a deleterious effect on the fatigue and erosion properties of the material [40,41].

Deformation behaviour

The deformation behaviour of the two phases is affected variously by their chemical composition, crystal structure, and stress state, as discussed above. In addition, two further effects must be taken into account:

- the slip length of dislocations in the binder phase is limited by the presence of WC grains
- the difference in hardness of the components leads to mutual plastic constraint during deformation, resulting in a 'harder' response of the soft binder phase and a 'softer' response of the hard WC phase [42].

The latter effect is considered to constitute the greatest single contribution to the flow resistance of the binder [43].

2.2.4 Post-production treatment

A number of techniques may be employed to bring the dimensions of the sintered component in line with those required, the most common of these being grinding [18]. A useful side-effect of grinding operations is that they introduce compressive stresses into the surface of the material, thus increasing its surface fracture toughness [38,44,45]

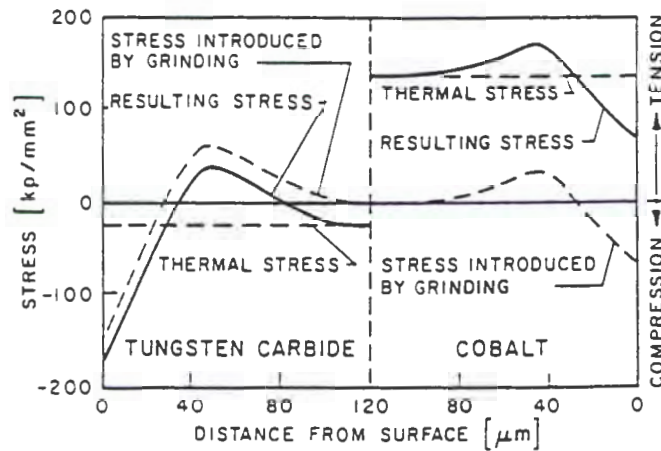


Figure 2.4: Stress distribution in an as-ground WC-Co sample [38]

2.3 Ultrafine WC-Co

As discussed in Section 2.2.2, the hardness of WC-Co is closely related to the binder mean free path. The equation linking these two parameters is in fact similar to the Hall-Petch equation governing the hardness of single phase materials [1]. Consequently, the hardness of WC-Co is found not only to increase, but to become increasingly sensitive to the microstructure as the binder mean free path decreases. A reduction in the binder mean free path may be achieved either by lowering the grain size or the cobalt content of the material. Grain size reduction is by far the most effective method, since the extent of cobalt reduction is limited by the need to maintain densification and fracture toughness levels.

Consequently, since the initial production of WC-Co, considerable effort has gone into developing processing technologies which have allowed ever-increasing control over the WC grain size of the final sintered product. This has resulted in the production of hardmetals with successively finer WC grains, culminating ultimately in the development of sub-micron (0.5-1 μm), ultrafine (0.1-0.5 μm) and nanocrystalline (<0.1 μm) WC-Co. A detailed account of the development of these processing techniques is given by Spriggs [4].

2.3.1 Production processes

The production of hardmetals with a closely-controlled grain size requires a two-fold approach:

1. WC powder of the desired grain size must be available
2. Processing parameters must be chosen to maintain the grain size at this level

A number of options are available for producing WC powder of the desired grain size. Through close control of conventional production processes (particularly the choice of raw material for the production of tungsten powder, and the reduction and carburisation processes), sub-micron levels may easily be attained [4]. However, the lower limit for the particle size of powder produced using these methods is considered to lie in the range 50-

150nm [46]. It is clear that in order to achieve further reductions, substantially different production methods are required. Such technologies are for the most part still very recent and include the spray conversion process, the chemical vapour reaction process [47], direct carburisation [48], and high-energy ball-milling of the elemental powders [49].

The high surface area of ultrafine and nanoscale powders inevitably results in a strong driving force for grain growth during consolidation. Existing liquid phase sintering technology is not sufficiently powerful to control this entirely, and hence the lower limit for the sintered grain size of hardmetals is currently estimated to be in the region of 200-300nm [46]. Unfortunately, no proven alternatives exist to liquid phase sintering, although novel consolidation methods such as solid state, flash, microwave, non-isothermal and rate-controlled sintering are being investigated [46,50,51].

2.3.1.1 Nanocarb

This study is concerned with the wear properties of ultrafine WC-Co sintered from powder produced through the spray conversion process. This process, developed by McCandlish and Kear at Rutgers University, and patented in 1994, is described in detail elsewhere [5,52,53] and only a brief outline will be given here.

The spray conversion process combines solution chemistry with gas-solid reaction processing to produce nanocrystalline WC-Co powders in which tungsten and cobalt are mixed at the molecular level. Aqueous solution-phase reactions between suitable combinations of soluble salts, followed by spray drying, yield powders which contain fine mixtures of tungsten and cobalt salts and which may be carburised in a fluidised-bed reactor to produce nanophase cobalt / tungsten carbide powder. Subsequent processing of the powder to produce the desired component is carried out using closely controlled conventional processes. The particular requirements and attributes of the powder are discussed extensively by Seegopaul [52].

The WC grain size of these powders has been estimated using XRD and TEM techniques to be less than 50nm, while sintered grain sizes of 0.2 μ m have been achieved. Furthermore, it is claimed that the spray conversion process produces a high level of compositional uniformity (due to mixing at the molecular level) and a narrow grain size distribution in both powders and

sintered parts, and that it eliminates particle non-uniformities which would otherwise contribute to abnormal grain growth [52].

2.3.2 Properties of ultrafine grades

2.3.2.1 Mechanical properties

Hardness

As expected, very high hardnesses, of up to 2300kg/mm^2 , have been observed in ultrafine grades [6]. However, work carried out by Roebuck [27] suggests that hardmetals with grain sizes below about $0.3\mu\text{m}$ may have hardnesses lower than those predicted by the Hall-Petch relationship, since at this point the deviation between the Hall-Petch relationship and an empirically-based power law relating hardness to microstructural parameters becomes significant.

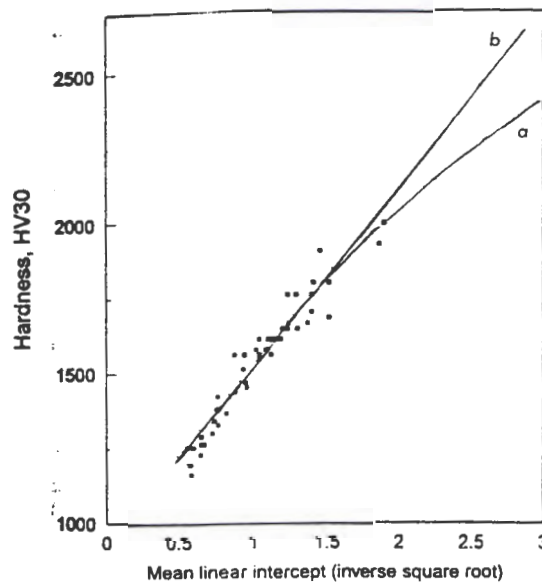


Figure 2.5: Dependence of WC-Co hardness on the inverse square root of the WC arithmetic mean linear intercept. The trend lines indicate the extrapolation of (a) the power law and (b) the Hall-Petch fits to the data [27].

Fracture toughness

While the hardness of WC-Co exhibits its greatest microstructural sensitivity at low grain sizes, the opposite is true for the fracture toughness: Keshavan and Jee [54] found fracture toughness and mean free path to be related through the equation:

$$K_{IC} \propto \lambda^{1/4}$$

Because of the different microstructural sensitivities of these two properties, the relationship between hardness and fracture toughness is strongly dependent on the grain size of the material. This has important implications for hardness/fracture toughness combinations in WC-Co components. As Figure 2.6 shows, the gradient of the graph of fracture toughness against hardness decreases with decreasing grain size [2,3]. Thus, while at high grain sizes, increases in hardness can only be achieved at the expense of fracture toughness, at low grain sizes it is possible to effect large changes in the hardness of the material (by changing the cobalt content) without compromising its reliability. Fine grained materials therefore tend to display greater toughness at high hardness than coarse grained materials of the same hardness.

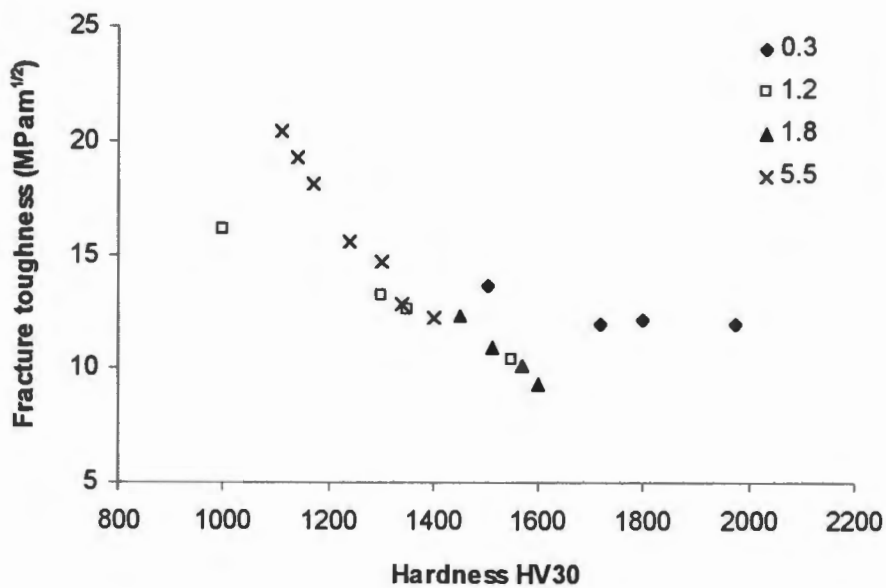


Figure 2.6: Dependence of fracture toughness on hardness for a series of alloys with grain sizes varying from 0.3 to 5.5 μm [3]

2.3.2.2 Sintering behaviour [46,53,55-59]

Due to the high surface areas of the powders used in the production of ultrafine WC-Co, a strong driving force for densification exists during sintering. In fact, it has been found that significant levels of densification (up to 75%) occur before the material reaches the liquid state [60]. Thus, the potential exists for rapid sintering at lower temperatures, with higher levels of densification. This has very positive implications for processing costs and the manufacture of components with low binder contents.

2.3.2.3 Composition

All ultrafine and sub-micron WC-Co grades contain small amounts of transition metal carbides which are added to the material to control grain growth during sintering. Grain growth inhibitors typically employed include VC, Cr_2C_3 , NbC and TaC. Of these, VC is considered to be the most effective and reliable, followed by Cr_2C_3 . The exact mechanism of grain growth inhibition is currently uncertain, although studies carried out on VC show that it interferes with the dissolution and reprecipitation of WC at the WC/Co interface [4,46,59,61].

The addition of grain growth inhibitors affects not only the sintered grain size of the component, but other material properties such as porosity, discontinuous grain growth, and hardness, and thus the levels and combinations of the inhibitors added must be chosen carefully to achieve the desired result [62]. For example, it has been shown that excessive VC additions can lead to a reduction in the transverse rupture strength of the material [63]. Cr_2C_3 additions, on the other hand are considered to contribute to solid solution strengthening of the binder phase [63], resulting in improved wear and mechanical properties of both ultrafine and conventional hardmetals [64,65]. Thus, it is considered that a combination of chromium and vanadium carbide is the most suitable additive for sub-micron carbides, since it combines the highly effective grain growth inhibition of VC with the advantageous influence on mechanical properties of Cr_2C_3 [63].

Ultrafine grades produced through the spray conversion process display a further compositional feature, namely that their binder phase has been shown to be enriched in tungsten and carbon compared to conventional materials [66]. This, together with the

amorphous phase detected in the binder of these materials in the course of the same study, may serve to strengthen the material.

2.3.2.4 Microstructure

The most significant difference between the microstructure of conventional and ultrafine grades is the occasional presence in ultrafine material of large isolated grains, with dimensions of the order of 10 μ m. These act as stress concentrators and therefore have a highly deleterious effect on material strength [67]. These grains are the result of discontinuous grain growth, which is defined as the rapid preferential growth of isolated WC grains, and is only observed in sub-micron and ultrafine grades, where a high driving force exists for grain growth during sintering. Discontinuous grain growth is promoted by chemical or geometrical irregularities, which lead to the nucleation of abnormal grains during sintering, followed by the preferred growth of these grains [46,62]. Examples of these irregularities include:

- coarse WC agglomerates in the powder compact
- local peaks in carbon concentration
- uneven grain growth inhibitor distribution
- individual grains or areas with non-stoichiometric compositions

In general therefore, ultrafine materials exhibit a high sensitivity to powder properties such as contamination and uniformity.

A second microstructural feature specific to ultrafine grades is the presence of cobalt inclusions in WC grains of material produced through the spray conversion process [68]. These have the effect of diminishing the amount of cobalt available in the binder phase, but may also act as crack arrestors.

2.3.3 Applications

Sub-micron WC-Co currently commands about 10-15% of the market for carbide products, and has found uses not only in areas requiring high wear resistance, but more specifically in those requiring good combinations of seemingly mutually exclusive properties such as hardness and fracture toughness. A number of these applications are discussed by Prakash [69].

A particularly good example of the way in which the properties of ultrafine WC-Co can be exploited is that of the miniature drills used to produce printed circuit boards [63]. Technical innovation in the printed circuit board industry has led to increasingly severe requirements of these drills, which must produce good quality holes, with sharp clean edges, at very precise positions, while maintaining high levels of reliability. These requirements necessitate high wear resistance, a high Young's modulus (and thus a high WC content) and high toughness, all of which seemingly-incompatible properties are provided by ultrafine WC-Co.

Chapter 3

EROSIVE WEAR

Wear is the progressive loss of material from the surface of a body, which occurs when the surface is subjected to repeated mechanical stresses arising from its interaction with a second body. These stresses may be generated by protrusions on contacting surfaces or by individual strikes from abrading or impacting particles. They result in the highly localised build-up of strain at the material surface, leading to eventual microfracture and material loss.

Wear processes are responsible for the progressive deterioration and premature failure of components in a wide variety of situations, but are of particular concern when they affect components which have been engineered to fine tolerances or a particular surface finish. In such cases, even small changes to the geometry of a system may result in operating conditions deviating significantly from the design, leading to a breakdown in the performance of the system. However, wear processes are also exploited in many operations: for example in machining, cleaning, or 'running' in of equipment.

Because the wear of a material is a result of its interaction with other bodies within a system, it must be regarded as being part of a system response, rather than a specific property of that material. Wear rates depend on a large number of parameters in the tribosystem, all of which interact in a complex manner. These parameters can be divided into two groups:

- the properties of the interacting bodies
- the kinematics of the interaction

Furthermore, in practical situations, wear processes are often complicated by the presence of other material degradation mechanisms, for example aqueous corrosion and high temperature oxidation, which may interact synergistically with the wear process resulting in enhanced rates of attack.

Erosive wear refers to surface material loss in an open system, brought about through repeated solid, liquid or gaseous impact. It includes, for example, blast erosion, cavitation erosion, and liquid droplet erosion. Again, these processes may interact with other materials degradation mechanisms, resulting in, for example, slurry erosion.

This study is concerned with the slurry erosion and cavitation erosion of WC-Co.

3.1 Slurry erosion

Materials exposed to slurry erosion environments are subject to the combined action of the erosive and corrosive components of the slurry and must ideally therefore be resistant to the synergistic interaction of these two material removal mechanisms. Slurry erosion is a factor in many industrial situations: for example, it affects components of the sea water pumping systems and the subsea pipelines used in oil and natural gas production. These systems are often very difficult to access and hence the costs of maintenance and replacement are very high [70,71]. In the mining industry, minerals are often transported in the form of slurries and the resultant erosion affects a wide range of components such as pumps, valves and pipelines.

Material response to slurry erosion environments depends on:

- its response to the erosive component of the slurry
- its corrosion properties
- its response to the interaction of these two degradation mechanisms at the specimen surface

These three parameters will be discussed in the following sections.

3.1.1 Particle erosion

The important variables determining a material's response to particle erosion are summarised below in Figure 3.1.

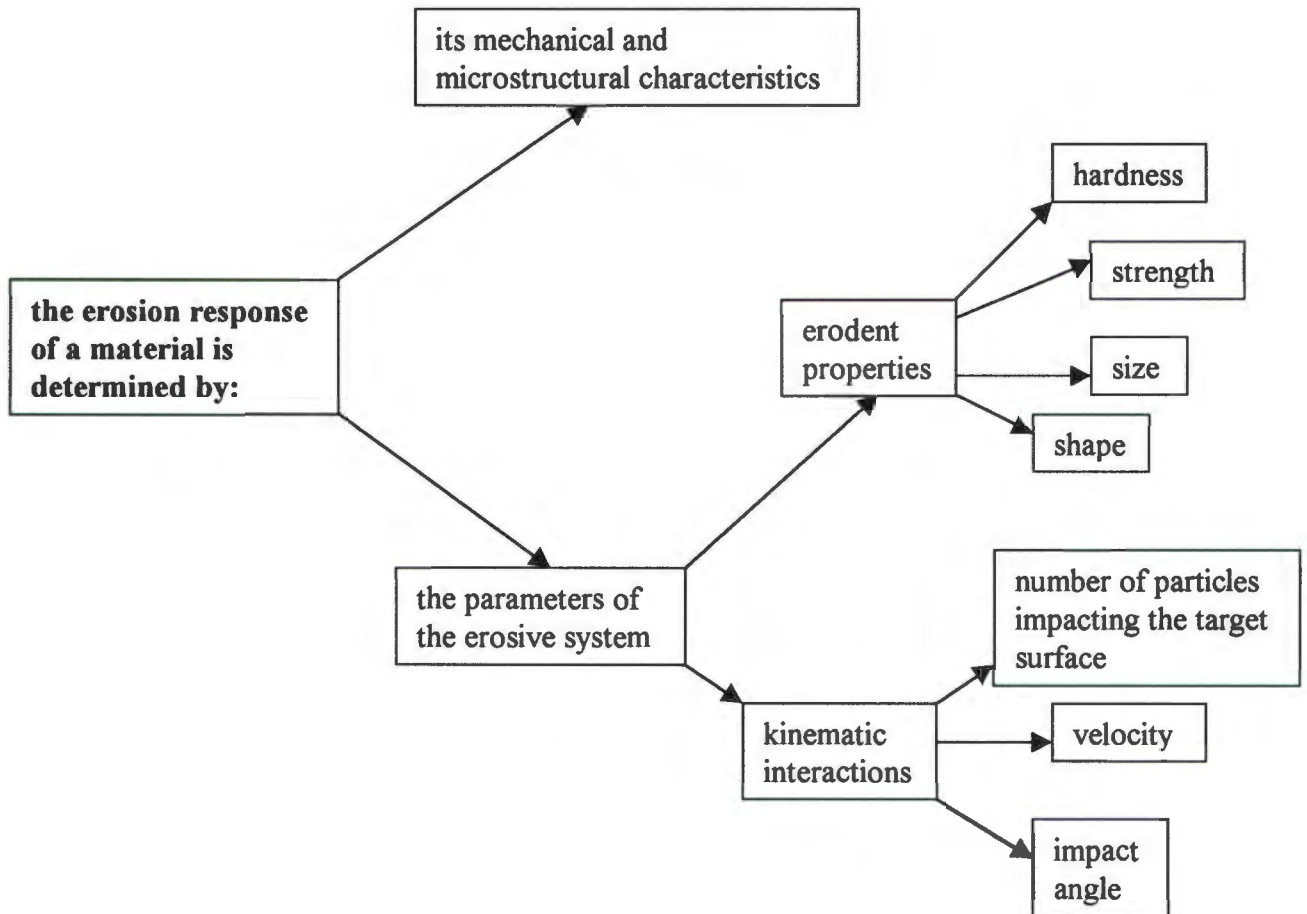


Figure 3.1: Flow chart illustrating the parameters which influence the erosion response of a material.

3.1.1.1 Target material properties

The properties of the target material largely determine the mode of material removal: ductile materials are considered to erode through a combination of microcutting and ploughing, while erosion in brittle materials results from the formation and interaction of cracks at the erodent impact site [72,73].

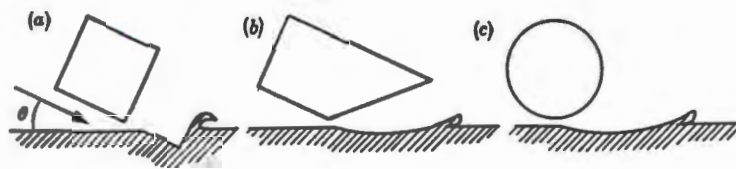


Figure 3.2: Modes of deformation observed in ductile materials [78]: (a) cutting deformation (b) ploughing deformation with an angular particle (c) ploughing deformation with a sphere

Microcutting in ductile materials is favoured when hard angular particles impact the surface at glancing angles: material is gouged out from the target surface as shown in Figure 3.2 [74]. Ploughing predominates at higher angles and results in the formation of extruded lips about the erosion crater. The extruded material may rupture from the surface immediately, if the particle velocity is sufficiently high, or may undergo further deformation due to the impact of fresh erodent particles or fragmented particles produced during the initial impact [75]. Eventually, the extruded lips become sufficiently work-hardened that they fracture from the target surface [75-80].

The two main crack systems operating during brittle erosion are:

- cone cracking [81]: this results from Hertzian elastic stresses which are set up by blunt erodents impacting the target surface at low velocities
- lateral and median cracking [82]: this occurs when angular particles travelling at high velocities impact the target surface, generating an elastic-plastic stress field.

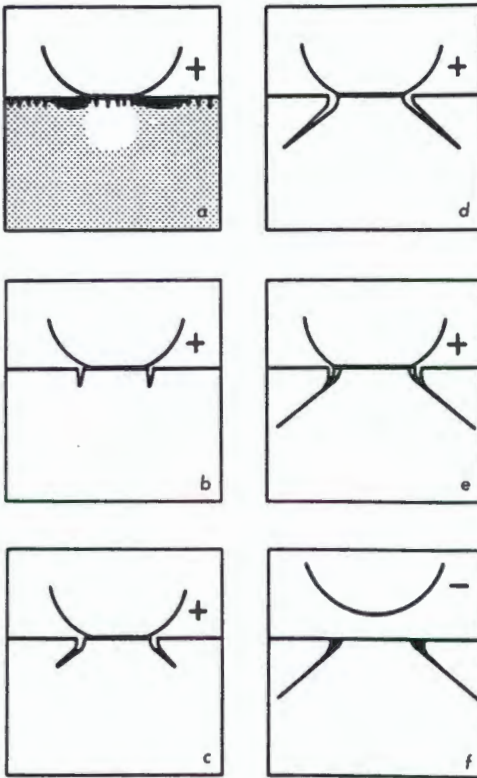


Figure 3.3: Sequence of events during cone-cracking [83]. Cracks form during the loading cycle and deviate outwards in order to avoid the compressive zone immediately beneath the indenter (this zone is indicated by the white region)

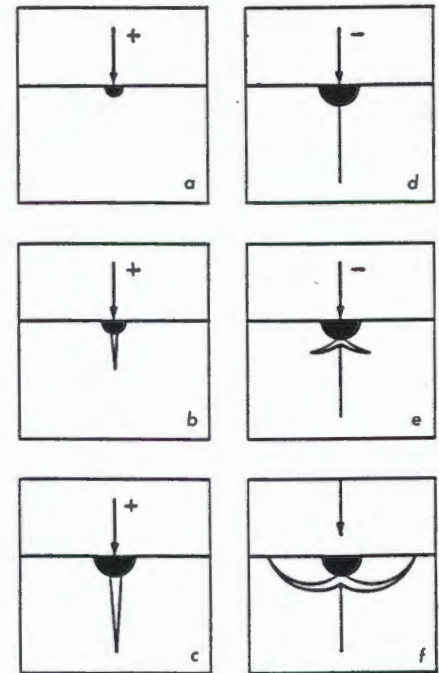


Figure 3.4: Sequence of events during lateral cracking [82]. Median cracks form during the loading cycle, due to the high stress concentration immediately beneath the indenter. Lateral cracks form during the unloading cycle, due to the tensile stresses imposed by the presence of the deformed material (indicated by the dark region)

Of the material removal mechanisms outlined above, only microcutting and lateral cracking habitually result in immediate material loss. Ploughing, cone cracking and median cracking merely contribute to surface damage, and material loss only occurs after a number of erodent impacts. Microcutting and lateral cracking are therefore considered to represent the most efficient material removal mechanisms.

From the above it is clear that two essential requirements for erosion resistance are sufficient hardness to resist microcutting and sufficient toughness to prevent cracking and chipping. However, experimental data shows these properties to be poor predictors of a material's response to erosion: for example, although a general correlation exists between hardness and

erosion resistance (see for example a study by Finnie, Wolak, and Kabil [84]), several exceptions exist to this trend and in particular a number of studies have shown that increasing the hardness of a material through work hardening or heat treatment does not improve its erosion response [79,80,85].

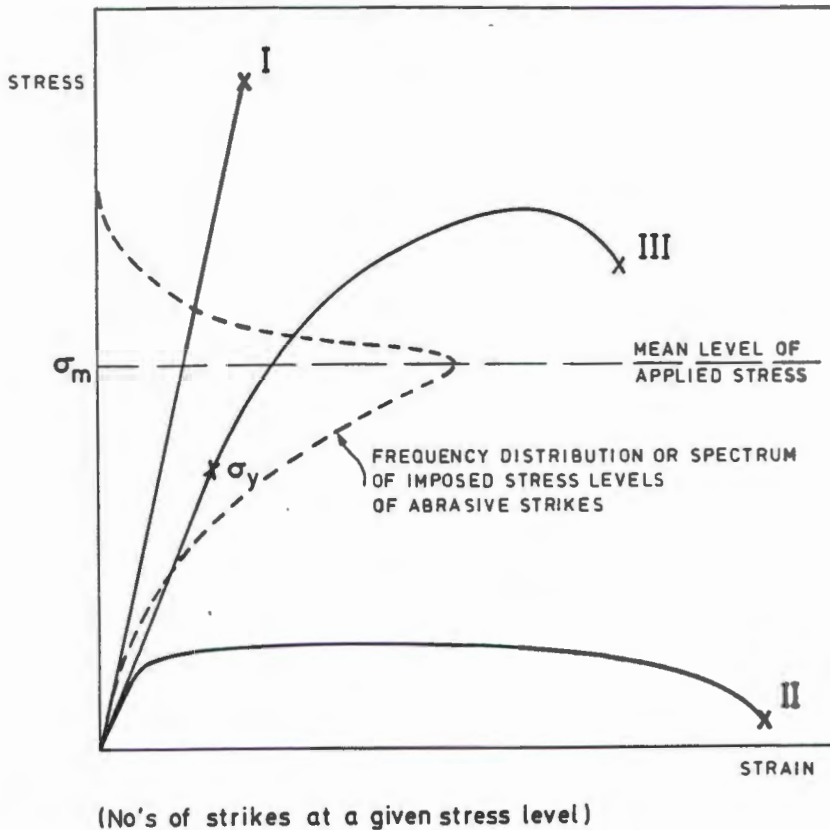


Figure 3.5: Hypothetical stress-strain curves for the wear of three classes of material superimposed upon the frequency distribution of abrasive or erosive strikes of a given stress magnitude [86] Material I has insufficient toughness to resist brittle erosion, material II has insufficient hardness to prevent cutting wear, while the hardness and toughness of material III are such that material removal will only occur after a number of erodent impacts

It is clear that other material properties must be considered in order to understand material erosion response. This is particularly important in the case of materials such as the hypothetical material III illustrated in Figure 3.5, which have sufficient hardness and toughness to resist microcutting and chipping. In this case, the predominant mode of erosion is ploughing deformation, and microfracture will only occur after successive erodent impacts.

Under these conditions, the erosion resistance of a material depends primarily on its ability to absorb impact energy without reaching a critical fracture strain. The most important parameter

in this respect is considered by Ball [86] to be the work hardening rate of the material: materials with high work-hardening rates are able to respond to erodent impact with only small strains and are therefore able to resist many such impacts before a critical fracture strain is attained.

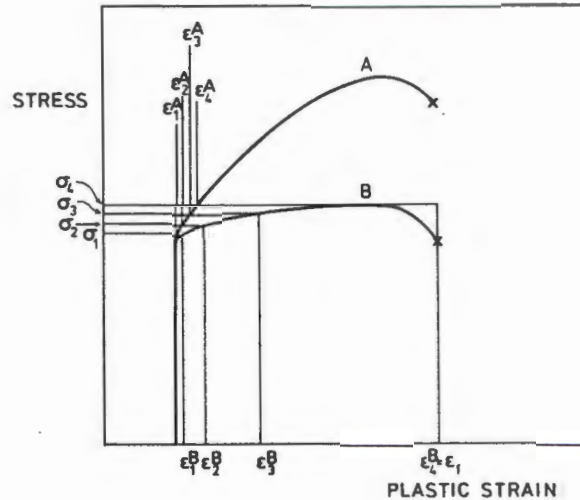


Figure 3.6: Hypothetical stress-strain curves for the wear of two materials A and B having identical yield stresses and strains to fracture, illustrating the influence of work-hardening characteristics on the material's ability to absorb plastic strain without failing [86]

3.1.1.2 The erosive system

Erodent properties

Mechanical properties: The mechanical properties of the erodent dictate the efficiency of the energy transfer from the particle to the target surface: this will be reduced if the particles deform or fracture on impact. Erosion rates are thus seen to increase with increasing particle hardness to reach a plateau when the erodent hardness is significantly greater than that of the target surface and erodent degradation no longer occurs on impact [73,87-89].

Size: The erosion rate of ductile materials has been found to be independent of erodent size for erodent particles greater than 100 μm in diameter. Below this threshold size, however, the erosion rate is seen to drop markedly with decreasing particle size [84,90]. This effect is

considered to be due to an increase in the local flow stress of the target material as the scale of the impact zone is diminished [73].

In contrast, the erosion rate of brittle materials has been found to increase continuously with increasing particle size. This is in accordance with theoretically derived relationships [73]. Below a certain threshold particle size, the erosion rate is found to decrease more rapidly with particle size than predicted, due to the increasing proportion of purely elastic impacts [91].

Shape: Angular particles are known to promote more efficient material removal mechanisms, namely microcutting and lateral cracking, and therefore produce higher erosion rates than spherical particles [89,92].

Kinematic interactions

Angle: Ductile materials display a maximum in erosion rate at impact angles between 20° and 30°: these conditions favour efficient material removal through microcutting [84]. In brittle materials, maximum erosion occurs at normal angles of incidence, when the extent of cracking due to particle impact is most severe [73].

Velocity: Erosion rates are related to the erodent velocity through a power law. Theoretical analyses of the microcutting mechanism predict velocity exponents of 2 for ductile materials [74], but in practice the values obtained generally lie between 2.3 and 3.0 [73]. This discrepancy may be attributed to the effects of ploughing, especially at high angles, but may also be related to the dependence of the local flow stress on the scale of the impact zone, as discussed above [84].

Theoretical analyses of brittle impacts predict velocity exponents of between 2.4 and 3.2 [73]. However, experimentally derived values for the velocity exponent are highly variable and generally significantly higher than predicted: exponents of between 1.7 and 7.0 have been reported [74,93-95]. The reason for this discrepancy between theoretical and experimental studies is unclear.

The erosion rate of brittle materials is found to decrease rapidly below a threshold value of impact velocity, due to the increasing proportion of purely elastic impacts [91].

Factors affecting kinematics at the target surface: Particle interaction and hydrodynamic effects exert a strong influence on the number, direction and velocity of the particles impacting the target surface. The values of these parameters at the target surface are therefore generally significantly different from those in the bulk of the system and hence are difficult to determine precisely.

Particle interaction effects denote the collisions which arise between impacting and rebounding particles at the target surface and which tend to reduce the total number of particles impacting it. These effects are prevalent at high particle concentrations and impact angles [96].

Hydrodynamic effects describe the tendency of carrier fluids to entrain the impacting particles and thus alter their direction and velocity. These effects become more pronounced as the viscosity of the carrier fluid increases and are stronger for small particles, which do not have sufficient momentum to resist deviation from their path [97-100]. However, they also tend to diminish the extent to which the surface is shielded by rebounding particles.

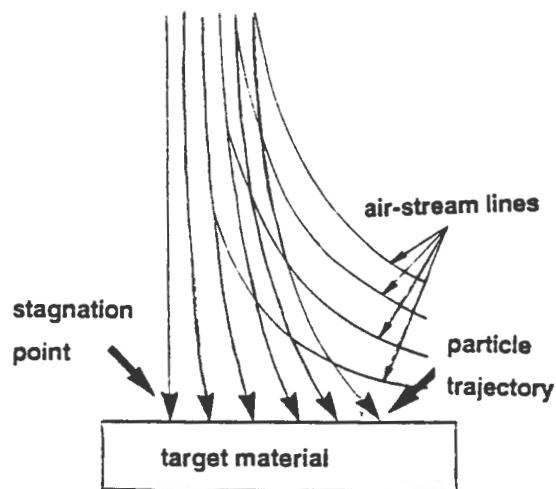


Figure 3.7: Deviation in particle trajectory caused by flow of the carrier fluid around the target [98]

Minimising the erosive potential of the system

The erosive potential of a system may be minimised through careful control of the variables outlined above. For example, the size and concentration of the erodent particles may be reduced through filtration or inertial separation; the operating parameters of the equipment may be changed (within the design limitations) to reduce particle velocity; and the geometry of the system may be altered to prevent particle impingement occurring close to the angle of maximum erosion.

3.1.2 Corrosion and erosion-corrosion interactions

The presence of a corrosive medium in the erosive system naturally represents a further degradation mechanism acting on the target material. However, its effect on the erosion rate is rarely merely additive since the two material removal mechanisms do not generally act in isolation. For example, particle impacts may render the surface more susceptible to corrosive attack, by removing passivating films and introducing higher dislocation densities. Conversely, corrosion may render a surface more susceptible to erosive attack by lowering its fatigue strength or introducing corrosion pits which act as stress concentrators [101].

The magnitude of this synergistic effect may be evaluated by the equation

$$S=T-(E+C)$$

where T is the total wear rate under combined erosive and corrosive attack, E and C are the wear rates resulting from the individual action of the erosive and corrosive mechanisms respectively, and S represents the additional wear due to synergistic erosion-corrosion interactions [102].

3.2 Cavitation

Cavitation refers to the growth and collapse of cavities in liquid subjected to local pressure fluctuations. The energy released during cavity collapse is sufficient to cause significant damage to adjacent surfaces, resulting in erosion. This phenomenon has the potential to occur in many hydrodynamic systems, such as pumps, valves, ship propellers, bearings, and turbines and has become increasingly prevalent as operating pressures in hydraulic equipment have been increased.

The pressure fluctuations necessary to induce cavitation in a liquid may originate either from the mechanics of fluid flow through the system, or from the vibration of an adjacent surface, as is the case in diesel engine cylinder liners [103,104]. It is the latter situation, termed vibratory cavitation, which is of interest in this study.

The intensity of cavitation erosion depends on the number of cavities formed, their collapse pressure, and their distance from the specimen surface. These are in turn dependent on the interaction of a number of parameters including pressure difference, liquid compressibility, liquid vapour pressure, viscosity, surface tension, temperature, and free and dissolved gas content [41].

Cavity collapse results either in the formation of a shock wave (if the collapse is symmetrical) or a microjet of liquid (if, due to the influence of a pressure gradient, the collapse is asymmetrical. Pressure gradients typically result from the presence of an adjacent surface or cavity collapse [105]). Furthermore, individual collapses may trigger the concerted collapse of a cloud of bubbles, producing a magnified shock wave [106]. Specimen erosion results from a combination of these mechanisms [107,108]. However, their relative importance is unclear and appears to vary with the geometry of the system and to depend on the type of erosion and the extent of cavitation development.

Cavity collapse typically generates pressures in the region of 10^2 - 10^3 MN/m² [109]. In some cases, these may be sufficient to cause surface pitting, while in others they will result in strain accumulation and eventual material loss.

Minimising the cavitation potential of the system

The cavitation erosion potential of a system may be minimised by proper design to prevent rapid variations in pressure [110]. Air injection [111,112] and the use of oil-water emulsions [113] have also been shown to reduce the extent of cavitation erosion.

3.2.1 Material response

Materials subjected to cavitation erosion experience large stresses and high strain rates, and their response is therefore generally difficult to predict since it cannot easily be related to processes occurring in conventional low strain rate tests. Thus, no strong correlations have been observed between bulk material properties, such as hardness and tensile strength, and the cavitation erosion rate, except for very narrow ranges of materials [114]. Furthermore, the performance of a material under other forms of erosive and abrasive attack is not necessarily a good indication of its resistance to cavitation attack [115,116].

Materials exhibiting high resistance to erosive attack are characterised by their capacity to withstand high strain rates and to absorb strain energy, and are found in general to exhibit a number of the following properties:

- a low strain rate sensitivity: materials with a high strain rate sensitivity, such as ferritic steels, undergo a ductile to brittle transition at high strain rates and exhibit high erosion rates due to brittle failure [114]
- absence of second phase particles and other erosion initiating sites [114,117]
- high work hardening rates [41]
- the ability to absorb energy without strain hardening, through phase transformations [41] or twinning [118]

Several studies have shown evidence that material removal during cavitation erosion occurs through a fatigue-like process [119,120], while Richman, McNaughton, and Rao have observed good correlations between cyclic deformation parameters and material removal rates [121,122]. TEM studies, however, have shown that the dislocation structure and

microstructure produced during cavitation erosion are entirely different from those normally associated with fatigue, and are instead typical of those produced by shock or impact loading [109,114].

Chapter 4

THE WEAR RESPONSE OF WC-Co

4.1 Slurry erosion

4.1.1 Particle erosion response

In common with other hard materials, WC-Co is highly resistant to erosive attack: for example, under conditions of liquid-borne particle erosion, the performance of the most resistant grades is similar to that of ceramics such as sintered alumina and silicon carbide [123,124].

It is generally accepted that the erosion rate of WC-Co under both airborne- and liquid-borne particle erosion increases monotonically with the binder content, as illustrated in Figure 4.1, and is therefore inversely related to the hardness [54,124-128]. However, more complex relationships have been observed in at least three studies.

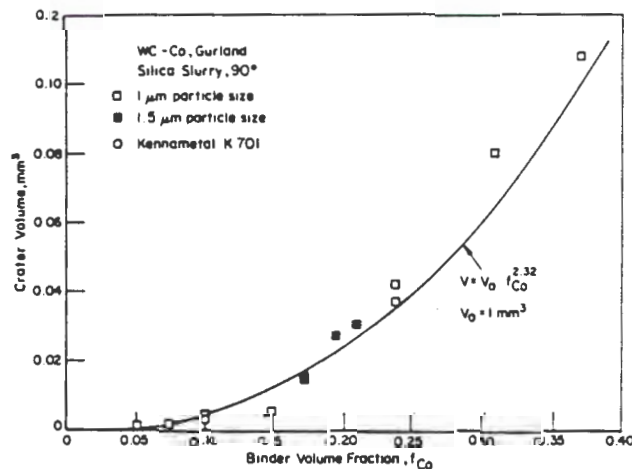


Figure 4.1: Plot of slurry erosion rate against binder content, showing monotonic increase of erosion rate with binder content [124]

Wright, Shetty and Clauer [129], in their study of the liquid-borne particle erosion of WC-Co, found the dependence of erosion rate on binder content to exhibit a transition at about 6wt%

cobalt. This is illustrated in Figure 4.2: for materials with over 6wt% binder, the erosion rate was observed to increase with binder content, while for materials with lower binder contents, the trend is reversed. This change in the microstructure/property relationship was attributed to the increasing importance of fracture toughness as a rate-controlling parameter. However, the high scatter observed in the data obtained from the low binder content materials suggests that it is the difficulty of sintering these materials to full density that is responsible for the increased erosion rates, rather than any fundamental change in the dependence of the erosion rate.

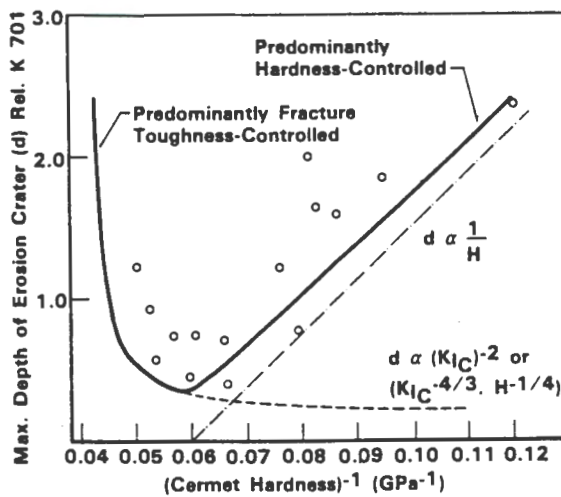


Figure 4.2: Wright's results for slurry erosion, plotted against inverse hardness [129]

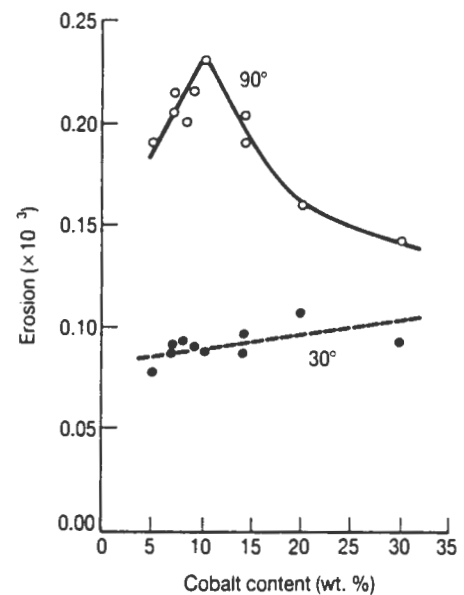


Figure 4.3: Pennefather's results for airborne particle erosion plotted against binder content [130]

Pennefather [131] and Ball and Paterson [132] have observed a considerably more complex relationship between erosion rate and cobalt content at impact angles of over 45°. This is illustrated in Figure 4.3 and is attributed to changes in the relative importance of parameters such as contiguity, fracture toughness and hardness. However, Pennefather did not observe any direct relationship between the erosion rate and any of these properties.

Studies of the relationship between erosion rates and other microstructural and system parameters fail to give a clear picture of the erosion response of WC-Co. With regard to the influence of grain size, no obvious dependence appears to exist: Wayne, Baldoni, and Buljan

[126] observed no correlation between erosion rates and grain size, while Reshetnyak and Kübarsepp [125] found the erosion rate to decrease with decreasing grain size. Conrad, Shin and Sargent [127] found the grain size to influence the erosion rate only at low velocities, when the erosion rate decreased with increasing grain size, while in a later study, Anand and Conrad [133] found the erosion rate to increase with increasing grain size until a plateau is reached.

Similarly conflicting observations have been made of the dependence of the erosion rate on impact angle: for example, some authors have found the angle of maximum erosion to be 60° [134], while others have found it to be 90° [128]. Velocity exponents ranging between 1.7 and 3.7 have been observed, which have been found to decrease with decreasing cobalt content [124] and increasing velocity [127].

A range of material removal mechanisms have also been observed, namely:

- extrusion and preferential removal of the binder phase followed by the loss of unsupported WC grains
- wear of WC grains [124]
- chipping and crushing of WC grains
- bulk deformation of the material through ploughing [131].

Anand and Conrad [133,135,136] have rationalised these results by postulating that two erosion regimes exist for multiphase materials such as WC-Co, and that the erosion response of these materials is determined by the relative dimensions of the microstructure and the crater formed by the impacting erodent. Their results indicate that when only a few (less than 10) WC grains are encompassed by the crater, a brittle mode of erosion occurs, with material loss occurring through cracking of the carbide grains. When the crater encompasses a large number of WC grains (over 100), erosion occurs through plastic displacement of the target along the cobalt phase. The size of the impact crater varies directly with the size and velocity of the erodent, and the cobalt content of the target.

In Anand and Conrad's study, the ductile mode of erosion was characterised by a low velocity exponent of about 2, a low angle of maximum erosion, and a strong correlation between

erosion rates and the square root of the binder mean free path. The brittle mode of erosion was characterised by a higher velocity exponent (between 3.1 and 3.7). Maximum erosion occurred at normal incidence, and the erosion rate increased rapidly with grain size when the WC grain sizes was low, and reached a plateau when the ratio of the impact crater area to the WC grain area was about 10.

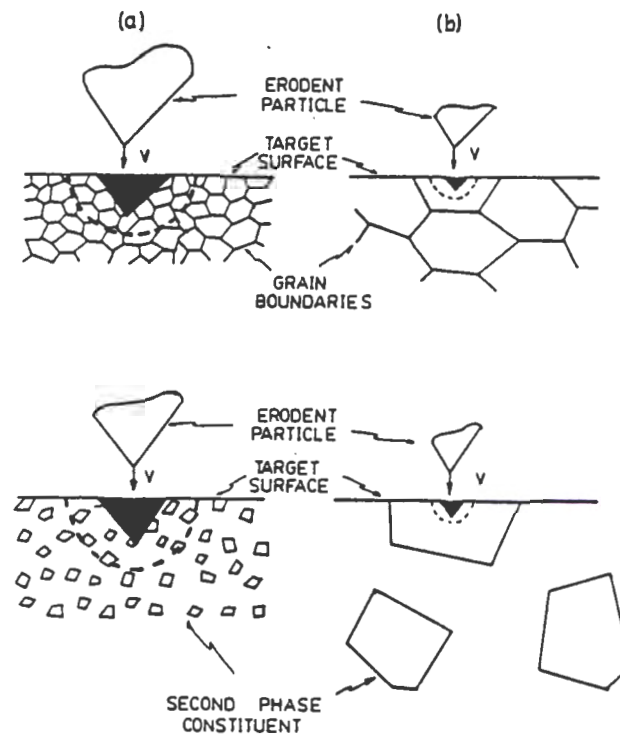


Figure 4.4: Schematic of scaling effects showing the influence of microstructure on erosion [133]
 (a) impact damage zone is appreciably larger than the microstructure size
 (b) impact damage is smaller than microstructure size.

4.1.2 Corrosion

The corrosion of WC-Co occurs through selective dissolution of the binder phase, and thus corrosion resistance decreases with increasing binder content. Due to the exaggerated attack of the binder phase which has been observed by Human and Exner [137] at carbide/binder interfaces, one might expect the corrosion resistance also to decrease with increasing microstructural refinement. However, electrochemical measurements of the rate of dissolution of the binder, carried out in the same study, revealed it to be independent of the grain size or the binder content. Similarly, Fernandez and co-workers [138], in tests on WC-6%Co found no correlation between corrosion rates and grain size.

4.1.3 Erosion-corrosion interactions

The response of hardmetals to an erosion-corrosion environment has been investigated by Wentzel [139,140], who subjected a series of hardmetals, with different binder compositions and corrosion properties, to slurry erosion. In these studies, significant increases in the slurry erosion rate were achieved by using a more corrosive carrier fluid, despite the fact that hardmetals subjected to the corrosive action of the carrier fluid alone showed no measurable mass loss during the test period [141]. Furthermore, materials subjected to an erosion-corrosion environment exhibited lower corrosion potentials than those subjected to purely corrosive environments. This observations indicate that a significant erosion-corrosion synergism operates during slurry erosion.

Corrosion resistant grades appear to be the most susceptible to erosion-assisted corrosion, since they experience the greatest drop in corrosion potential when subjected to the slurry jet. This appears to be due to the fact that under erosive conditions, these materials are no longer able protect themselves from the corrosive environment by forming a passive layer. As a result, the increases in slurry erosion rate observed with more corrosive carrier fluids showed no dependence on the binder composition, and no correlation was observed between the slurry erosion rate and the corrosion resistance. The main determinant of the materials' slurry erosion response appeared instead to be their hardness.

4.2 Cavitation erosion

A cursory glance at the existing data for the cavitation erosion of WC-Co suggests that the material response to this form of erosion must be highly complex: as Figure 4.5 shows the cavitation erosion resistance of WC-Co is significantly lower than would be expected from its hardness, being similar to that of tool steels and an order of magnitude lower than that of WC-Ni [41]. Furthermore the microstructure/property relationships are complex and unpredictable, and appear to depend on the choice of binder material.

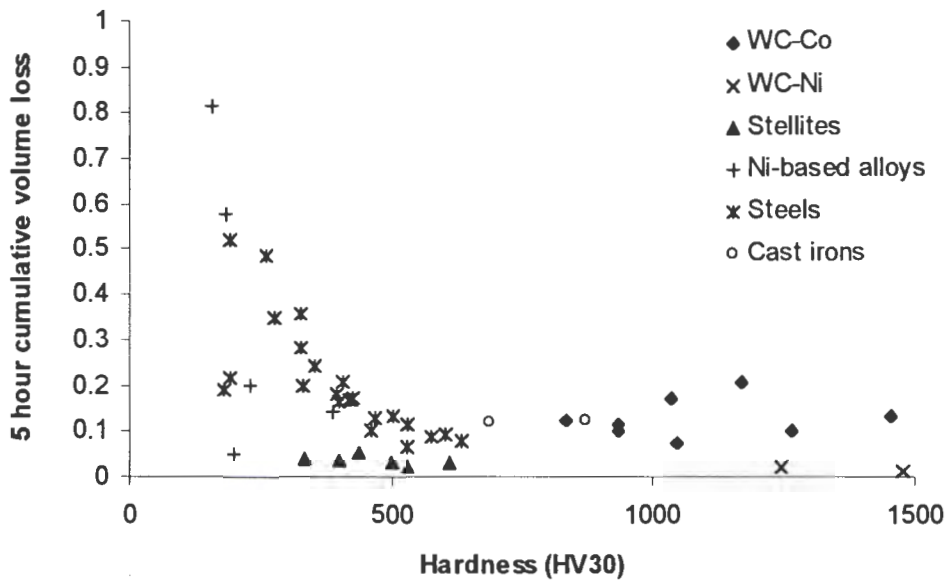


Figure 4.5: Plot of cavitation erosion damage against hardness [41]

Heathcock [41], in his work on hardmetals with binder contents of between 6wt% and 25wt%, found that the cavitation erosion rates of WC-Co (illustrated in Figure 4.6) decreased with increasing binder content, reaching a minimum at 15wt% cobalt, at which point they increased again. The limited results available for WC-Ni, however, suggest that for this material, the erosion rates increase with increasing binder content. Hankey's results [130], obtained from hardmetals with binder contents of between 5 and 30wt%, divided into two groups according to grain size, are illustrated in Figure 4.7. This shows a peak in erosion rate to occur at binder contents of 7wt% and 12wt% for the 1.8 μ m and 2.8 μ m grades respectively. Furthermore, while Heathcock's results show the erosion rate to increase with increasing grain size, no strong grain size dependence is observed in Hankey's study.

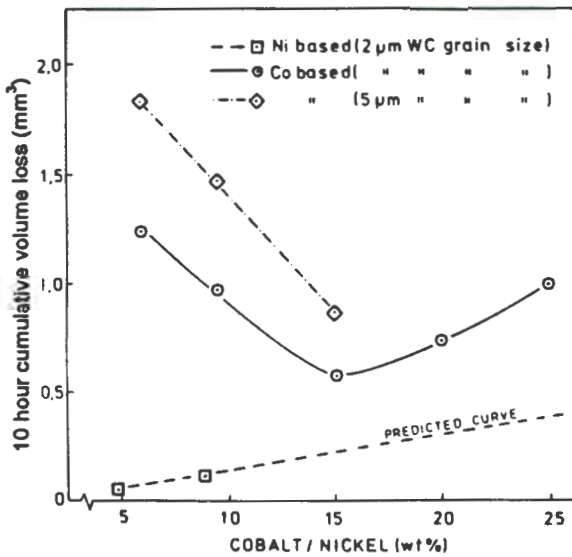


Figure 4.6: Heathcock's cavitation erosion results, plotted as a function of binder content [132]

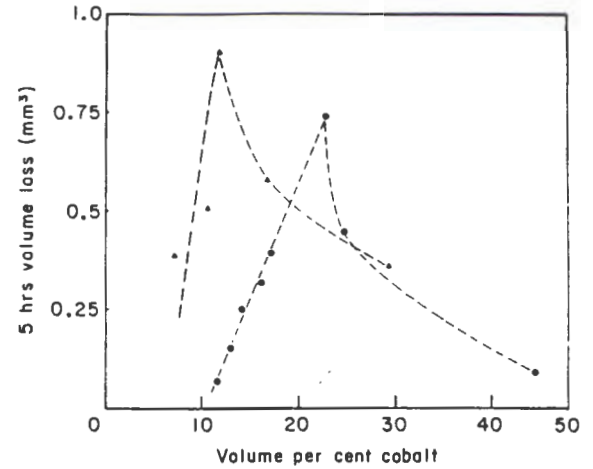


Figure 4.7: Hankey's cavitation erosion results, plotted as a function of binder content [130] (\blacktriangle = 1.8 μm grain size; \bullet = 2.8 μm grain size)

Various explanations have been advanced to account for these results. The poor performance of WC-Co alloys relative to WC-Ni alloys has been attributed to their inferior corrosion resistance [132]. However, Heathcock [41] suggests it may be due to stresses imposed at the WC/Co interface following the contraction of the cobalt phase which occurs during the f.c.c. \rightarrow h.c.p. transformation. The latter explanation appears most likely since it also accounts for the poor performance of WC-Co alloys relative to softer and less corrosion-resistant materials such as tool steels.

The peak in erosion rate observed by Hankey is considered to be due to a change in erosion mechanism: below the critical percentage of binder, the erosion response is controlled by the WC skeleton. As the binder content decreases, the hardness of the material and the contiguity of the WC skeleton increase, imparting strength and rigidity to the material and increasing its ability to withstand shock. Above the critical percentage of binder, erosion is controlled by the properties of the cobalt binder. The observed decrease in erosion rate is considered to be due to the increase in the fracture toughness of the material and an increase in the extent of the cobalt f.c.c. \rightarrow h.c.p. transformation. As discussed in Section 3.2.1, phase transformations are considered to increase the ability of materials to absorb strain energy during cavitation erosion.

The explanations advanced for the observed decrease in erosion rate appear to be unsatisfactory, for a number of reasons. Firstly, no grain fracture is observed in surfaces subjected to cavitation erosion [142], and thus it appears unlikely that fracture toughness would be a controlling parameter in this process.

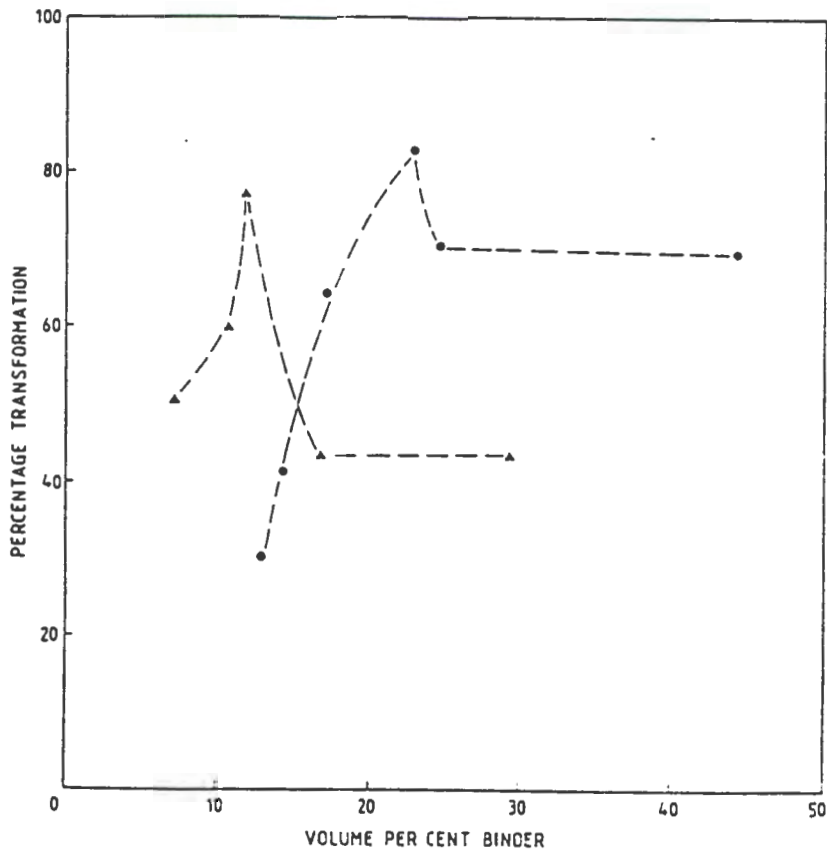


Figure 4.8: Percentage of the cobalt binder transforming during testing, as a function of total binder content [142] (\blacktriangle = 1.8 μm grain size; \bullet = 2.8 μm grain size)

Secondly, given the poor cavitation erosion performance of WC-Co (particularly relative to WC-Ni), it is questionable whether the transformation of the binder phase really increases the erosion resistance of this material. It is particularly interesting in this regard to examine Hankey's data for the extent of phase transformation occurring during cavitation erosion [142]. This data was obtained through X-ray diffraction measurements, and is shown in Figure 4.8, plotted against cobalt content. It is apparent from comparison of Figures 4.7 and 4.8 that a strong correlation exists between the erosion rate of WC-Co and the extent of the phase transformation occurring during testing. From this it appears that the phase transformation is

deleterious to the erosion performance of WC-Co, and that the extent of the transformation is the controlling parameter determining erosion rates.

4.3 Erosion of ultrafine WC-Co

No published data is currently available for the erosion response of ultrafine WC-Co. However, Jia and Fischer [6] found in their study of the abrasive wear of ultrafine and conventional hardmetals that the abrasion resistance of the best ultrafine material was approximately twice that of the closest conventional material. This improvement in abrasion resistance was attributed to the combination of increased hardness, reduced WC grain fracture and a ductile mechanism of material removal.

Chapter 5

EXPERIMENTAL MATERIALS

5.1 Introduction

The erosion performance of four ultrafine WC-Co grades, sintered from powder produced through the spray conversion process, was evaluated during this project. These grades were of similar WC grain sizes, but varying cobalt contents. A further twelve commercially-available WC-Co grades of varying cobalt contents and grain sizes were tested to provide data for comparison. These grades were divided according to their grain size into groups of fine, standard and coarse WC-Co. The nominal grain size of the materials tested is given in Table 5.1, and the different grades are illustrated in Figure 5.1.

Grade	Nominal grain size
UF (ultrafine)	0.3 μ m
F (fine)	0.8 μ m
S (standard)	1.2 μ m
C (coarse)	4 μ m

Table 5.1: Nominal grain size of the materials tested

For each grade, specimens were produced containing 6, 8, 10, and 15 wt% cobalt. While the standard and coarse grades consisted entirely of WC and cobalt, the fine and ultrafine grades also contained grain growth inhibitors to minimise grain growth during sintering. The ultrafine grades were experimental materials and thus it was possible to prepare them all using exactly the same amount of grain growth inhibitor, namely 0.8 wt% VC. Unfortunately this was not possible with the fine grades, which are commercial grades, and in these, the amount and composition of the grain growth inhibitor varied with the cobalt content, as detailed in Table 5.2.

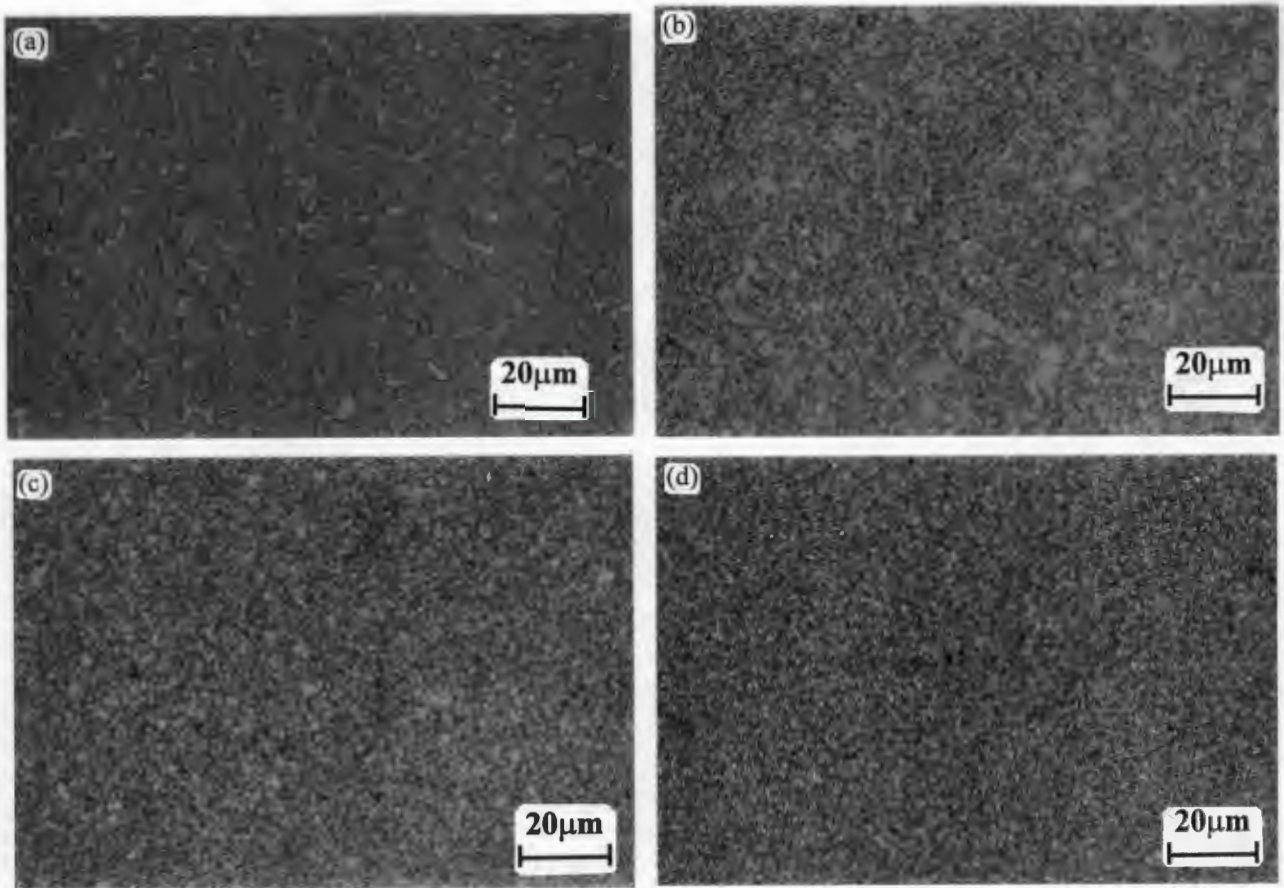


Figure 5.1: Optical micrograph showing typical microstructures of the grades tested: a) C6 (coarse grade) b) S6 (standard grade) c) F6 (fine grade) d) UF6 (ultrafine grade).

Grade	Grain growth inhibitor
F6	0.2 wt% VC
F8	0.2 wt% VC + 0.2 wt% Cr ₂ C ₃
F10	0.3 wt% VC + 0.2 wt% Cr ₂ C ₃
F15	0.3 wt% VC + 0.6 wt% Cr ₂ C ₃

Table 5.2: Amount and composition of grain growth inhibitor used in Fine grades. The number in the sample code indicates the cobalt content in wt%.

All the specimens tested were milled, pressed and sintered at Boart Longyear Research Centre, Krugersdorp, South Africa, using commercially available powders. Quality control of the sintered specimens was carried out through magnetic saturation and density measurements, and microscopic examination. The specimens were further characterised through coercivity, hardness and fracture toughness evaluation. The results of these tests are presented in the following sections.

5.2 Quality control

5.2.1 Experimental details

Density: The density of each grade was determined using the Archimedes submersion method, as detailed in ASTM test method B311-86.

Magnetic saturation: The magnetic saturation measurements were carried out on an LDJ model SM-8100 saturation induction measuring system. Four specimens were tested from each grade and an average taken.

Microscopic examination: Optical microscopy was carried out using a Reichart MeF3A microscope. The specimens were examined for porosity, free carbon, eta phase and discontinuous grain growth. Specimen preparation and examination was carried out in accordance with the relevant ASTM procedures [143,144].

5.2.2 Results and discussion

The results of the density and magnetic saturation tests are given in Table 5.3. The magnetic saturation measurements are expressed in three forms: the specific magnetic saturation of the composite, the specific magnetic saturation of the binder phase (calculated using the nominal binder content of the composite) and the specific magnetic saturation of the binder phase expressed as a percentage of that of pure cobalt.

Grade	Density (g/cm ³)	Magnetic Saturation (e.m.u./g)	Normalised MS (e.m.u./g)	MS relative to pure Co (%)
UF6	14.73	102±2	1700	85
UF8	14.52	146±1	1830	91
UF10	14.27	186±1	1860	93
UF15	13.80	282±1	1880	94
F6	14.84	111±2	1850	92
F8r	14.70	130±6	1630	81
F8	14.66	144±1	1800	90
F10r	14.45	130±2	1300	65
F10	14.47	184±2	1840	92
F15	14.01	281±2	1870	93
S6	14.91	113±1	1880	94
S8	14.76	149±1	1860	93
S10r	13.22	191±1	1910	96
S10	14.50	184±1	1840	92
S15	13.96	285±1	1900	94
C6	14.92	113±1	1880	94
C8	14.72	149±1	1860	93
C10	14.50	186±1	1860	93
C15	14.02	270±1	1800	90

Table 5.3: Density and magnetic saturation measurements for test specimens. The error quoted represents one standard deviation. (r indicates grades which were remade)

Density: Through comparison of the data in Tables 5.3 and 5.4, it can be seen that the measured densities of the standard and coarse grades correlate well with the theoretical values, but are in general slightly lower. The difference between the theoretical and experimental

values is due to the fact that the theoretical determination of density does not take into account the presence of porosity.

However, it must be noted that the density of grade S10 is significantly lower than expected.

Cobalt content (wt%)	Density (g/cm ³)
6	14.95
8	14.74
10	14.53
15	14.04

Table 5.4: Theoretical density of WC-Co, based on densities of 15.63g/cm³ and 8.9g/cm³ for WC and Co respectively

The densities of the fine and ultrafine grades are in general lower than the theoretical values: this is due to the presence of grain growth inhibitors.

Magnetic saturation: The specific magnetic saturation of the binder phase can be seen to vary in general between 1800 and 1900 e.m.u/g. This represents between 90 and 95% of the specific magnetic saturation of pure cobalt. These values lie well within the WC+ β section of the WC-Co phase diagram, indicating that the presence of a third phase is unlikely and that the compositions of the binders of these hardmetals are broadly similar.

The exceptions to this are the grades UF6, F8 and F10, for which the specific magnetic saturation of the binder phase is respectively 85%, 81% and 65% of that of pure cobalt. The binder phase of these materials is expected to contain high concentrations of tungsten, and, since it is considered that the initiation of η phase occurs when the specific magnetic saturation of the binder is less than 78% of that of pure cobalt [19], there is a strong likelihood of the presence of a third phase.

Microscopic examination: Initial examination of the polished specimen surfaces showed the porosity levels of the majority of grades to be <A02 B00 C00, as defined by the ASTM standard [143]. The exceptions to this are:

- grade S10: as expected from its low density, this contained massive porosity, as illustrated in Figure 5.2(a). In addition, significant macroscopic warping of the specimens was evident
- grade UF8: free carbon was observed at the edges of a few specimens [Figure 5.2(b)]

The high levels of porosity in grade S10 are considered to be due to an excessively high temperature gradient at the start of the sintering cycle, which results in rapid sintering of the surface of the specimen. Gasses formed from the lubricant added to the powder during milling are therefore unable to disperse and remain trapped inside the specimen, causing massive porosity.

The presence of free carbon in grade UF8 is due to insufficient control of the carbon balance of the furnace during sintering. Free carbon does not in itself have a strong effect on the properties of WC-Co, but high carbon levels are known to reduce the efficiency of grain growth inhibitors and thus may be associated with discontinuous grain growth in sub-micron materials.

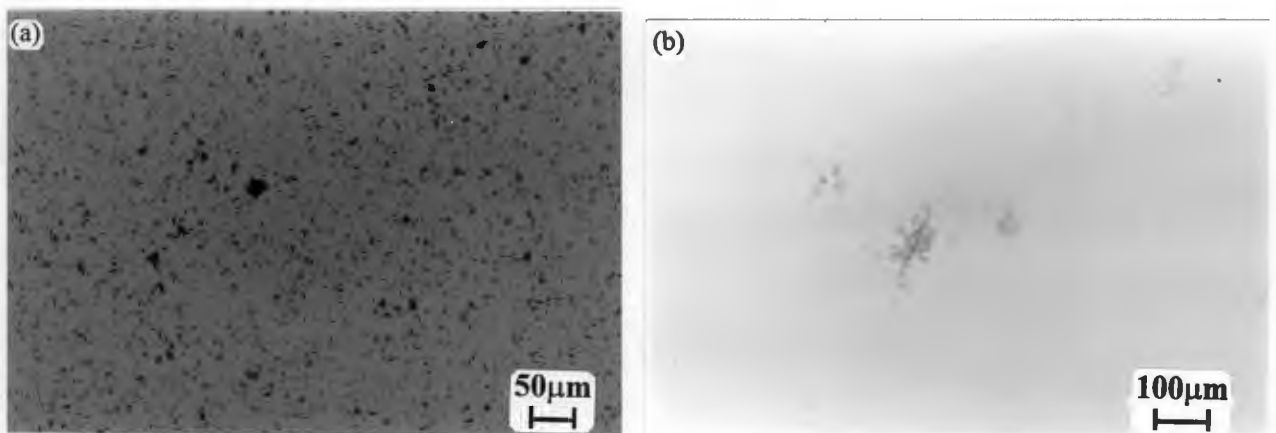


Figure 5.2: Optical micrograph showing porosity detected in the specimens: (a) massive porosity in grade S10, due to improper de-waxing procedure; (b) typical rosettes of free carbon, observed at the edges of some UF8 specimens

During microscopic examination of the etched specimens, the following defects were also encountered:

- grades F8 and F10: as expected from the low specific magnetic saturation of their binder phases, these grades displayed extensive tracts of η phase, which are illustrated in Figure 5.3.

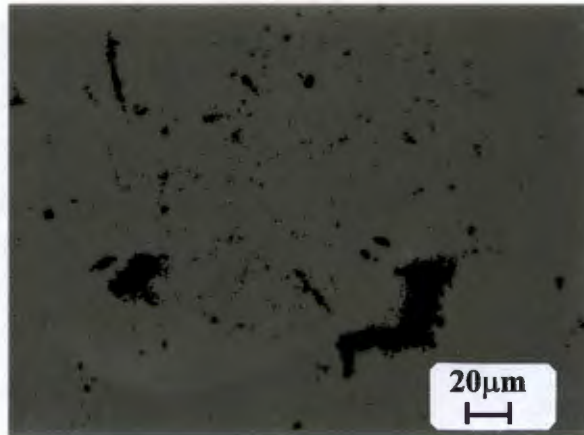


Figure 5.3: Optical micrograph showing typical formations of η phase observed in specimen F8

- grade UF8: a small amount of discontinuous grain growth was observed in some specimens. This effect may be related to the high carbon levels observed in this material, and is illustrated in Figure 5.4.

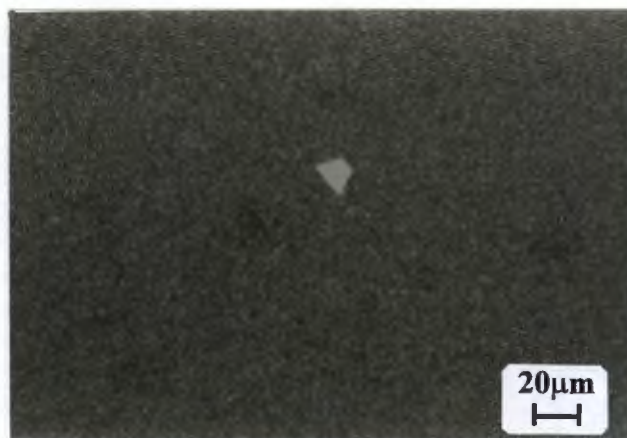


Figure 5.4: Optical micrograph showing isolated area of discontinuous grain growth observed in specimen UF8

- grade F15: extensive cobalt pools were observed in these specimens, as shown in Figure 5.5. These observations were confirmed through microhardness testing, which showed the

hardness of these areas to be significantly lower than that of the rest of the material. Cobalt pools result from improper milling procedure.

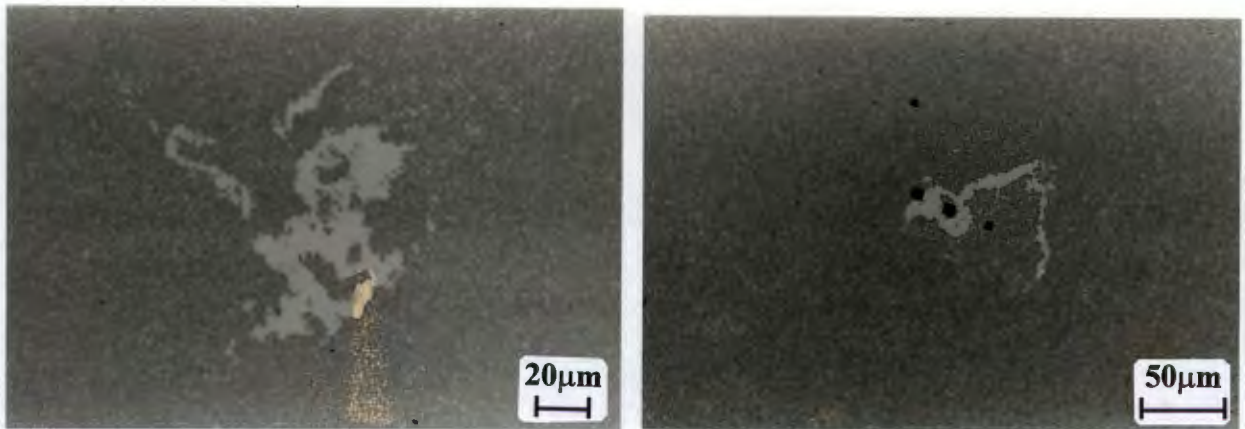


Figure 5.5: *Optical micrographs showing typical morphology of cobalt pools observed in grade F15. The identity of the phase is confirmed by the size of the microhardness indents*

5.2.3 Outcome of quality control testing

Following quality control testing, grade S10 was rejected and remade due to the presence of massive porosity and specimen warping. Grades F8 and F10 were also rejected and remade due to the presence of extensive tracts of η phase.

Grade UF8 was accepted for testing despite the occasional presence of free carbon and discontinuous grain growth. The level of discontinuous grain growth was considered to be acceptable in terms of industry standards [145] and specimens were individually screened for free carbon before testing.

Grade F15 was also accepted for testing, since cobalt pooling is only considered to have an adverse effect on material performance under highly specific applications such as the fast machining of metals [146].

5.3 Material characterisation

5.3.1 Experimental details

Hardness: The hardness of the materials was determined using a Vickers hardness indenter with a 30 kg load. Four indents were made per grade and the indentation diagonal lengths were measured using a Portascan machine.

Fracture toughness: Short rod fracture toughness tests were carried out for a number of grades on a Terratek systems model 4200 fractometer, following a modified version of the ASTM standard B771-87. The geometry of the specimens required for this test is fairly complex, and unfortunately specimens were not available for all the WC-Co grades examined in this study. Specimen dimensions were as follows:

Diameter:	9.52±0.025 mm
Length:	14.29±0.051 mm
Chord angle:	55.0°
Slot thickness:	0.33 mm

Four specimens were tested for each grade. The residual stresses in the material and the plasticity at the crack tip were both assumed to be negligible and thus no correction factor was used to calculate the fracture toughness.

Coercivity: Coercivities were determined using a Koerzimeter 1.094 measuring set in accordance with International Standard ISO 3326-1975 (E). The specimens used were cylindrical with a radius of 5mm and a height of 14mm. Four specimens were tested for each grade and an average taken.

Microstructural parameters: The microstructural parameters of the materials tested were determined from the coercivity using the procedure devised by Fang and Eason [19].

Stereological analysis [147] has shown the grain size to be related to the other microstructural parameters through the equation:

$$L_{wc} = \lambda(1-C) \frac{(1-f_v)}{f_v} \quad (1)$$

where L_{wc} is the mean linear intercept of the WC grains

λ is the binder mean free path

C is the contiguity

f_v is the volume fraction of cobalt

The mean free path has been shown by Fischmeister and Exner [148] to be related to the coercivity through the following empirical relationship:

$$H_c = \frac{73}{\lambda} \quad (2)$$

where H_c is the coercivity

Experimental data [148] shows that the contiguity of a WC-Co alloy may be described by an equation of the form:

$$C = 1 - 1.03 \exp(-5f_v) \quad (3)$$

By substituting equations (2) and (3) into equation (1), we obtain an equation for the WC grain size in terms of the cobalt volume fraction and the coercivity:

$$L_{wc} = 73 [1 - 1.03 \exp(-5f_v)] \frac{(1-f_v)}{H_c f_v} \quad (4)$$

5.3.2 Results and discussion

Table 5.5 gives the hardness, fracture toughness and coercivity data for all the grades tested, while the calculated values for the WC grain size and the binder mean free path are listed in Table 5.6.

Grade	Hardness (HV30)	Fracture toughness (MPam ^{1/2})	Coercivity (Oe)
UF6	2114±14	12.5±2.4	509±10
UF8	1976±8	12.8±1.4	458±4
UF10	1883±10	12.8±2.2	430±6
UF15	1602±7	11.7±1.5	308±3
F6	1711±4	-	271±4
F8	1764±9	-	348±3
F10	1707±10	-	310±1
F15	1364±10	14.1±1.6	159±1
S6	1557±6	10.9±0.9	183±2
S8	1526±15	10.9±0.4	159±1
S10	1404±7	-	143±2
S15	1163±10	13.5±0.2	99±1
C6	1255±5	15.8±0.2	68±2
C8	1244±8	-	84±1
C10	1201±5	15.7±0.3	81±1
C15	1012±5	18.8±0.2	57±1

Table 5.5: Hardness, fracture toughness and coercivity data for all grades tested. The error quoted represents one standard deviation.

Grade	Grain size (μm)	Mean free path (μm)
UF6	0.48	0.14
UF8	0.49	0.16
UF10	0.47	0.17
UF15	0.52	0.24
F6	0.91	0.27
F8	0.65	0.21
F10	0.66	0.24
F15	1.01	0.46
S6	1.3	0.40
S8	1.4	0.46
S10	1.4	0.51
S15	1.6	0.74
C6	3.6	1.07
C8	2.7	0.87
C10	2.5	0.90
C15	2.8	1.28

Table 5.6: Microstructural parameters for all the grades tested, calculated from the coercivity, using Fang and Eason’s procedure [19]

The average grain size for each of the four sets of materials tested is indicated in Table 5.7.

Grade	Grain size (μm)
UF	0.49 \pm 0.02
F	0.81 \pm 0.18
S	1.4 \pm 0.1
C	2.9 \pm 0.5

Table 5.7: Average grain size of each of the four sets of materials tested

Unfortunately, the use of coercivity measurements to calculate microstructural parameters provides no information on the grain size distributions within individual grades. However, a qualitative estimate of the grain size distributions may be obtained from the micrographs shown in Figure 5.1. From these it can be seen that the microstructure of ultrafine and coarse grades is highly uniform, while the WC grain size of individual fine and standard grades exhibits a wide variation.

5.3.2.1 Relationship between mechanical properties and microstructural parameters

The dependence of hardness and fracture toughness on the binder mean free path is illustrated in Figures 5.6 and 5.7 respectively.

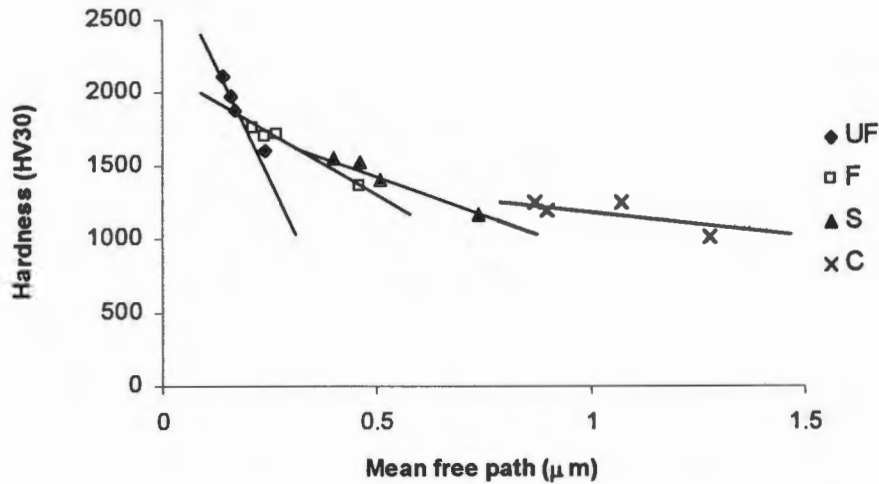


Figure 5.6: Plot of hardness against calculated mean free path

As Figure 5.6 shows, the sensitivity of hardness to the mean free path increases as the grain size decreases, such that the hardness of ultrafine grades exhibits a very strong dependence on the mean free path. This is consistent with previous studies of WC-Co hardness, which show it to be related to the microstructural parameters through a Hall-Petch type equation [1].

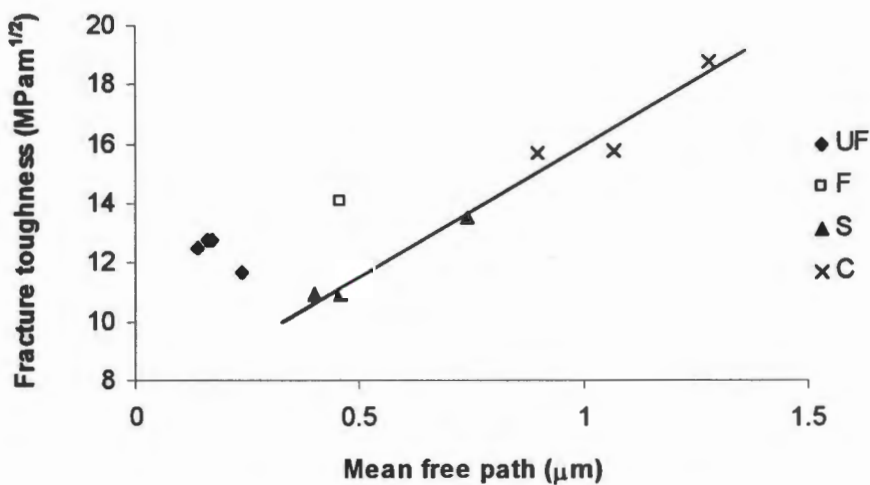


Figure 5.7: Plot of fracture toughness against mean free path

The limited data available for the fracture toughness of WC-Co grades indicates that for hardmetals with grain sizes above $1\mu\text{m}$, the fracture toughness increases in an approximately linear fashion with the binder mean free path.

By contrast, the fracture toughness of ultrafine hardmetals is considerably higher than would be expected from the trends observed in conventional materials and shows no obvious dependence on the binder mean free path. Furthermore, Table 5.5 shows that the scatter in the fracture toughness data obtained from ultrafine grades is significantly higher than that of the data obtained from the conventional materials. This implies that the fracture toughness may have been influenced strongly by the presence of defects, and could therefore be raised still further by improving processing methods.

The reasons for the observed fracture behaviour of ultrafine grades are unclear. However, the results imply that a different fracture mechanism may be operating in ultrafine grades. Previous studies of the relationship between the fracture toughness and the mean free path have indicated that the sensitivity of the fracture toughness to this parameter decreases with decreasing mean free path [54]. This may explain the fact that the fracture toughness of ultrafine grades is independent of cobalt content.

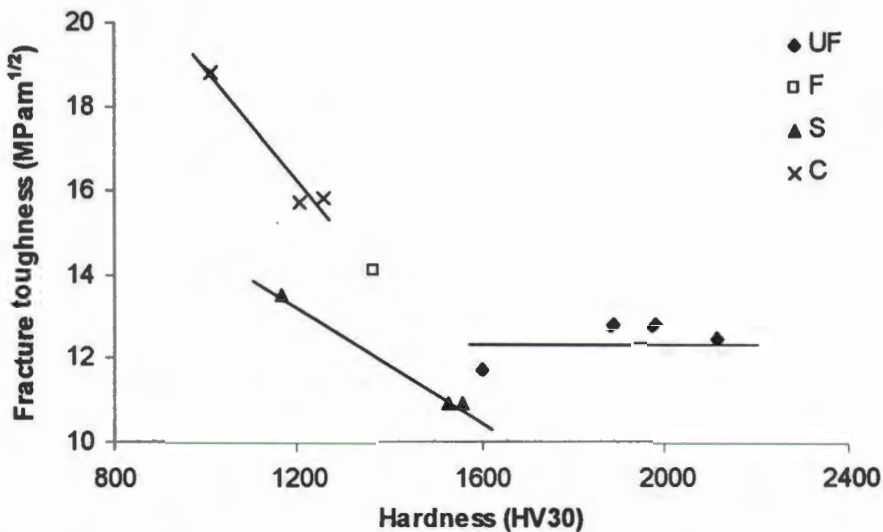


Figure 5.8: Plot of terra tek fracture toughness against hardness for all those grades for which terra tek data was available

The plot of fracture toughness versus hardness, shown in Figure 5.8, confirms the findings of O'Quigley and co-workers [2] and Sacks and co-workers [3]: namely that the sensitivity of fracture toughness to the material hardness decreases with decreasing grain size. The two graphs shown Figures 5.6 and 5.7 indicate that the reason for this is the difference in microstructural sensitivity of the two properties: the hardness becomes increasingly sensitive to the microstructure as the binder mean free path is reduced, while the fracture toughness exhibits the opposite trend.

5.4 Summary

1. A series of 16 WC-Co alloys of varying grain size and cobalt content has been produced and subjected to quality control through microscopic examination and determination of the density and magnetic saturation. The hardness, fracture toughness and coercivity of each grade has been measured and microstructural parameters have been calculated from the coercivity measurements.
2. Following quality control, three grades have been rejected and re-made due to the presence of η phase and massive porosity. Some free carbon and discontinuous grain growth has been observed in one ultrafine grade; the presence of free carbon was sporadic and the grain growth very limited, so the grade was retained for testing. Extensive cobalt pooling was observed in one fine grained material. This is not considered to affect the general properties of the material, and so this grade was also retained.
3. The calculated microstructural parameters indicate that the average grain size of the materials tested is $0.49\mu\text{m}$, $0.81\mu\text{m}$, $1.4\mu\text{m}$, and $2.9\mu\text{m}$ for the ultrafine, fine, standard and coarse grades respectively. The fine and coarse grades display a considerably more uniform microstructure than the standard and fine grades.
4. The hardness of the materials tested becomes increasingly sensitive to the microstructure as the binder mean free path of the material decreases.
5. The fracture toughness of ultrafine grades is higher than would be expected from the trends observed in conventional materials, and shows no dependence on the cobalt content.
6. The sensitivity of the fracture toughness to the hardness decreases with decreasing grain size of the material.

Chapter 6

EXPERIMENTAL METHODS

6.1 Slurry erosion

6.1.1 The jet impingement rig

Slurry erosion testing was carried out on a jet impingement rig designed and built by Wentzel [141], and based on the original rig devised by Zu [149]. A rig is illustrated in Figure 6.1.

During the operation of this rig, carrier fluid is pumped from the holding tank to the ejector, where the difference in diameter between the input and output nozzles results in the formation of a region of low pressure. This low pressure region draws erodent from the funnel into the ejector, by means of a vertical suction tube. The erodent and the carrier fluid are mixed to form a slurry jet which is accelerated through the ejector and impinges on the specimen surface.

After striking the specimen, the slurry falls back into the funnel and is separated into its constituent parts by a gravity filtering system: the erodent particles sediment out, while the carrier fluid fills the funnel until it overflows into a second container. Any erodent particles which have become entrained by the carrier fluid sediment out into this second container, while the carrier fluid, now almost entirely free of entrained erodent, fills this container and overflows into the holding tank. The cycle now recommences, with the carrier fluid being pumped through the system once more, while the erodent is again drawn into the ejector through the vertical suction tube.

The extent of erosion of the specimen is monitored through periodic mass loss measurements.

During the course of this study, the rig was modified through the insertion of a cooling coil in the water tank: this was considered necessary since continuous operation of the pump causes

the temperature of the carrier fluid to rise until it reaches a maximum of 50°C. Such a large temperature rise will affect not only the corrosivity, but also the viscosity of the carrier fluid and will consequently alter the velocity and erodent concentration of the slurry jet.

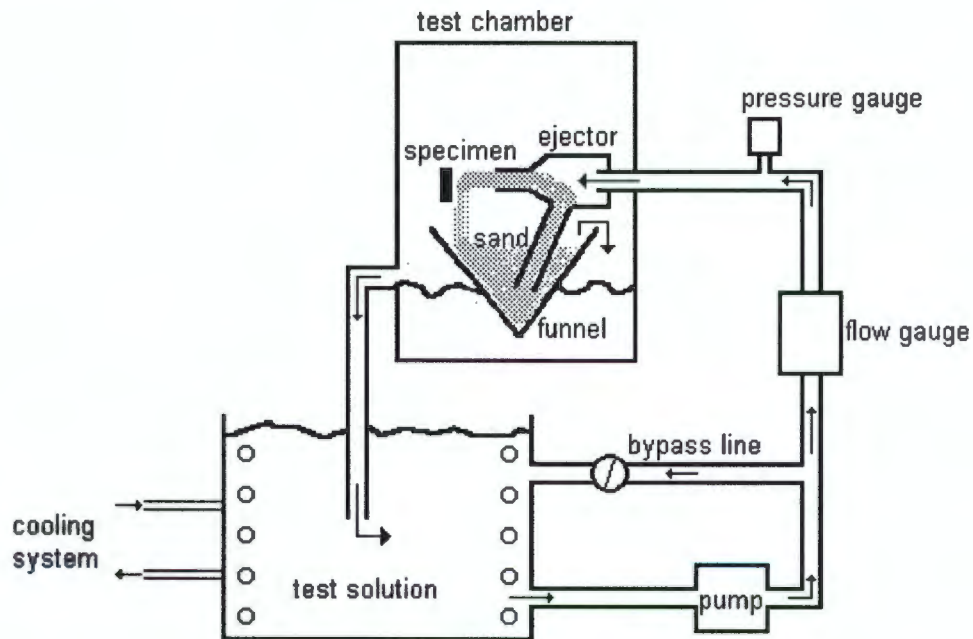


Figure 6.1: The slurry jet erosion rig

The design of the slurry rig allows close control over a number of test parameters, such as the erodent concentration of the slurry jet, its velocity and the angle of impact. The erodent concentration of the slurry can be altered by changing the dimensions of the venturi; the velocity of the slurry jet can be controlled by adjusting the bypass valve to change the feed pressure; and the impact angle may be varied between 0° and 90° by rotating the specimen holder about its horizontal axis.

The advantages of the rig are as follows:

- it is simple to operate
- it is capable of producing rapid erosion damage
- only small specimens are required
- erosive damage is restricted to a very small section of the rig

6.1.2 Test parameters

The operating parameters adopted for slurry erosion testing are summarised in Table 6.1.

Operating parameter	Value
Erodent	2kg of 500 μ m silica sand
Carrier fluid	200l tap water
Operating temperature	$\pm 25^\circ\text{C}$
Impact angle	75°
Test time	5 minutes – 1 hour
Erodent concentration	16wt%
Impact velocity	6.4ms^{-1}
Erodent impact rate	101 kg hour^{-1}
Specimen	18mm diameter disc

Table 6.1: Summary of the operating parameters employed for slurry erosion testing

Erodent: Silica sand, which is considered to be the most commonly occurring natural abrasive contaminant [73], was chosen as the erodent. The sand used in this study was 20/40 density silica sand, supplied by Consol Industrial Minerals, and having the following characteristics:

- nominal particle size: 500 μ m
- particle shape: round
- hardness: 1100 kg/mm²
- density: 2.7 g/cm³

A scanning electron micrograph of the erodent is shown in Figure 6.2.

Prior to use, the erodent was sieved to remove all particles greater than 710 μ m or smaller than 425 μ m. The size distribution of the remaining sand is given in Table 6.2.

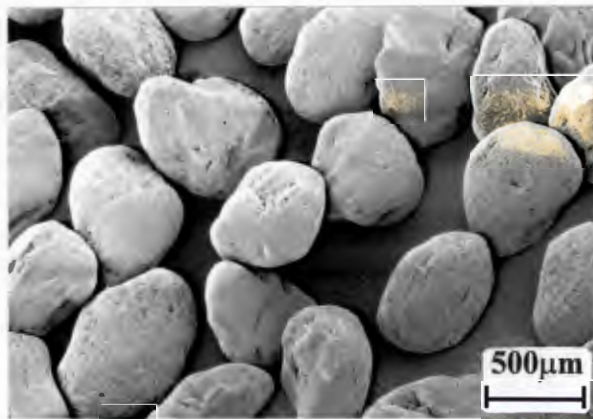


Figure 6.2: Scanning electron micrograph of unused erodent

Particle size	Fraction
600-710	0.24
500-600	0.69
425-500	0.07

Table 6.2: Size distribution of silica sand used for slurry erosion (determined from data supplied by the manufacturer)

Continuous recycling of the erodent is known to produce a gradual alteration of erodent properties, which will lead to progressive changes in the test conditions [150]. Erodent degradation in the slurry jet erosion rig has been monitored by Wentzel [141], who found no significant degradation to occur after four hours testing. Consequently, the erodent was replaced at four hour intervals.

Impact angle: In this study, the impact angle was set at 75° , which has been shown by Wentzel [140] to be the angle of maximum erosion for standard grade hardmetals with 6wt% binder content.

Test time: The mass loss of the specimens was monitored at intervals of between 5 minutes and 1 hour, depending on the erosion resistance of the material. Test times were chosen such that at least 1mg mass loss occurred between successive measurements.

Calibration: Both the velocity and the erodent concentration of the slurry jet were maintained at a constant value throughout this study. The rig was calibrated by directing the slurry jet into a measuring cylinder: the velocity and the flow rate of the slurry jet were determined by measuring the time required to fill the cylinder, while the erodent concentration was calculated from the density of the slurry collected.

6.1.3 Test procedure

1. The holding tank of the slurry rig was filled with 200l of tap water, while two kilograms of unused sieved silica sand were washed in tap water and placed in the funnel shaped container.
2. Each specimen was prepared as detailed in Section 6.3, cleaned ultrasonically in alcohol, dried, and allowed to cool (to ensure accurate mass measurement). The specimen was then weighed to an accuracy of 0.1mg.
3. The specimen was positioned in the specimen holder with its orientation indicated by the inscribed mark. The specimen holder was then set to the impact angle required and

secured to the top of the impact chamber, thus positioning the specimen 30mm from the output nozzle, directly in the path of the slurry jet.

4. The specimen was subjected to the action of the slurry jet for a pre-determined time, during which the carrier fluid was maintained at a constant temperature through the operation of the cooling system. The specimen was then removed from the holder, cleaned ultrasonically in alcohol, dried, cooled and weighed.
5. This procedure was repeated until four successive constant mass loss measurements were obtained.
6. Mass loss measurements were converted to volume loss and the steady state erosion rate and incubation time of the specimen (defined in Figure 6.3) were determined through regression analysis.

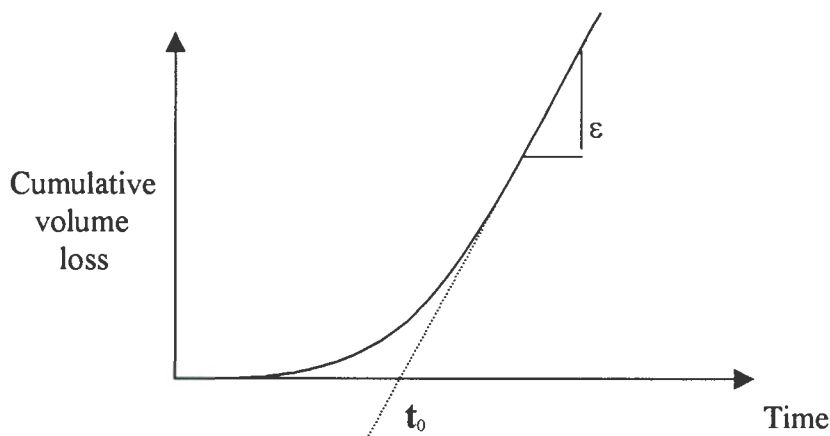


Figure 6.3: Illustration of the steady state erosion rate, ϵ , and the incubation time, t_0 , on a graph of cumulative volume loss against time

6.1.4 Reproducibility

The reproducibility of the slurry erosion tests was determined by testing two C10 specimens under identical conditions in a tap water slurry. The data obtained is presented graphically in Figure 6.4, while Table 6.3 gives the calculated slurry erosion data for the two specimens.

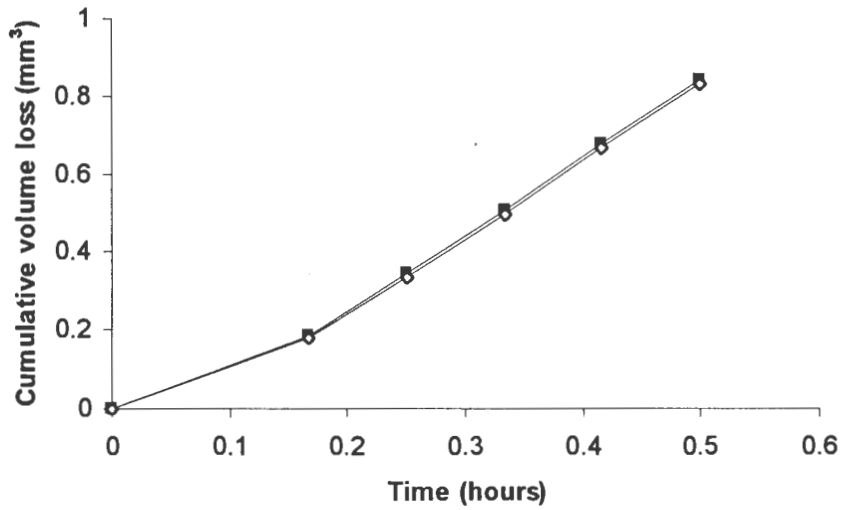


Figure 6.4: Graph of cumulative volume loss against time for two C10 specimens

	Steady state erosion rate (mm ³ /hour)	Incubation time (hours)
Specimen 1	1.95	0.0766
Specimen 2	1.97	0.0753
Average	1.96	0.0760
Standard deviation	0.01	0.0009

Table 6.3: Slurry erosion data for two C10 specimens tested in tap water

It is clear that the data for the two specimens are in excellent agreement, with neither the standard deviation of the incubation period, nor that of the steady state erosion rate exceeding 1% of the average value.

The principal sources of error during slurry erosion are considered to be:

- Erosion of the venturi: changes in the dimensions of the venturi will affect the velocity and the erodent concentration of the slurry jet. These two parameters were monitored closely throughout the study in order to ensure that the components of the venturi could be replaced as soon as any significant change was detected
- Slight temperature fluctuations ($\pm 4^{\circ}\text{C}$) due to variations in atmospheric temperature
- Smoothing of the erodent surface due to repeated impacts

6.1.5 Determination of the dependence of erosion rates on impact angle

As discussed in Section 3.1.1.2, a target surface subjected to slurry erosion experiences erodent impact over a wide distribution of angles, due to the entrainment of the particles by the carrier fluid, which is forced to deviate as it approaches the surface [98]. Thus the geometry of the erosion scar formed will depend upon, and give an indication of, the angular dependence of the erosion rate of that material [151,152].

This effect was evaluated in the present study using four grades of different grain sizes, each containing 6wt% cobalt binder. These were subjected to slurry erosion at a 90° impact angle, until equal volumes had been lost from the surface of each specimen (to within 0.5%). The diameters of the erosion scars formed were then measured using vernier callipers: it is expected that as the angle of maximum erosion decreases, the erosion scars will become shallower and wider.

6.2 Cavitation erosion

6.2.1 The vibratory cavitation erosion rig

Cavitation erosion testing was carried out on a vibratory cavitation erosion rig designed and built by Heathcock [41] and based on the stationary specimen mounting method adopted by Preece [153]. This method is considered to be superior to the vibratory specimen method ASTM G32-72, since it eliminates the risk of fatigue failure of the specimen and avoids the difficulties involved in producing a suitable specimen for insertion in the drill horn.

The rig is illustrated in Figure 6.5.

The specimen is held in a beaker of the fluid immediately beneath the tip of a vibrating drill, which produces cavitation events in the thin layer of fluid separating it from the specimen. The drill is mounted on vertical sliding bars which allow the separation distance and thus the cavitation intensity to be altered. The separation distance can be measured using the micrometer mounted on one of the bars. The temperature of the cavitating fluid is controlled through the use of a thermoregulating system and a magnetic stirrer, while that of the drill horn is maintained constant through use of a fan.

The extent of erosion of the specimen is monitored through periodic mass loss measurements.

The advantages of the vibratory cavitation system are its simplicity, the fact that it produces rapid erosion damage and that it allows the intensity of the erosive attack to be closely controlled. However, the application of its results is restricted by the fact that it only models those systems in which cavitation is produced by a vibrating surface (for example, diesel engine cylinder liners).

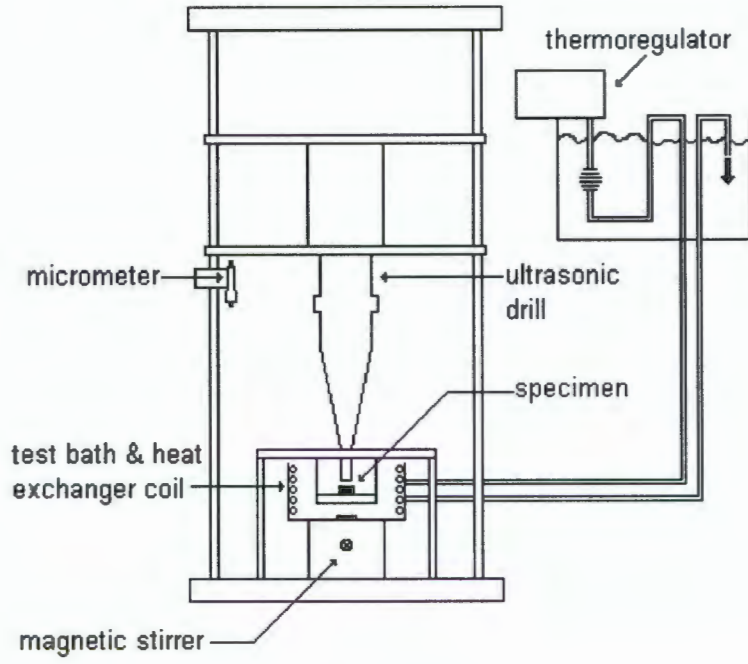


Figure 6.5: The vibratory cavitation erosion rig

6.2.2 Test parameters

The operating parameters adopted for cavitation erosion testing are summarised in Table 6.4.

Operating parameter	Value
Cavitation medium	Distilled water
Temperature	31° to 34°C
Separation distance	0.35mm
Test time	30 minutes to 10 hours
Amplitude	100 ± 3 μm
Frequency	20 ± 0.2 kHz
Specimen	13mm diameter disc

Table 6.4: Summary of the operating parameters employed for cavitation erosion testing

Temperature: The temperature of the cavitating fluid was maintained between 31° and 34°C by the thermoregulating system. This is close to the temperature of maximum cavitation erosion, determined by Heathcock [41] as being 35°C.

Separation distance: The separation distance between the drill tip and the specimen during testing was 0.35mm. This was found by Heathcock [41] to produce maximum cavitation intensity.

Test time: The mass loss of the specimens was monitored at intervals of between 30 minutes and 10 hours, depending on the erosion resistance of the material. Test times were chosen such that at least 1mg mass loss occurred between successive measurements.

6.2.3 Test procedure

1. The rig was warmed up for an hour using a dummy specimen, in order to allow the cavitating fluid to reach the test temperature, the drill to warm up and expand to its maximum length, and the gas content of the fluid to equilibrate.
2. Each specimen was prepared as detailed in Section 6.3, cleaned ultrasonically, dried, and allowed to cool to ensure accurate mass measurement. The specimen was then weighed to an accuracy of 0.1mg.
3. The specimen was positioned in the specimen holder at a given orientation, indicated by the inscribed mark. The specimen and the holder were clamped in the mounting platform, which was then submerged in distilled water.
4. After setting the appropriate separation distance between the specimen and the drill tip, the drill was clamped into place and the specimen subjected to the erosive action for a pre-determined time.
5. This procedure was repeated until four successive constant mass loss measurements were obtained.
6. Mass loss measurements were converted to volume loss and the steady state erosion rate and incubation time of the specimen (defined in Figure 6.3) were determined through regression analysis.
7. The TiAl drill tip was refaced and the distilled water replaced after every 8 hours testing.

6.2.4 Reproducibility

The reproducibility of the cavitation erosion tests was determined by testing four S6 grades under identical conditions. The plots obtained are given below in Figure 6.6.

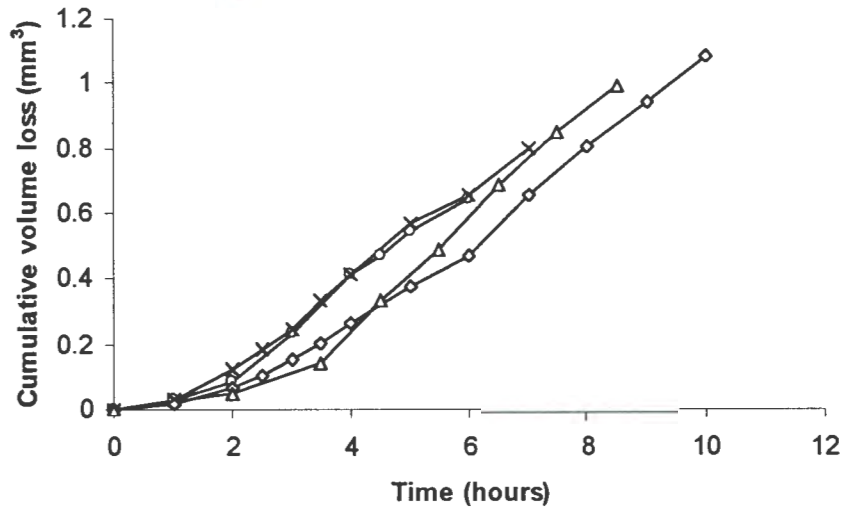


Figure 6.6: Plot of cumulative volume loss against time for four S6 specimens

	Steady state erosion rate (mm ³ /hour)	Incubation time (hours)
Specimen 1	0.154	1.43
Specimen 2	0.147	1.28
Specimen 3	0.137	2.13
Specimen 4	0.171	2.61
Average	0.152	1.86
Standard deviation	0.0143	0.621

Table 6.5: Cavitation erosion results for four different S6 specimens

The calculated values of the steady state erosion rate and incubation time for each of the specimens are listed in Table 6.5. From this it may be seen that the steady state erosion rates are in good agreement, with the standard deviation being equivalent to 9% of the average erosion rate. The incubation times, however, exhibit a high scatter, with the standard deviation being equivalent to 33% of the average incubation time. The high scatter of the incubation

periods relative to the steady state erosion rates is probably due to the high sensitivity of the initial erosive attack to minor surface flaws.

The principal sources of error during cavitation erosion are considered to be:

- Unavoidable cooling of the rig during specimen change-over. This causes the drill horn to contract, thus introducing a slight uncertainty in the determination of the separation distance and causing a small variation in resonant frequency. The temperature of the distilled water typically drops by a few degrees during this period and the time required for it to return to equilibrium temperature may represent a significant proportion of the test time for materials with low erosion resistance
- The standard error in determining the separation distance (about 10 μ m) combined with the effects of possible bevelling of the specimen introduced during polishing

6.3 Specimen preparation

The specimens used for both slurry and cavitation erosion were discs of either 13mm or 18mm diameter and 10mm height, which were supplied with their sides ground flat and parallel. Before testing these specimens were:

1. polished with 9 μ m diamond suspension, using the procedure outlined below, in order to eliminate the stresses introduced by grinding. The cavitation erosion specimens were then polished further using 0.25 μ m diamond paste.
2. demagnetised, to ensure accurate mass measurements
3. marked with a diamond scribe in order to allow them to be replaced in the specimen holder in the same orientation after each mass loss measurement

6.3.1 Polishing procedure

The polishing procedures required to eliminate the residual stresses introduced by grinding were determined using the method developed by Exner [38]: the surface of the specimen is indented after each polishing step and the total length of the Palmqvist cracks formed at the corners of the indent is measured. The residual stresses are considered to have been eliminated when a maximum indentation crack length is observed. Separate polishing procedures were determined for ultrafine, fine, standard and coarse grades, each based on the behaviour of the corresponding 6wt% binder content grade.

The specimens tested were hot-mounted to minimise bevelling and polished using a Struers Rotomodule automatic polishing system with a Struers DP Plan polishing cloth charged with 9 μ m diamond suspension. The polishing increment was one minute in the case of sub-micron grades and 30 seconds in the case of standard and coarse grades, for which material removal occurs more rapidly.

After each polishing increment four indents were produced in each specimen using a 50 kg load. The lengths of the Palmqvist cracks produced at the corners of each indent were then

measured using a Reichart MeF3A microscope. No measurements were carried out on the as-ground material, due to the difficulty of distinguishing the cracks from the grinding lines. The amount of material removed during polishing was estimated by measuring the decrease in length of the diagonals of the previous Vickers indentations. This is related to the thickness of the layer removed through the equation:

$$A = \frac{D_1 - D_2}{2} \cdot \cot \frac{\alpha}{2} = 0.143(D_1 - D_2)$$

where A = thickness of the layer removed
 D_1 and D_2 = diagonals of Vickers indentation before and after polishing
 α = angle between the faces on the top of the Vickers pyramid (136°)

This procedure was repeated until a maximum crack length was achieved. Further polishing using finer grit was not considered necessary since it has been shown not to produce any further decrease in residual stress [38].

The results obtained are illustrated in Figures 6.7 and 6.8, which show the change in crack length occurring during successive polishing operations. Figure 6.9 gives an indication of the change in surface fracture toughness which is brought about by polishing.

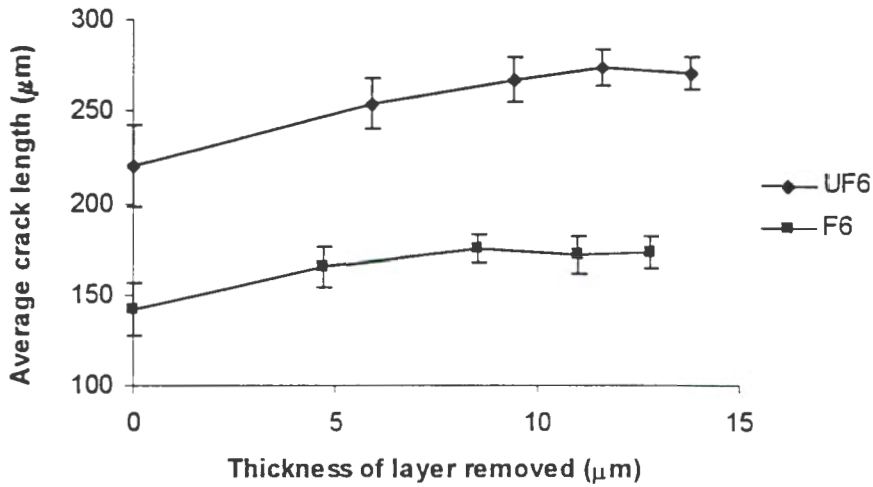


Figure 6.7: Average Palmqvist crack length as a function of total thickness of surface layer removed, for fine and ultrafine grades. Each data point represents one minute of polishing. The first measurement was taken after one minute of polishing. The error bars represent one standard deviation.

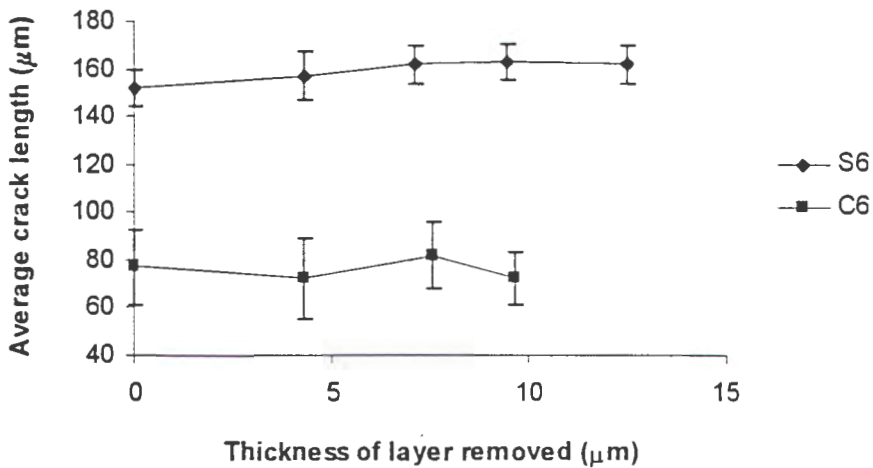


Figure 6.8: Average Palmqvist crack length as a function of total thickness of surface layer removed, for standard and coarse grades. Each data point represents 30 seconds of polishing. The first measurement was taken after 30 seconds of polishing.

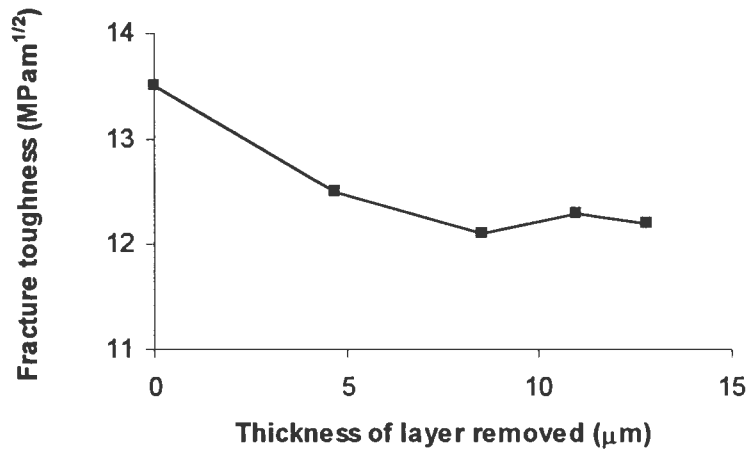


Figure 6.9: Palmqvist fracture toughness of the F6 grade (calculated using the equation developed by Shetty [154]) plotted as a function of the total thickness of material removed. The first measurement was taken after 1 minute of polishing.

The results obtained confirm that residual tensile stresses are present in the surface of WC-Co after grinding operations: as Figure 6.9 shows, these may increase the surface fracture toughness of the material by over $1.5 \text{ MPam}^{1/2}$.

From Figure 6.7 it can be seen that maximum crack length in UF6 and F6 grades is achieved after 4 and 3 minutes' polishing respectively. Figure 6.8 shows the Palmqvist crack length in S6 grades to reach a maximum after 1.5 minutes. The Palmqvist crack lengths for grade C6 did not show any net increase during the monitoring period and it must be assumed that residual stresses due to grinding are removed in the first 30 seconds of polishing.

From these results it was considered that in all cases 5 minutes' polishing using $9\mu\text{m}$ diamond suspension would be sufficient to eliminate the residual stresses introduced by grinding.

6.4 X-ray diffraction

X-ray diffraction spectra were taken from four coarse grade specimens in order to monitor the extent of the f.c.c. \rightarrow h.c.p. phase transformation occurring during cavitation erosion. The extent of phase transformation has previously been shown to reach a plateau at the end of the incubation period [142]. Spectra were obtained from the specimens before and after the erosion test. The uneroded specimen was polished to a surface finish of $0.25\mu\text{m}$.

X-ray diffraction was carried out using a Phillips diffractometer fitted with a monochromator and the following parameters were adopted:

- Radiation Cu $K\alpha$
- Start Angle (2θ) 40°
- End angle (2θ) 56°
- Step interval 0.05°
- Count time 10s
- Current 25mA
- Voltage 40kV

The ratio of the h.c.p. to f.c.c. phase in the cobalt binder was estimated from the maximum intensities of the h.c.p. (101) and the f.c.c. (111) peaks. More detailed calculations of the integrated intensities of the peaks are prevented by the large degree of overlap between the h.c.p.(101) and the WC (111) peaks.

Chapter 7

RESULTS

7.1 Slurry erosion

The results obtained from slurry erosion testing, carried out as detailed in Section 6.1, are presented in Table 7.1. Also included, in the fourth column of the table, is the erosion resistance of each grade. This is defined as the reciprocal of the steady state erosion rate and is a measure of the relative lifetime of the grade in this erosive environment.

Grade	Steady state erosion rate (mm ³ /hour)	Incubation time (hours)	Erosion resistance (hour/mm ³)
UF6	0.125	0.66	8.00
UF8	0.127	0.39	7.87
UF10	0.167	0.28	5.99
UF15	0.436	0.45	2.29
F6	0.395	0.84	2.53
F8	0.302	1.10	3.31
F10	0.222	1.23	4.50
F15	2.17	0	0.461
S6	0.840	0.47	1.19
S8	0.919	0.31	1.09
S10	1.14	0.26	0.877
S15	1.57	0.23	0.637
C6	1.65	0.16	0.606
C8	1.59	0.14	0.629
C10	1.96	0.08	0.510
C15	2.42	0.07	0.413

Table 7.1: Summary of the steady state erosion rate, incubation period, and erosion resistance for all grades tested

7.1.1 Influence of microstructural parameters on slurry erosion rates

The dependence of the steady state erosion rate of the materials on their WC grain size is illustrated in Figure 7.1.

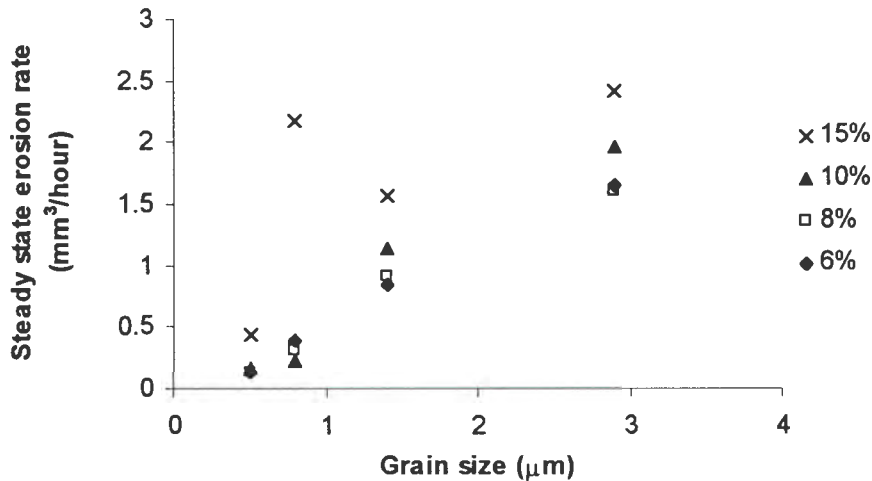


Figure 7.1: Steady state erosion rates of all the materials tested, plotted as a function of grain size. The legend gives the binder content of the material in wt%.

This figure clearly shows that the steady state erosion rate of grade F15 is highly anomalous, being between five and ten times greater than that of the remaining fine-grained materials, and almost as high as that of the least resistant coarse grain material.

Scanning electron micrographs of the eroded surface of grade F15, shown in Figure 7.2, indicate that the poor performance of this material is due to the presence of cobalt pools. These are subject to almost immediate erosive attack, followed by the rapid loss of large sections of the material. Since the poor erosion resistance of this material is entirely due to a defective production process, data from this grade has been excluded from all subsequent analyses.

The data for the remaining grades exhibits a general trend of increasing erosion rate with increasing grain size.

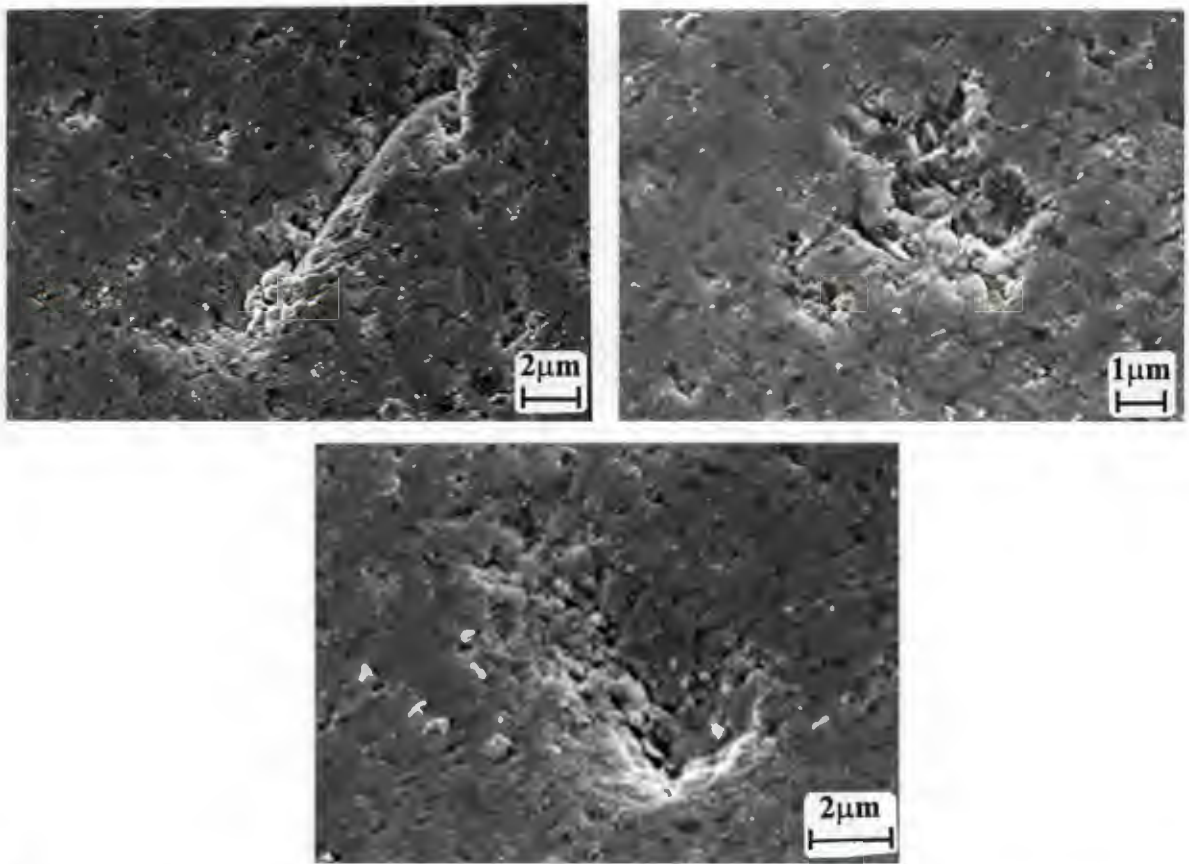


Figure 7.2: Scanning electron micrographs of single impact sites in grade F15, showing preferential ductile erosion of the cobalt phase, followed by the loss of large sections of material

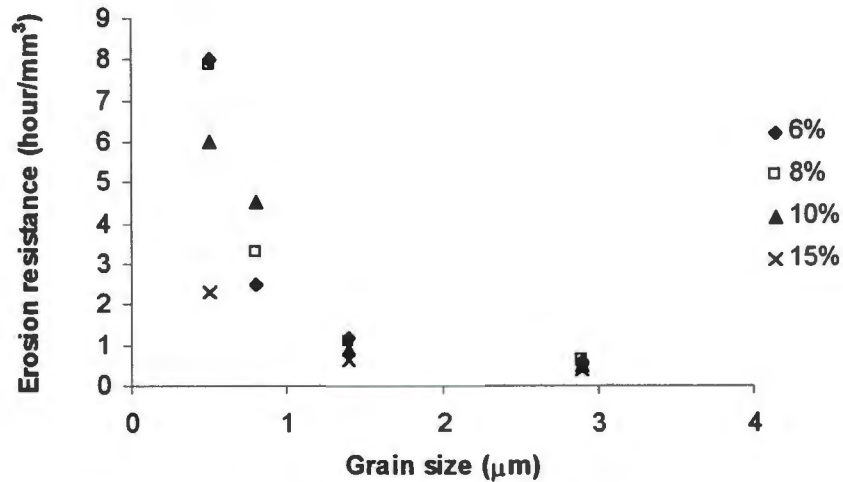


Figure 7.3: Erosion resistance plotted as a function of grain size for all materials tested, except F15. The legend indicates the binder content in wt%

In Figure 7.3 the erosion data is plotted in terms of the erosion resistance. The resulting graph highlights the dramatic increases in resistance which may be achieved by decreasing the grain size below about $1\mu\text{m}$. For example, the best-performing ultrafine material has an erosion resistance which is six times that of the most resistant standard grade.

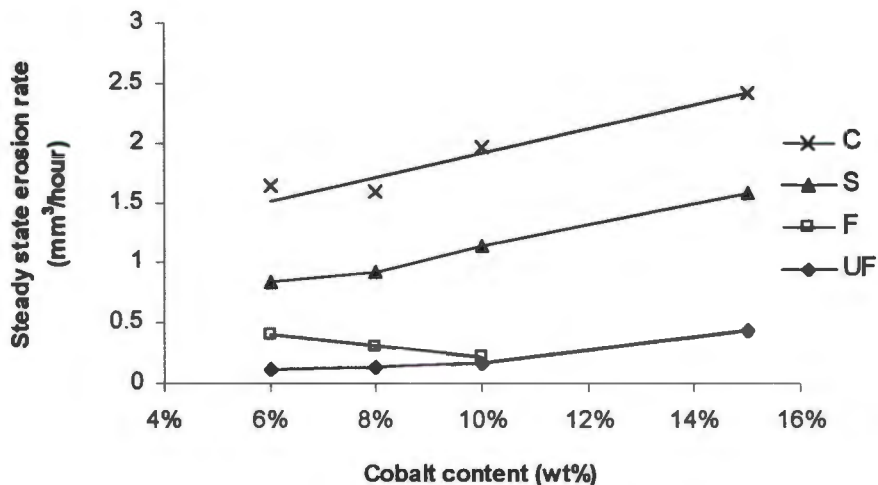


Figure 7.4: Steady state erosion rates plotted as a function of cobalt content.

The dependence of the erosion rate of the materials on their cobalt content is illustrated in Figure 7.4. This figure shows that in general the erosion rate for each grade increases with increasing cobalt content. The exception to this is the fine grade, in which the erosion rate is

seen to decrease with increasing cobalt content. This is likely to be due to the fact that grades F8 and F10 have a slightly finer microstructure than F6 (as detailed in Table 5.6) and contain additions of Cr_2C_3 , which, as discussed in Section 2.3.2.3, tend to strengthen the binder phase.

The erosion resistance of the materials tested is plotted against the binder mean free path in Figure 7.5. This shows that at the transition from standard grades to sub-micron grades, the sensitivity of the erosion resistance to the binder mean free path begins to increase dramatically.

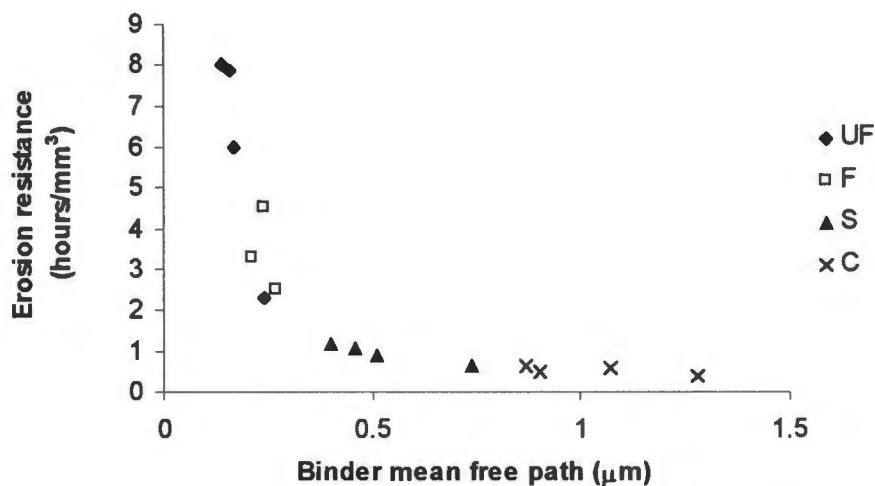


Figure 7.5: Erosion resistance plotted as a function of the binder mean free path.

7.1.2 The influence of mechanical properties on erosion resistance

The relationships between erosion resistance and the hardness and fracture toughness of the material are shown in Figures 7.6 and 7.7 respectively.

Figure 7.6 shows that, as expected, the erosion resistance increases with increasing hardness. However, a transition in this relationship is observed as the hardness of the composite increases above 1600 kg mm^{-2} . This corresponds to the transition from standard grades to fine and ultrafine grades. Above this point, the erosion resistance of the material becomes highly sensitive to the hardness, and as a result, ultrafine materials may display erosion resistances

which are over six times greater than that of the most resistant Standard material, despite a hardness increase which is of at most 35%.

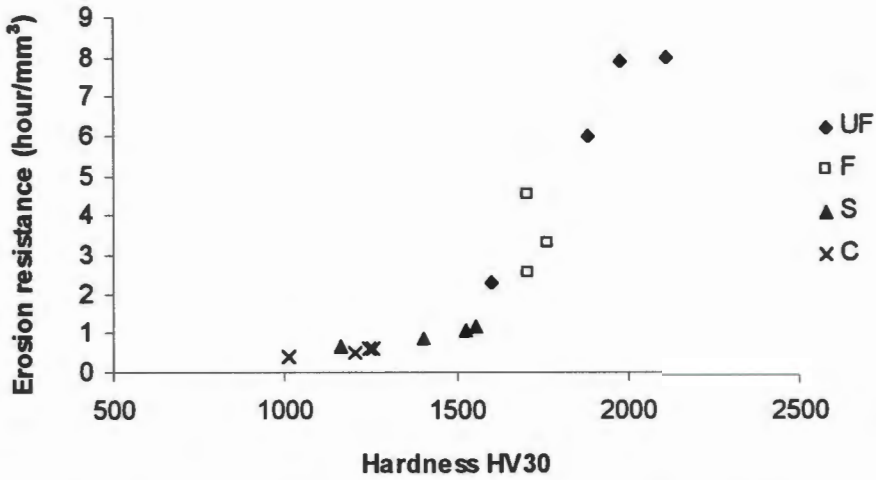


Figure 7.6: Variation of erosion resistance with hardness

Figure 7.7 shows that for standard and coarse grades, increases in erosion resistance are coupled with significant fracture toughness losses. Ultrafine materials, however, display approximately constant fracture toughness of the same magnitude as standard grades, and therefore the combinations of erosion resistance and fracture toughness observed in these grades are significantly higher than those observed in coarser grades.

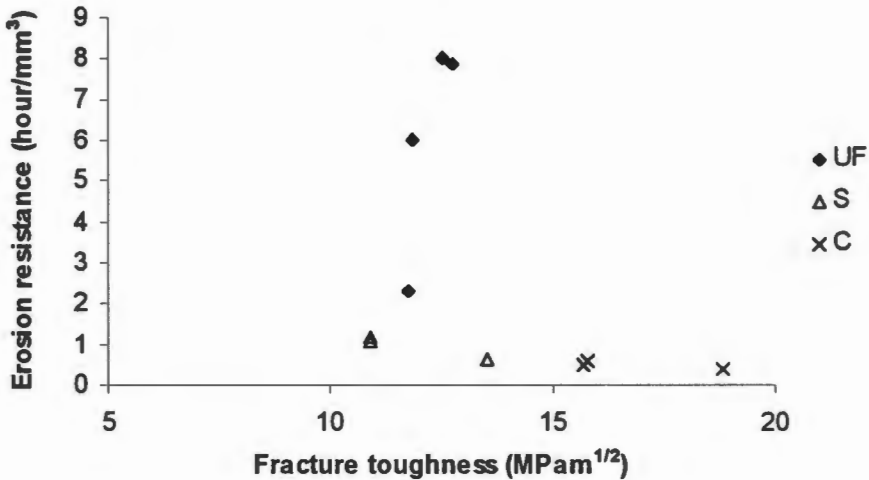


Figure 7.7: Variation of erosion resistance with fracture toughness

7.1.3 Angular dependence of erosion rates

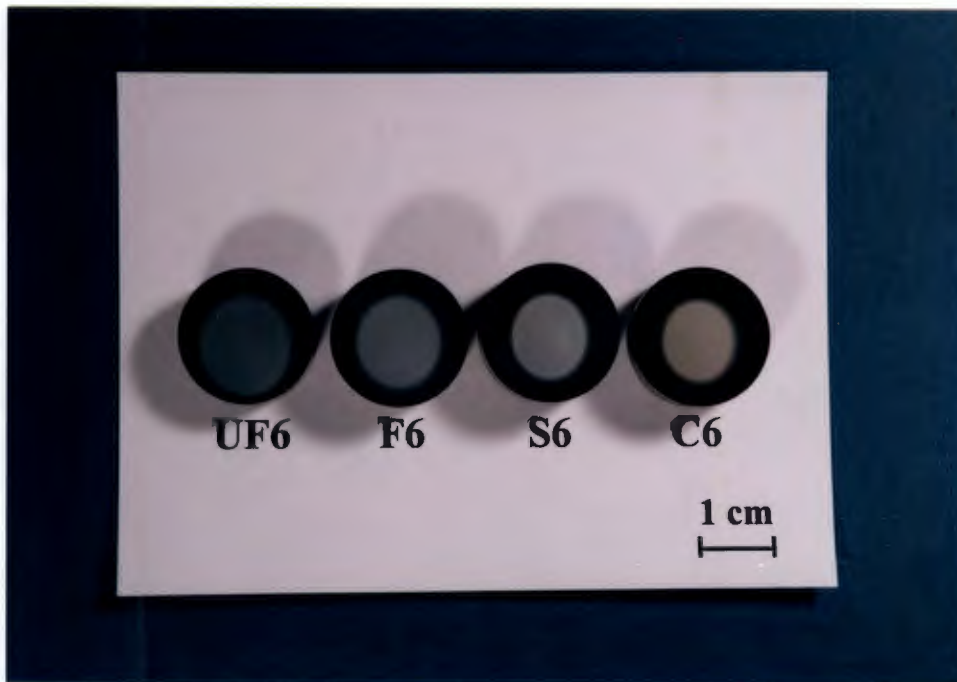


Figure 7.8: Erosion scars of equal volume formed on a series of grades containing 6wt% binder. Note different scar diameters

As Figure 7.8 shows, a macroscopically visible difference exists between the diameters of the erosion scars produced in the four materials tested. The diameter of the erosion scars increases with decreasing grain size of the material, despite their identical volume.

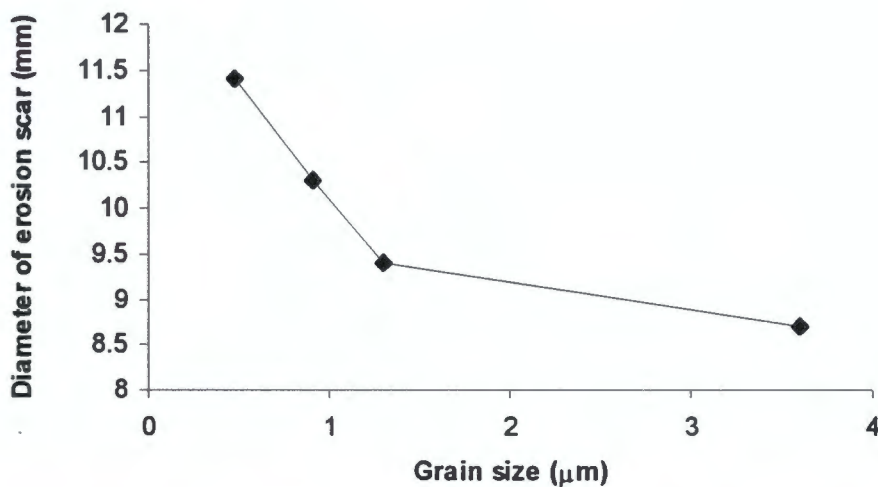


Figure 7.9: Diameter of erosion scars of identical volume, plotted as a function of grain size

When the measured diameters of these scars are plotted against grain size, as shown in Figure 7.9, it can be seen that this increase is particularly sharp for materials with grain sizes below about $1\mu\text{m}$.

These results imply that as the grain size of the materials decreases, an increasing proportion of their erosive wear occurs at low angles of impact, so that wider and shallower erosion scars are formed. In particular, sub-micron materials exhibit significantly more material loss at low angles of impact than do standard and coarse materials.

7.1.4 Microscopic examination of eroded areas

Microscopic examination of the eroded surfaces of the materials tested shows two distinct erosion mechanisms to be in operation. The transition between these mechanisms occurs at a grain size of approximately $1\mu\text{m}$.

Scanning electron micrographs of single impact sites in fine and ultrafine materials, shown in Figure 7.10, reveal that during erodent impact, material is smeared across the target surface in a manner similar to that observed in adhesive wear. Very little penetration of the surface by the erodent is observed. The dimensions of the single impact sites, which are of the order of $2\mu\text{m}$, are considerably larger than those of the microstructure, so that the area encompassed by the impact zone may contain up to about 20 WC grains. Micrographs taken after multiple erodent impacts show bulk material loss to occur [Figure 7.11(a)]. The eroded areas display relief on a scale greater than that of the microstructure, and contain individual WC grains which appear well-defined and unaffected by the erodent impact [Figure 7.11(b)].

By contrast, response to erodent impact in coarse grained materials occurs on a scale smaller than that of the microstructure. This gives rise to a number of distinct features, many of which are shown in Figure 7.12. In this micrograph we may observe cracking, deformation and displacement of WC grains, as well as the extrusion and preferential removal of the cobalt binder which is followed by the loss of single unsupported WC grains. In the eroded areas, the material loss and the surface relief are on the scale of the microstructure [Figure 7.13] and the

steady state erosion area consists mainly of heavily deformed, chipped and crushed WC grains, but also exhibits evidence of the recent loss of whole WC grains [Figure 7.14].

The response of standard grades to erosion is illustrated in Figure 7.15. This shows the erosion process to be a mixture of the two modes outlined above. Erodent impact sites encompass a small number of grains, and although some chipping and cracking of WC grains does occur, grains in steady state erosion areas are generally much better defined than is the case for coarse grained material.

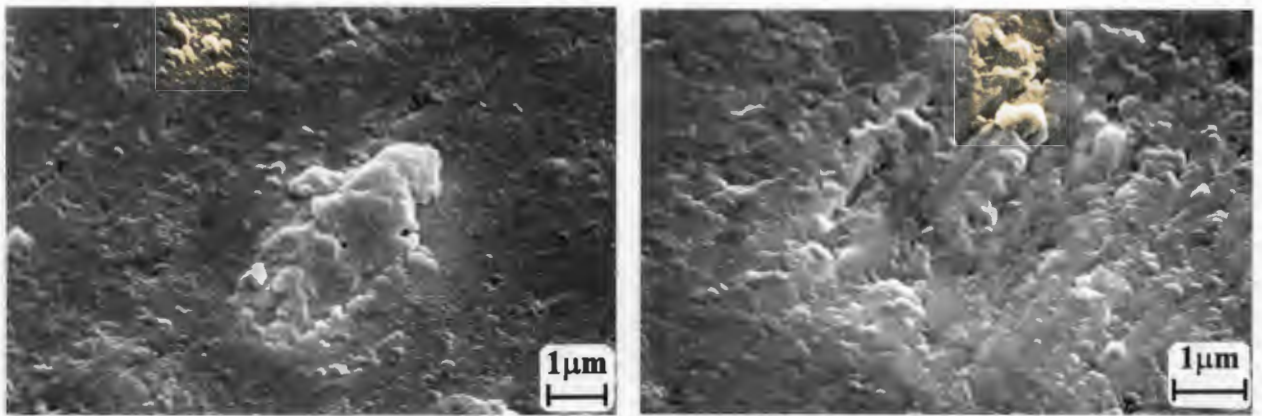


Figure 7.10: Scanning electron micrographs of single impact sites in grade UF15

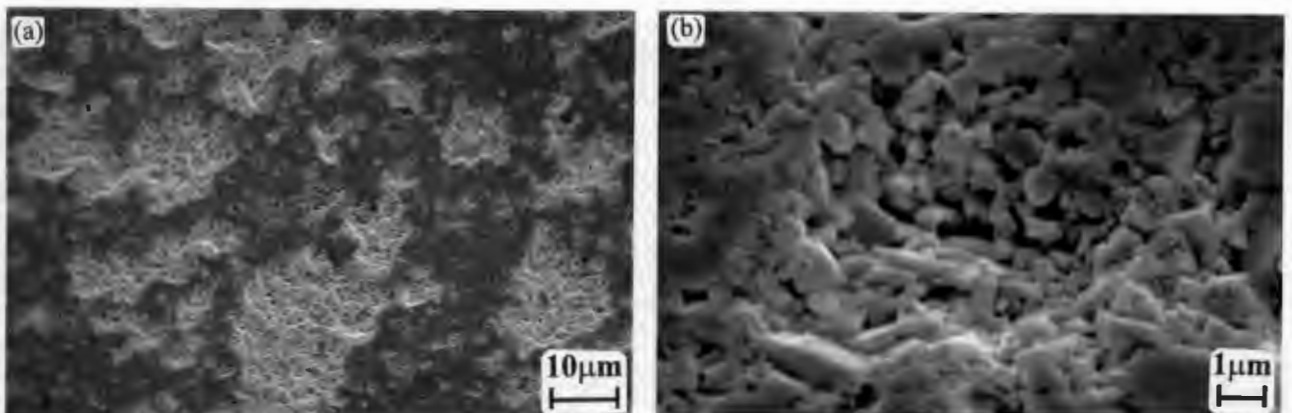


Figure 7.11: Scanning electron micrographs of fine-grained alloy F6 subjected to multiparticle impact

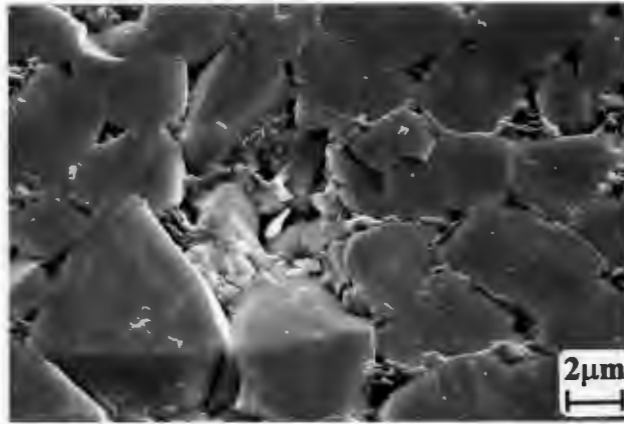


Figure 7.12: Scanning electron micrograph of the coarse WC-Co alloy C6, showing a variety of material responses to erodent impact: deformation of WC grains, cracking and crushing of WC grains, extrusion and deformation of binder phase, displacement of WC grains, and loss of single grains

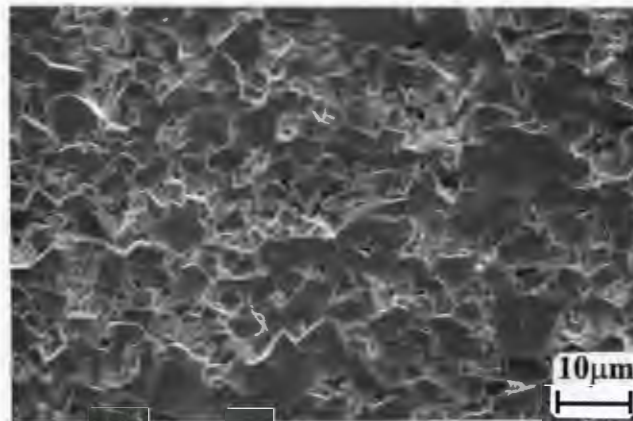


Figure 7.13: Scanning electron micrograph of coarse-grained alloy C6 subjected to multiparticle impacts. Note material removal occurs on the scale of the microstructure

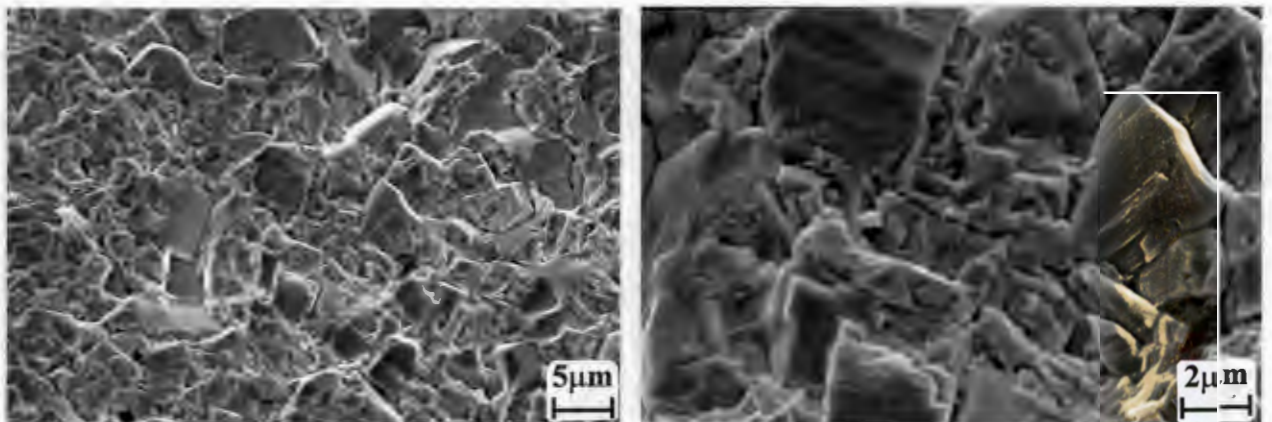


Figure 7.14: Scanning electron micrographs of eroded areas in coarse grained alloy C6. Note highly deformed, chipped and crushed WC grains, and sites where the loss of WC grains has occurred

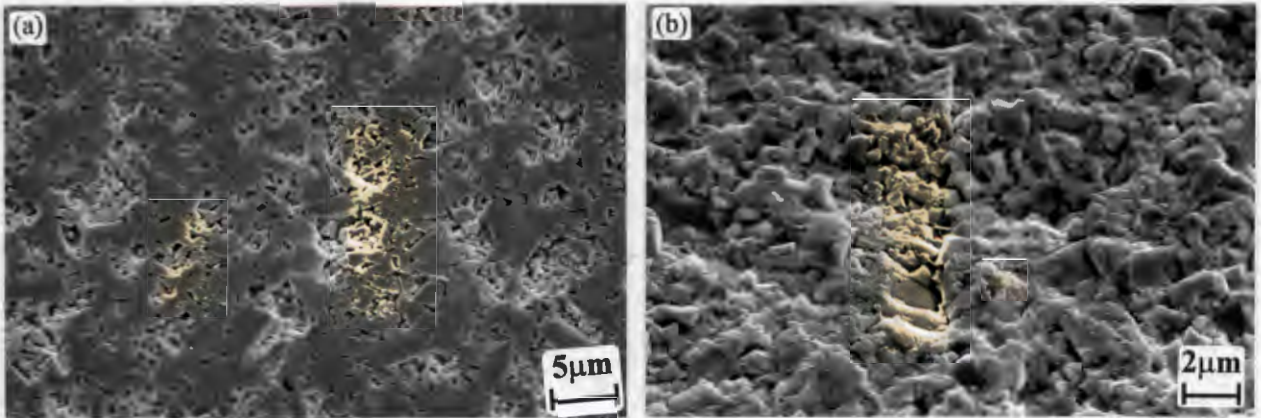


Figure 7.15: Scanning electron micrographs of eroded areas in standard grade S6: (a) initiation period; (b) steady state erosion regime

7.1.5 Influence of defects on material performance

The effect of cobalt pooling on slurry erosion performance is discussed in Section 7.1.1.

The influence of discontinuous grains and non-uniform grain size on the slurry erosion performance is illustrated by the micrographs shown in Figure 7.16. From these it may be seen that large grains in non-uniform microstructures tend to be retained in the eroded surface and hence may exert a protective effect on the material beneath them. They also exhibit a greater tendency to crack formation.

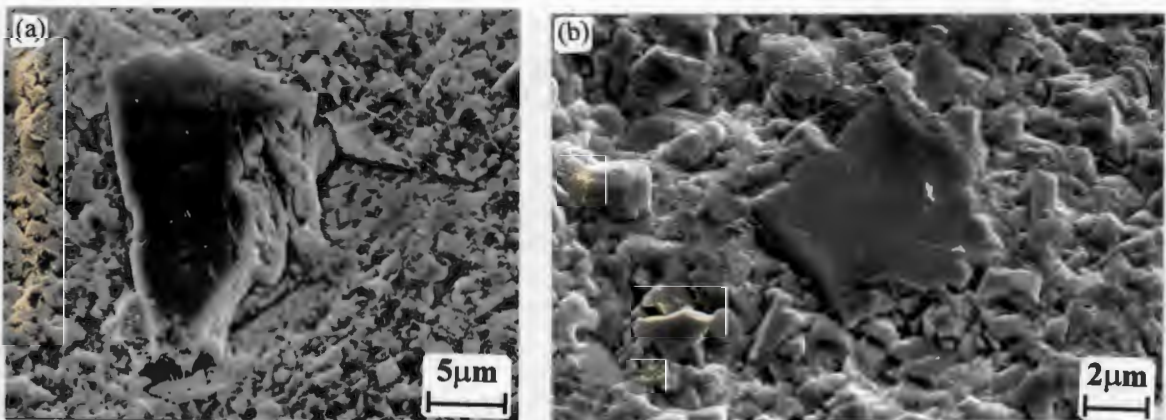


Figure 7.16: Scanning electron micrograph of eroded areas of grades with non-uniform grain size: (a) grade F6; (b) grade S6. Note that large grains tend to be retained in the eroded surface

7.1.6 Summary

1. The slurry erosion response of 16 WC-Co alloys of varying grain size and cobalt content has been evaluated. A general trend has been observed of increasing erosion resistance with decreasing grain size and decreasing cobalt content.
2. A transition in the slurry erosion behaviour of the materials has been observed at a grain size of approximately $1\mu\text{m}$: as the grain size of the material decreases below this value, a significant increase in the sensitivity of the erosion resistance to the binder mean free path and the hardness is observed. As a result, the erosion resistance of ultrafine grades may be up to six times that of the best-performing standard grade.
3. The high erosion resistance of ultrafine grades is achieved without any sacrifice in fracture toughness (relative to coarser grades) and thus high combinations of these two properties are realised.
4. Sub-micron materials are much more susceptible to erosion at low angles of attack than are standard and coarse materials, and thus exhibit wider, shallower erosion scars.
5. The erosion of sub-micron materials occurs through a bulk process, while that of coarser materials occurs on a scale similar to that of the microstructure.
6. The presence of cobalt pools has a highly deleterious effect on the slurry erosion resistance of WC-Co, while discontinuous grains may help protect underlying material from erosive attack.

7.2 Cavitation erosion

The results obtained from cavitation erosion testing, carried out as detailed in Section 6.2, are presented in Table 7.2.

Grade	Steady state erosion rate (mm ³ /hour)	Incubation time (hours)	Erosion resistance (hour/mm ³)
UF6	0.0145	12.7	69.0
UF8	0.0320	5.2	31.3
UF10	0.0396	5.4	25.3
UF15	0.0793	1.7	12.6
F6	0.0578	3.6	17.3
F8	0.0771	2.2	13.0
F10	0.0752	1.9	13.3
F15	0.112	-	8.93
S6	0.152	1.4	6.58
S8	0.112	1.9	8.93
S10	0.135	1.5	7.41
S15	0.103	1.9	9.71
C6	0.247	1.6	4.05
C8	0.178	2.1	5.62
C10	0.141	2.5	7.09
C15	0.131	2.4	7.63

Table 7.2: Summary of the steady state erosion rate, incubation period and erosion resistance for all the grades tested

As is the case with the slurry erosion data, the values of erosion resistance tabulated above correspond to the reciprocal of the steady state erosion rate and are an indication of the relative lifetimes of these materials under cavitation erosion conditions.

The steady state erosion rates of all the materials tested are plotted in Figure 7.17 as a function of grain size. From this it may be seen that the erosion rate decreases with decreasing grain size. It must be noted that grade F15 (which, like the specimen subjected to slurry erosion, contains cobalt pools) does not in this case appear to exhibit the highly anomalous steady state erosion rate recorded during slurry erosion (see Figure 7.1). The data for this grade was

therefore included in the analysis. Anomalous behaviour was, however, observed during the incubation period: this is discussed in Section 7.2.4.

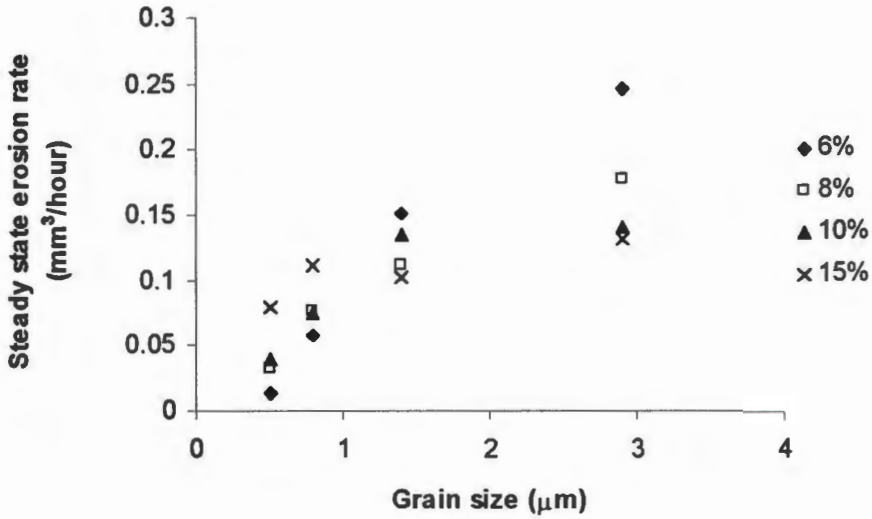


Figure 7.17: Plot of steady state erosion rate against grain size for all the materials tested. The legend gives the binder content in wt%.

The plot of erosion resistance against grain size, given in Figure 7.18, highlights the dramatic increases in erosion resistance which may be achieved by reducing the grain size of the material below about 1 µm. In fact, the erosion resistance of the best-performing ultrafine material is over seven times that of the most resistant standard material.

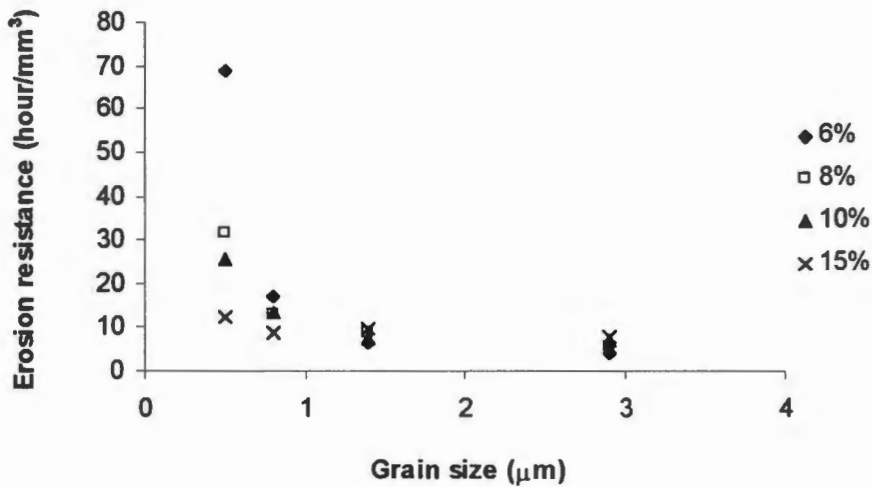


Figure 7.18: Plot of erosion resistance against grain size for all the grades tested. The legend gives the binder content in wt%.

The dependence of erosion rates on cobalt content is illustrated in Figure 7.19, which shows that the erosion behaviour of the materials tested may be divided into two regimes: for sub-micron grades, erosion rates increase with increasing cobalt content, while for standard and coarse grades, erosion rates decrease with increasing cobalt content. The erosion response of the materials in these two regimes will be considered separately in the following two sections.

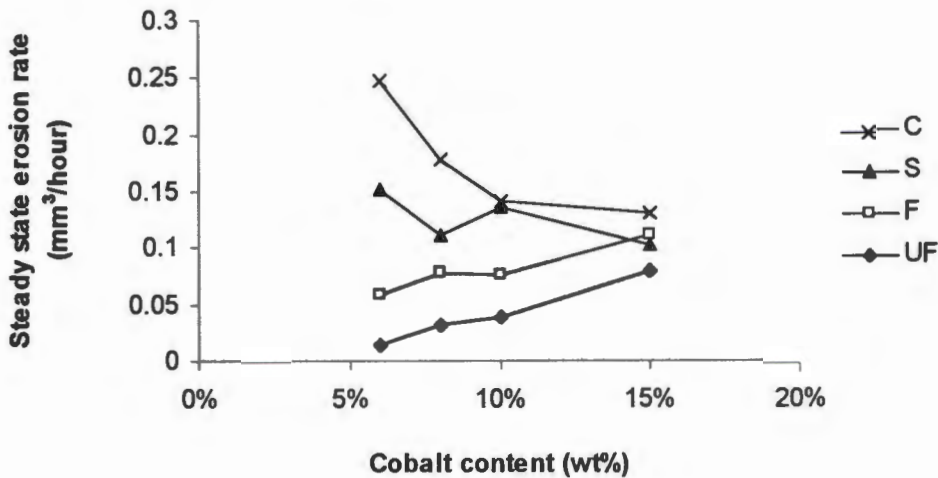


Figure 7.19: Plot of steady state erosion rate against cobalt content for all the grades tested

7.2.1 Cavitation erosion response of fine and ultrafine materials

The dependence of the erosion resistance of fine and ultrafine materials on hardness and binder mean free path is illustrated in Figures 7.20 and 7.21. These show that the erosion resistance of ultrafine grades is strongly dependent on both the hardness and the binder mean free path, and increases with increasing hardness and decreasing binder mean free path.

The dependence of fine grades on these parameters is less marked, but the data obtained is consistent with the trends observed in ultrafine grades.

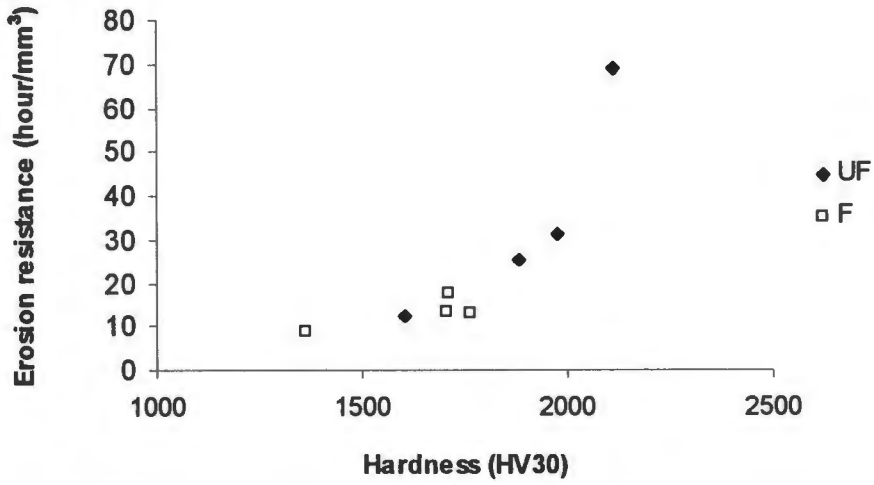


Figure 7.20: Plot of erosion resistance against hardness for fine and ultrafine grades

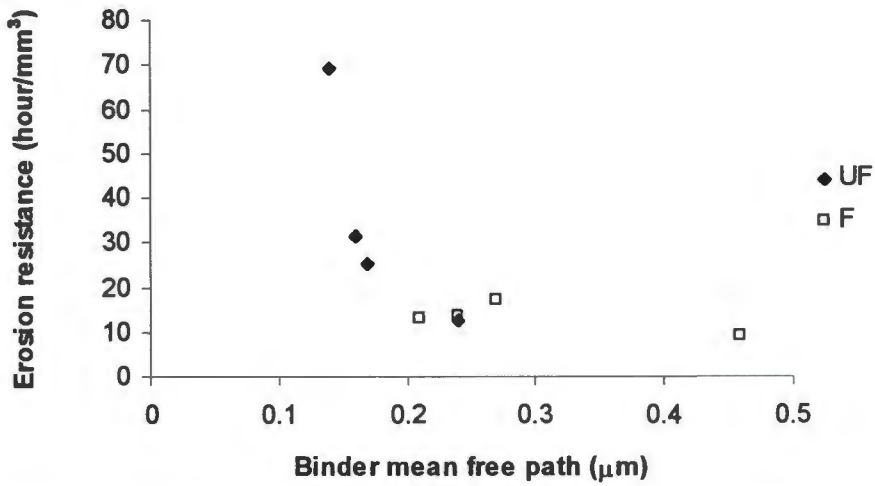


Figure 7.21: Plot of erosion resistance against binder mean free path for fine and ultrafine grades

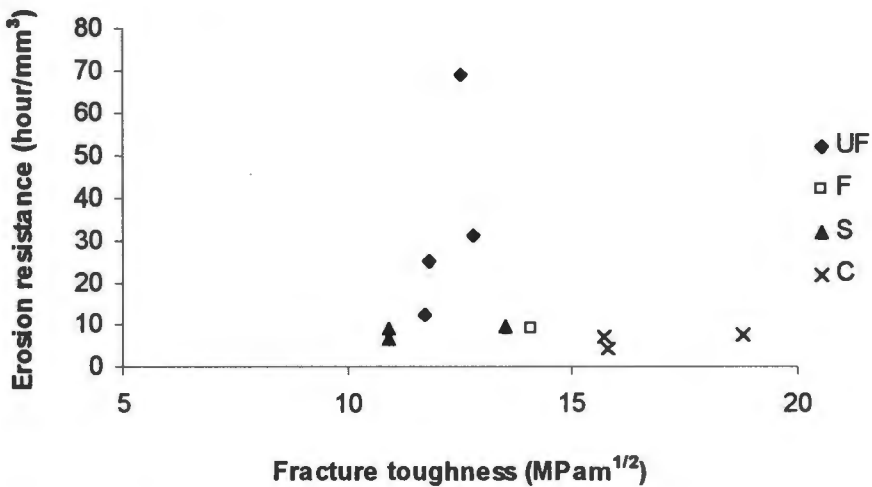


Figure 7.22: Plot of erosion resistance against fracture toughness for all the grades tested

Figure 7.22 gives the erosion resistance of all the grades tested as a function of fracture toughness. This shows that, as is the case for slurry erosion, ultrafine grades may exhibit very high combinations of erosion resistance and fracture toughness relative to standard and coarse grades.

7.2.1.1 Microscopic examination of the eroded areas in fine and ultrafine grades

Scanning electron micrographs of ultrafine grades taken from the edges of the eroded area [Figure 7.23(a)] and during the incubation period [Figure 7.23(b)] reveal that initial erosive attack of these materials results in the formation of deep craters. These craters are dispersed evenly across the specimen surface and do not appear to be associated with material defects [Figure 7.24]. Erosion progresses through the lateral expansion and eventual coalescence of these craters [Figure 7.25(a)], resulting in a steady state eroded area with a high level of relief, and which contains small islands of uneroded material [Figure 7.25(b)]. Scanning electron micrographs taken from the eroded areas of grade F6 [Figure 7.26] reveal similar evidence of bulk material removal, although the craters formed do not appear to be as deep as for ultrafine materials.

Figure 7.27 shows that the WC grains in the eroded areas of ultrafine grades do not appear to be affected by the erosive attack, being clean, sharply defined and undeformed.

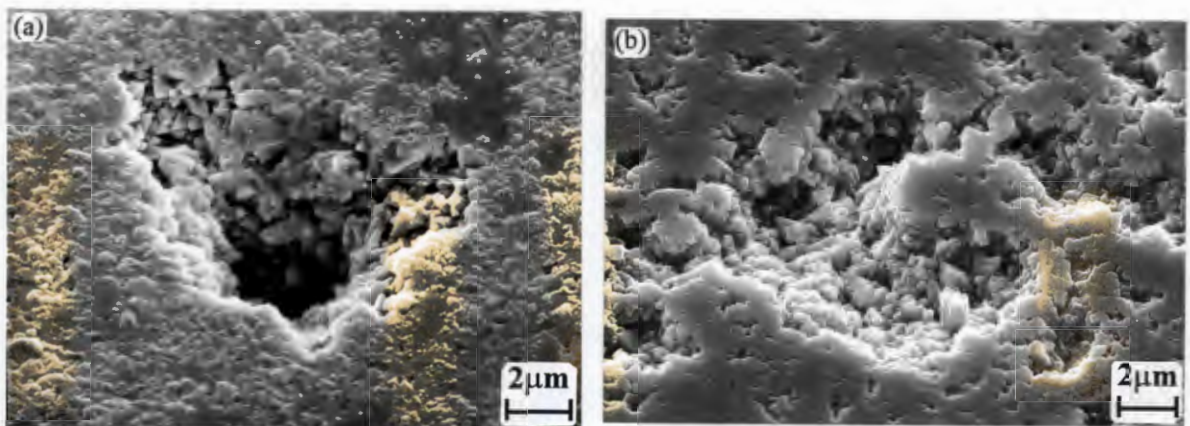


Figure 7.23: Scanning electron micrographs of craters formed in ultrafine grades during cavitation erosion: (a) UF15; (b) UF8



Figure 7.24: Scanning electron micrograph of grade UF15 showing the even distribution of discrete craters across the specimen surface

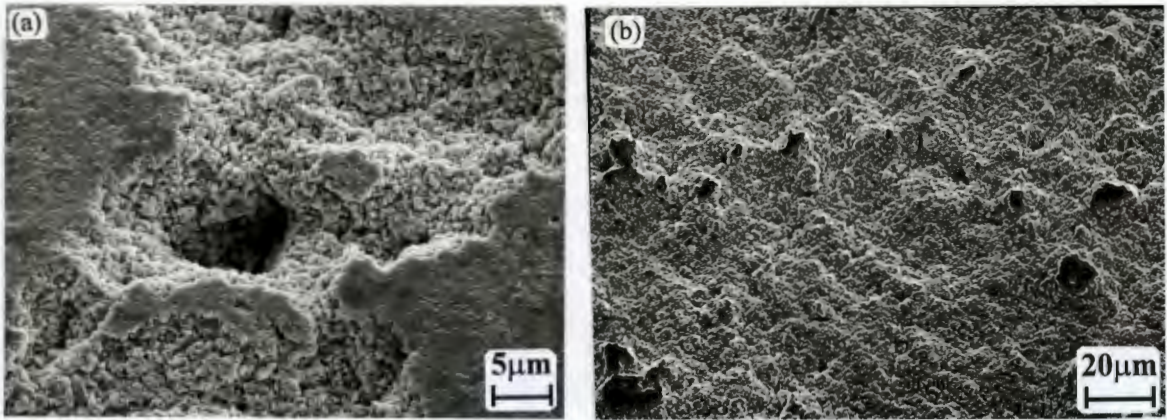


Figure 7.25: Scanning electron micrograph of the eroded surface of grade UF15: (a) erosion craters merging; (b) steady state eroded surface, showing relief on a scale greater than the microstructure and small islands of uneroded material

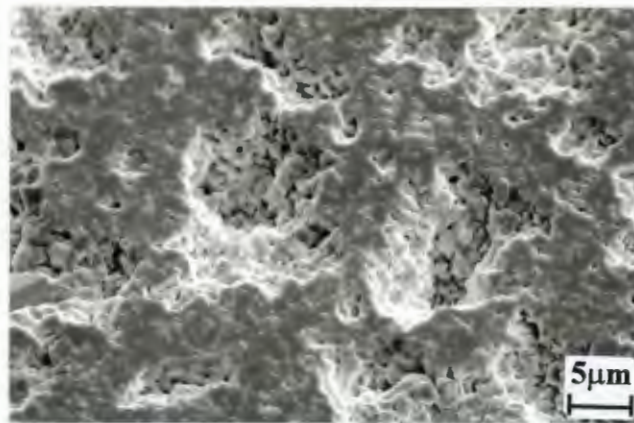


Figure 7.26: Scanning electron micrographs of the eroded surface of grade F6 showing bulk material loss

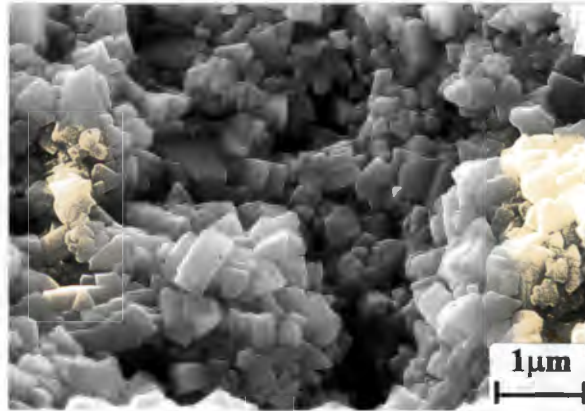


Figure 7.27: Scanning electron micrograph of eroded area in grade UF8 showing clean, sharply defined and undeformed WC grains

7.2.2 Cavitation erosion response of standard and coarse materials

The dependence of the erosion resistance of standard and coarse materials on their hardness, binder mean free path and fracture toughness is illustrated in Figures 7.28, 7.29, and 7.30 respectively. These show that, when considered individually, both the standard and coarse grades exhibit decreasing erosion resistance with increasing hardness, decreasing binder mean free path and decreasing fracture toughness. However, it must be noted that the trends observed in relation to the binder mean free path and the fracture toughness are not very strong, and that none of the three parameters accounts entirely for the erosion behaviour observed across the two sets of materials.

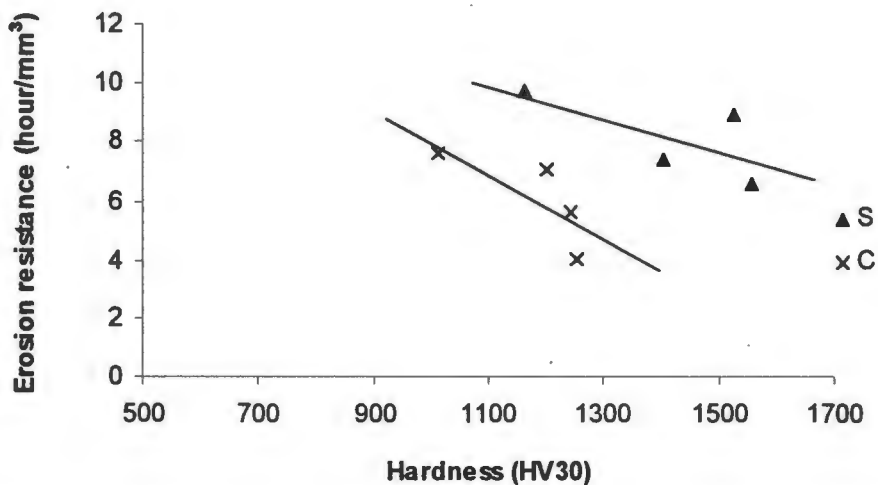


Figure 7.28: Plot of erosion resistance against hardness for standard and coarse grades

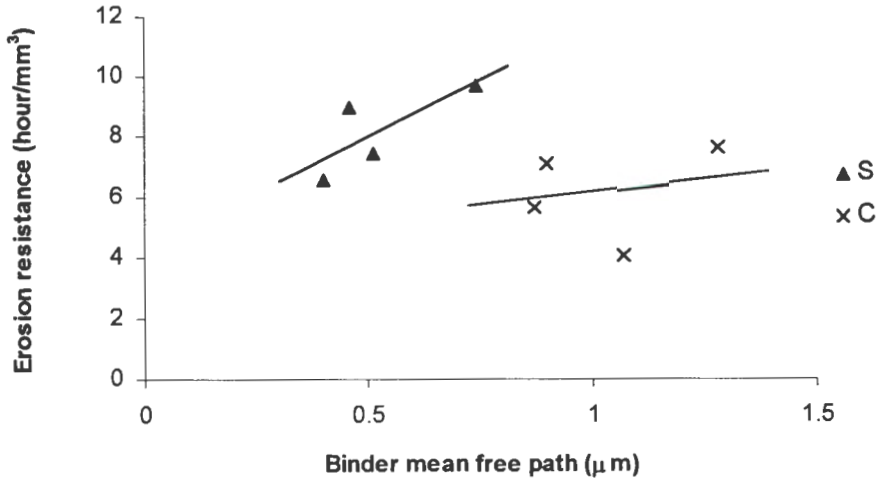


Figure 7.29: Plot of erosion resistance against binder mean free path for standard and coarse grades

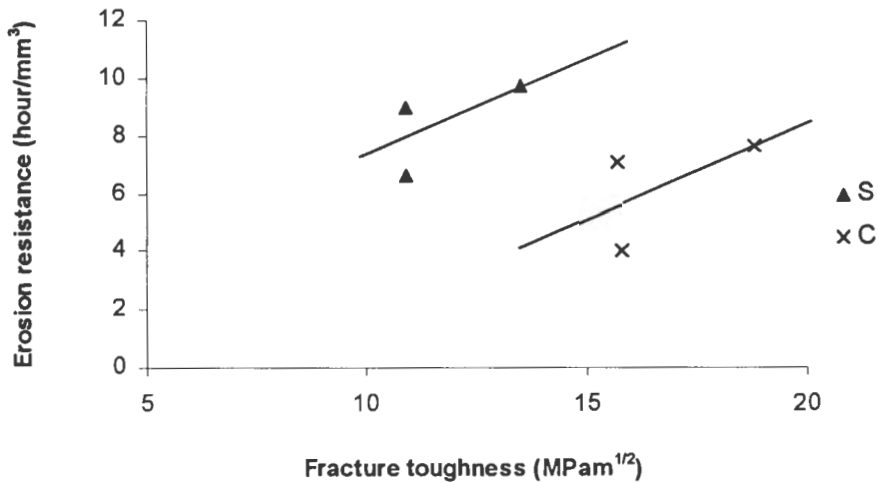


Figure 7.30: Plot of erosion resistance against fracture toughness for standard and coarse grades.

7.2.2.1 Microscopic examination of eroded areas in standard and coarse grades

Scanning electron micrographs taken from the edge of the eroded area in coarse-grained material [Figure 7.31] indicate that erosion proceeds through the preferential removal of the cobalt phase, followed by the loss of single unsupported WC grains. The eroded areas formed are shallow and contain relief which is on the scale of the microstructure. No evidence is observed of bulk material removal.

The eroded areas of the coarse grades subjected to cavitation erosion are highly featureless compared to those of the specimens subjected to slurry erosion (see Section 7.1.4). There is

no evidence of extrusion of the cobalt phase or displacement of the WC grains. The WC grains themselves show no evidence of deformation or fracture [Figure 7.32]. Small amounts of retained cobalt appear to adhere to the grains [Figure 7.32(b)].

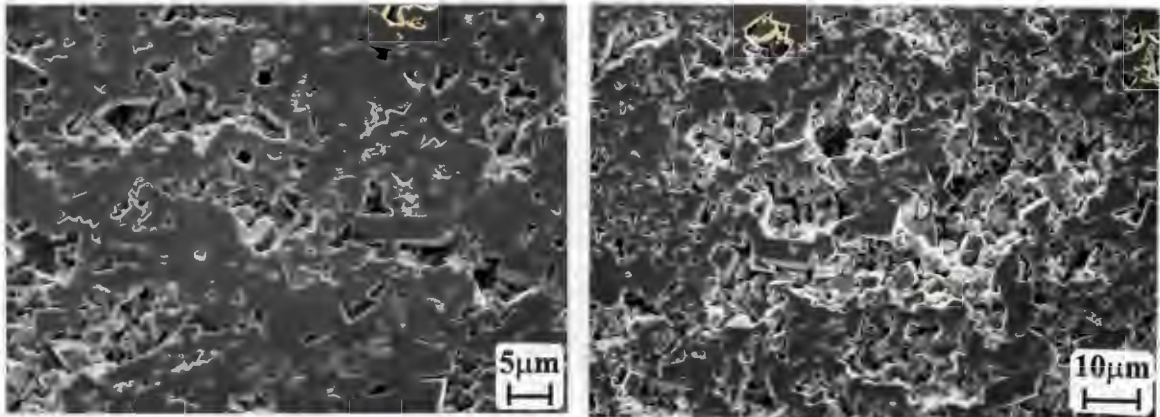


Figure 7.31: Scanning electron micrographs taken at the edge of the eroded area on grade C10. Note uniform erosive attack leading to the loss of single WC grains. Note also evidence of corrosion products at the WC/Co interface

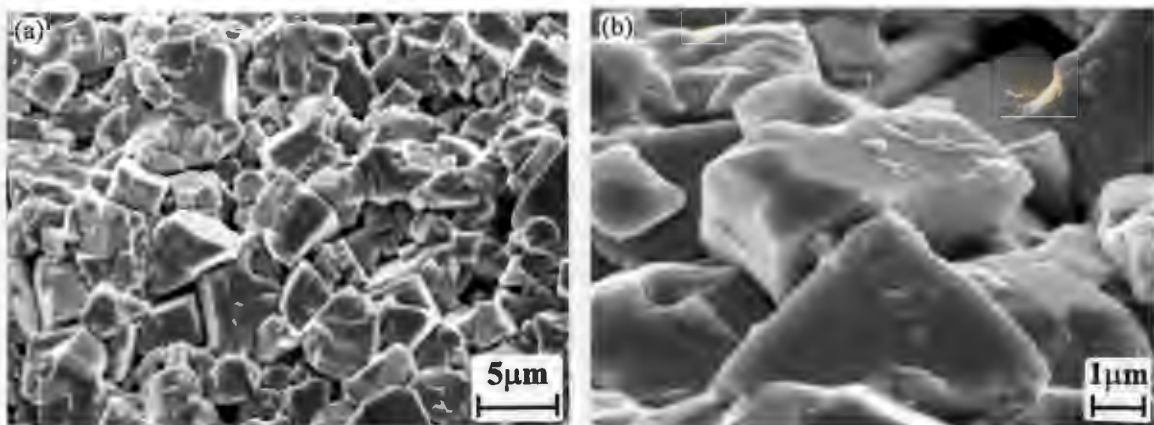


Figure 7.32: Scanning electron micrographs of eroded areas on grade C10. Note well-defined WC grains as well as what appear to be flakes of cobalt retained on the specimen surface

7.2.2.2 X-ray diffraction of uneroded and eroded areas in coarse grades

Typical X-ray diffraction spectra obtained from eroded and uneroded coarse grade specimens, as detailed in Section 6.4, are shown in Figures 7.33 to 7.35

Comparison of Figures 7.33 and 7.34 shows that a noticeable decrease in the relative proportion of f.c.c. cobalt present in the surface of the material occurs during the erosion process. This serves to confirm that the stresses induced by cavitation erosion result in a partial transformation of the binder phase.

As explained in Section 6.4, the relative proportions of the two cobalt phases present at the surface of each specimen were estimated from the ratio of the maximum intensities of the h.c.p. (101) and the f.c.c. (111) peaks. The results obtained from the eroded and uneroded surfaces of the four grades examined are presented in Table 7.3, along with the erosion resistance of each grade. The observed variation in the initial h.c.p./f.c.c. ratio indicates that the proportion of h.c.p. phase present in the uneroded surface decreases with increasing cobalt content of the material. The proportion of h.c.p. cobalt present in the eroded surface, however, does not appear to depend closely on the cobalt content. Consequently the extent of transformation of the binder phase during testing appears to increase with increasing cobalt content, as does the erosion resistance.

Specimen	C6	C8	C10	C15
Erosion resistance (hours/mm ³)	4.06	4.90	7.09	7.30
h.c.p./f.c.c. ratio of cobalt phase in uneroded surface	1.09	0.89	0.86	0.51
h.c.p./f.c.c. ratio of cobalt phase in eroded surface	1.04	1.16	1.38	1.32
Difference in h.c.p./f.c.c. ratios	-0.05	0.27	0.52	0.81

Table 7.3: *The erosion resistance and binder phase crystal structure of four coarse-grained specimens of varying cobalt contents*

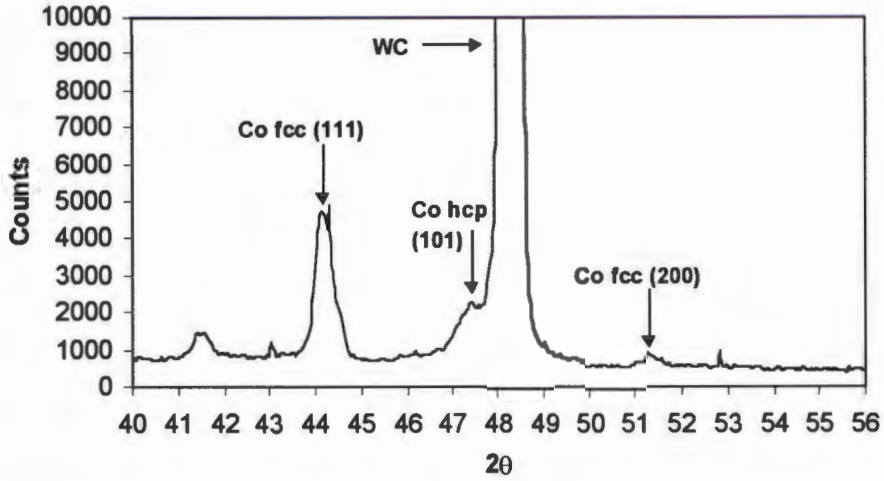


Figure 7.33: Typical X-ray diffraction spectrum from polished C15 sample

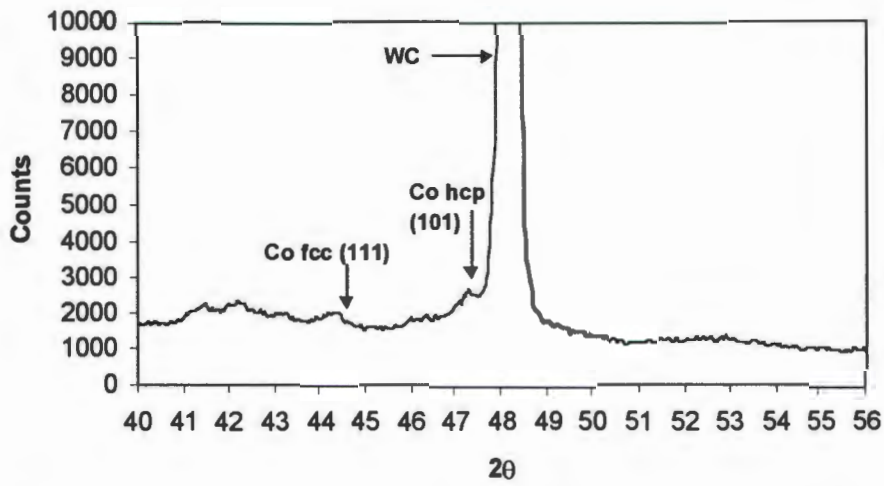


Figure 7.34: Typical X-ray diffraction spectrum from eroded C15 sample

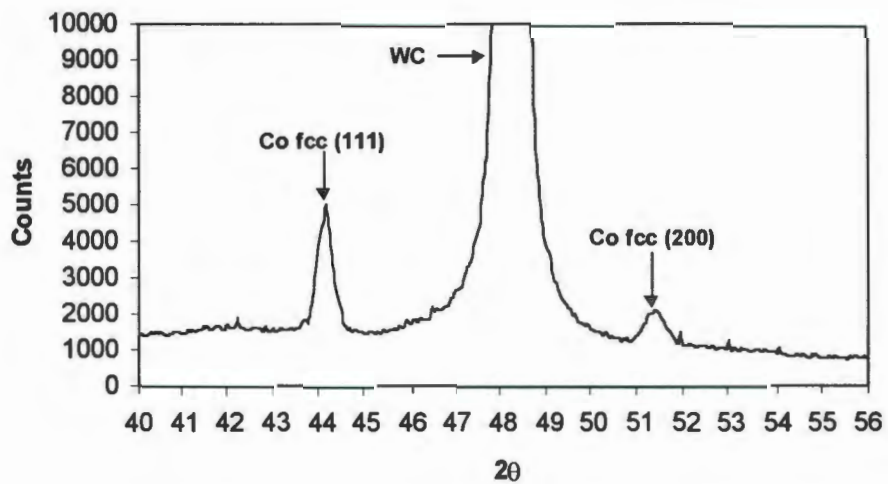


Figure 7.35: Typical X-ray diffraction sample from ground C15 sample

From comparison of the three spectra shown in Figures 7.33 to 7.35, it is interesting to note that the width of the main WC peak in the spectrum obtained from the ground surface is much greater than that of the corresponding peaks in the spectra obtained from the polished and eroded surfaces. This indicates that the level of deformation of the WC grains on the surface of polished and eroded specimens is much lower than that of the WC grains on the surface of the ground specimen.

7.2.3 Influence of defects on erosion performance

7.2.3.1 Cobalt pools

As mentioned previously, the presence of cobalt pools in grade F15 does not appear to impact negatively on the steady state erosion rate of the material. However, as Figure 7.36 shows, it does have a strong effect on the incubation behaviour of the material. By comparing its erosion rate to that of grade S15, it can be seen that although the steady state erosion rates of the materials are almost identical, grade S15 exhibits a pronounced incubation period, whereas grade F15 does not. The erosion rate for F15 is, in fact, approximately constant throughout the test period, with the exception of a small peak, which occurs after about four hours testing.

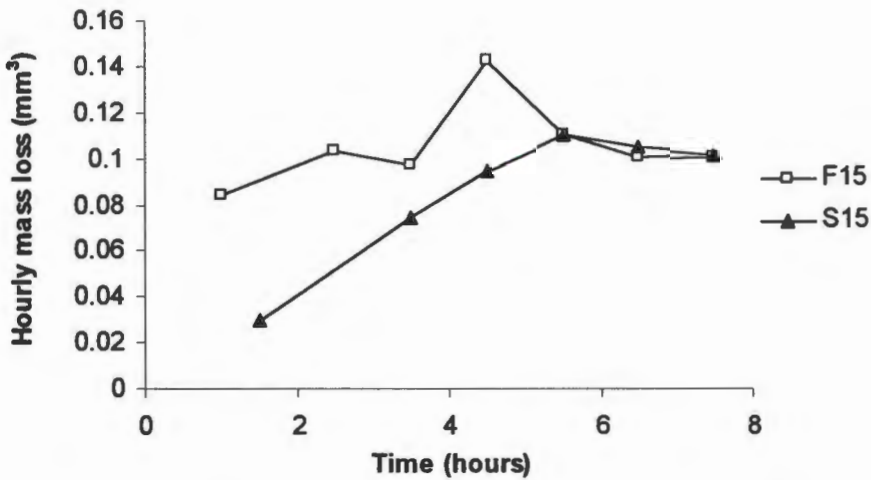


Figure 7.36 Plot of erosion rate (defined as the average hourly mass loss) against time for fine and standard grades containing 15 wt% cobalt. Note that although the steady state erosion behaviour of the two grades is identical, their behaviour during the incubation period differs significantly

Scanning electron micrographs taken from grade F15 after 30 minutes' exposure to cavitation show that no bulk material loss appears to occur: erosion appears instead to proceed through the loss of single WC grains. However, the eroded areas exhibit non-random shapes, as shown in Figure 7.37 which indicates that erosive attack may be concentrated at the sites of cobalt pools.

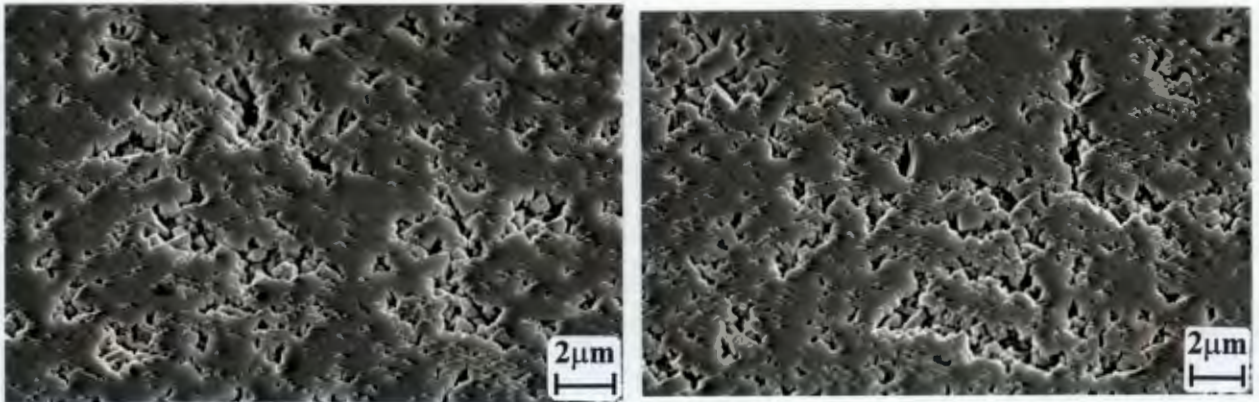


Figure 7.37 Scanning electron micrographs of grade F15 subjected to 30 minutes cavitation erosion. Note non-random shape of eroded areas.

7.2.3.2 Discontinuous grain growth

The scanning electron micrographs shown in Figure 7.38 indicate that preferential attack may occur at sites of discontinuous grain growth.

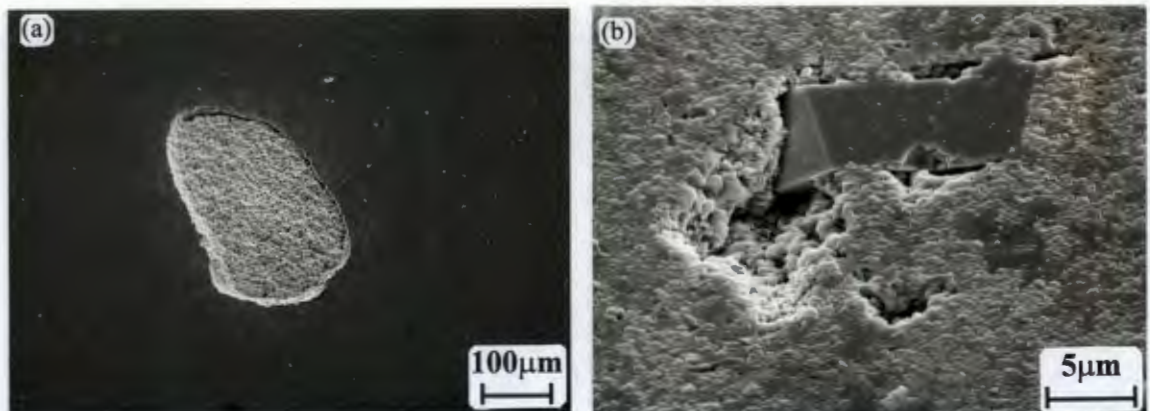


Figure 7.38 Scanning electron micrographs showing preferential erosive attack occurring at sites of discontinuous grain growth: (a) This micrograph shows the site of a cluster of discontinuous WC grains in grade UF6 which have experienced rapid preferential erosion after only three hours testing. The remaining surface appears to be unaffected by erosive attack. Note: no further testing was carried out on this specimen.

(b) This micrograph shows preferential erosive attack occurring in grade UF15 at the interface between a discontinuous WC grain and the bulk of the material.

7.2.4 Summary

1. The cavitation erosion response of 16 WC-Co grades of varying grain size and cobalt content has been evaluated. A general trend has been observed of increasing erosion resistance with decreasing grain size. The relationship between erosion resistance and cobalt content has been found to vary with the grain size of the material: sub-micron materials exhibit increasing erosion resistance with decreasing cobalt content, while for the standard and coarse grades, the trend is reversed.
2. The erosion resistance of sub-micron materials is highly sensitive to the binder mean free path and the hardness, and thus these materials exhibit erosion resistances which may be up to seven times greater than that of the best-performing standard grade.
3. The high erosion resistances of sub-micron materials are achieved without any significant drop in fracture toughness levels (relative to the coarser grades), and thus high combinations of these two properties may be realised.
4. The erosion resistance of coarse and standard grades does not appear to depend strongly on the hardness, fracture toughness or binder mean free path.
5. Material removal from sub-micron grades occurs through a bulk process, while in standard and coarse grades erosion proceeds through the preferential removal of the cobalt phase, followed by the loss of single unsupported WC grains.
6. X-ray diffraction spectra from coarse grades indicate that the level of deformation of WC grains at the surface of the eroded specimens is very low.
7. The extent of the f.c.c. \rightarrow h.c.p. transformation occurring during cavitation erosion appears to increase with increasing cobalt content, as does the erosion resistance of the material.
8. The presence of cobalt pools does not appear to have a strong effect on the cavitation erosion resistance of WC-Co, but preferential attack has been observed at sites of discontinuous grain growth.

Chapter 8

DISCUSSION

8.1 Introduction

The vast majority of applications for WC-Co exploit its high resistance to wear and erosion, and thus an understanding of its response to tribological environments has major commercial implications. However, the development of such an understanding is complicated by the fact that as a composite material, WC-Co displays properties which vary over a particularly wide range and which are strongly dependent on its microstructural parameters. In particular, recently-developed ultrafine WC-Co grades have exhibited properties and property combinations which represent a significant departure from those of conventional WC-Co composites. Furthermore, the tribological performance of any material depends critically on the type of system it is exposed to, and the exact parameters of that system.

The following discussion evaluates the response of WC-Co composites of highly varying microstructures, including ultrafine grades, to two substantially different erosive systems, namely cavitation erosion and slurry erosion. An attempt is made to elucidate the microstructure / property trends governing the material response to each type of erosive attack. The performance of ultrafine grades is considered in particular detail and the effects of the two erosive systems are compared and contrasted.

8.2 Slurry erosion

8.2.1 Scaling effects

In this study, the slurry erosion response of a range of WC-Co composites has been investigated through mass loss measurements, microscopic observation of the eroded surfaces, and evaluation of the geometry of the erosion scars. Each of these three approaches has

indicated that a transition in the erosion response of the material occurs as the WC grain size falls below $1\mu\text{m}$.

The erosion response of materials with grain sizes below $1\mu\text{m}$ is characterised by erosion rates which are significantly lower than those of more coarse-grained materials, and which exhibit a high sensitivity to hardness and binder mean free path. The wide, shallow shape of the erosion scars formed indicates that erosion occurs preferentially at lower angles than for more coarse grained materials. Material loss appears to result from the removal of small flakes of material formed as surface material is smeared in the direction of erodent impact. This process acts on the bulk material and does not appear to affect individual WC grains. By contrast, the erosion response of coarse grained materials appears to occur on a scale smaller than that of the microstructure, so that the two phases are sampled separately and respond individually. Material response consists of the deformation, cracking, chipping, and displacement of WC grains, combined with the extrusion and preferential removal of the cobalt binder phase which is followed by the loss of single unsupported WC grains.

It must be noted that since the angular dependence of erosion in sub-micron grades is different to that in coarser grades, it is likely that the impact angle of 75° employed during this study does not represent the angle of maximum erosion for the former grades: this may account in part for the low erosion rates observed.

The observations outlined above are broadly consistent with those of Anand and Conrad, who have undertaken extensive research into the importance of scaling effects in the erosion of WC-Co [133,135,136]. It is considered that the erosion response of WC-Co is highly dependent on the scale of the impact zone relative to the microstructure: when the impact zone encompasses less than 10 WC grains, material removal occurs mainly through the brittle response of individual WC grains, while if the impact zone encompasses more than 100 grains, the material response consists mainly of bulk ductile deformation. The former condition is termed the brittle erosion regime, while the latter is termed the ductile erosion regime.

Some differences are observed, however, between the results of this study and those of Anand and Conrad. Firstly, whereas Anand and Conrad's work showed cracking and crushing of WC grains to be the main method of material removal in the brittle regime, microscopic

observations in this study indicate that significant material loss may also occur through the extrusion and preferential removal of the cobalt binder phase, and the consequent loss of unsupported single WC grains (see for example Figure 7.14(b))

Secondly, the transition points in this study seem in general to occur at significantly lower ratios of the impact zone to the microstructure than those determined by Anand and Conrad. For example, Figure 7.10 shows the size of the impact zone in fine and ultrafine materials to be typically of the order of $2\mu\text{m}$, and thus the number of WC grains encompassed by it will be at most 20. This is considerably lower than the minimum number of grains per impact zone considered necessary for full ductile deformation to occur, and yet fine and ultrafine grades display all the characteristics of ductile deformation. Furthermore, standard grades, for which impact zones encompass only a few WC grains [Figure 7.15], and which should display all the characteristics of the brittle erosion regime, instead display only limited cracking, while material removal seems to occur mainly through the preferential removal of the binder phase and loss of unsupported WC grains.

These differences are likely to be due to the fact that much higher velocities, of between 35 and 93 m/s, were used Anand and Conrad's study, and that the erodent employed, Al_2O_3 , is angular in shape and has a hardness of over 2000 kg/mm^2 . By contrast, SiO_2 , the erodent used in the present study has a hardness of about 1000 kg/mm^2 . The low velocities and the use of an erodent which is rounded in shape and softer than any of the materials tested, will tend to limit grain fracture and hence promote a ductile deformation response.

The difference in erodent hardness is also probably responsible for the difference between the features observed in the ductile regime in this study and those documented by Anand and Conrad. In the latter study, impact damage in the ductile regime is shown to result in a large degree of penetration by the erodent, producing appreciable plastic deformation, with the formation of ridges and lips at the crater edges. By contrast, in this study, impact damage in the ductile regime is characterised by virtually no penetration of the material by the erodent, and consequently typical features of ductile erosion, such as extruded lips of material, are absent. Instead, the material appears to have been smeared across the target surface, in a manner corresponding more closely to adhesive wear than to abrasive wear.

The latter observations correspond with those made by Jia and Fischer [6] on Nanocarb surfaces abraded by ZrO_2 . In both cases, the abrasive is considerably softer than the target material, and hence is unable to penetrate it: instead, the surface material is smeared in the direction of erodent impact. By contrast, Jia and Fischer have shown that when Nanocarb is abraded using diamond or SiC, the surfaces reveal features typically associated with ductile ploughing.

8.2.2 Relationship to mechanical and microstructural properties

8.2.2.1 Sub-micron grades

Sub-micron materials subjected to a slurry erosion environment respond in bulk to erodent impact, and hence the relationship between their erosion resistance and material properties is relatively simple. The erosion resistance is strongly dependent on bulk material deformation properties, such as hardness, and exhibits a high level of sensitivity to the binder mean free path, since, as discussed in Section 2.2.2, this parameter largely characterises the bulk deformation behaviour of the composite.

The erosion resistance of sub-micron materials appears to be much more sensitive than the hardness to microstructural parameters. Consequently, a three-fold increase in erosion resistance may be achieved by decreasing the grain size of the material from $0.9\mu\text{m}$ to $0.49\mu\text{m}$, while the corresponding increase in hardness is of only 25%. This high structure sensitivity of the wear properties of WC-Co has been observed in previous studies [54,125].

8.2.2.2 Standard and coarse grades

The erosion response of standard and coarse grades is dependent on the individual response of the WC and cobalt phases, which are sampled separately. Material response is therefore not directly dependent on bulk parameters, but instead depends on the properties of the individual phases, and on the microstructural parameters.

WC grains respond to erodent impact through plastic deformation, cracking and chipping. The extent of these processes is dictated by the WC grain size. The cobalt binder responds to erodent impact through ductile ploughing. The removal of the cobalt binder phase then leads to the loss of single WC grains. The rate of removal of the cobalt binder phase depends on the binder mean free path. The relative importance of the response of each phase can therefore be evaluated by considering the dependence of the overall erosion resistance on the WC grain size and the binder mean free path.

Figure 8.1 shows a portion of the graph of erosion resistance against binder mean free path (given in full in Figure 7.5), which has been scaled so as to emphasise the behaviour of standard and coarse grades. This shows that although the erosion resistance of standard and coarse grades is not as sensitive to the binder mean free path as that of sub-micron grades, the binder mean free path remains an important parameter. By contrast, very little influence of grain size is observed: the trends for the two grades are in good agreement and no significant drop in erosion resistance is observed at the transition from standard to coarse grades.

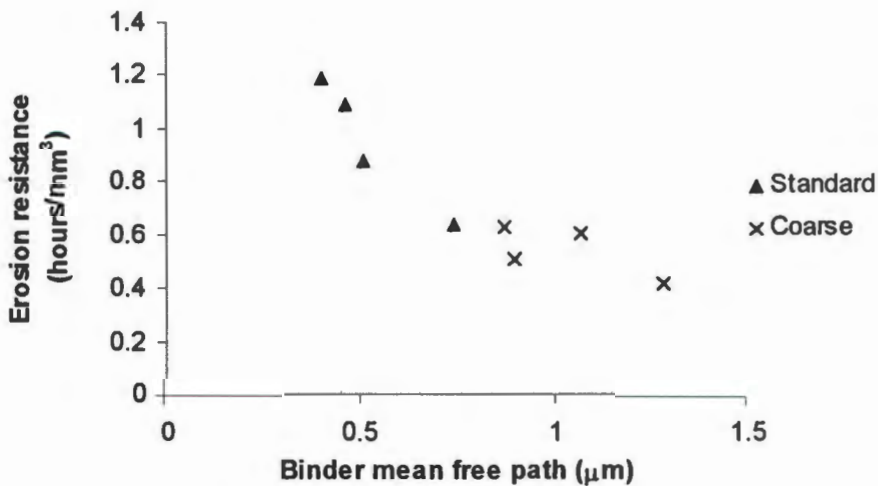


Figure 8.1: Erosion resistance of standard and coarse grades plotted as a function of binder mean free path

Thus it is apparent that although in this erosion regime significant chipping and cracking of WC grains is observed, particularly in coarse grades, this process does not represent a significant contribution to the overall erosion rates, which are instead highly dependent on the rate of removal of the binder phase and the consequent loss of single unsupported WC grains.

These results are in contrast to those obtained by Anand and Conrad, who found that the erosion response in this regime was not strongly dependent on the binder mean free path. Instead erosion rates were found to increase with increasing grain size, until a plateau was reached. The differences between the results obtained in these two studies are explained by the different parameters of the two systems: the erodent used by Anand and Conrad, Al_2O_3 , is considerably more angular than SiO_2 , and the impact velocities were substantially higher. These two factors promote outright crushing of the WC grains, which represents a significant contribution to material removal since it causes the loss of entire grains. Grains which have merely been chipped and cracked, however, tend to be retained by the microstructure until sufficient cobalt phase has been removed to allow the entire grain to fall out. Chipping and cracking processes do not therefore represent a significant contribution to material removal.

Thus it would seem that the term 'brittle erosion regime' is not an accurate description of the material response observed in the present study: a more suitable appellation would appear instead to be 'localised erosion regime'.

Given these results, the angular dependence of erosion rates, as demonstrated by the geometry of the erosion scars, cannot be explained in terms of a change from a ductile to a brittle regime. It is likely, therefore, that the reduced susceptibility of standard and coarse grades to low angle erosive attack is due to a shielding effect whereby protruding WC grains prevent erodent impact on the binder phase at low erosion angles.

8.2.2.3 Influence of fracture toughness on erosion response

Given that no cracking is observed in sub-micron materials in response to erosive impact, and that the cracking and chipping observed in standard and coarse materials is not considered to have a significant influence on the erosion process, it appears unlikely that the erosion response of the materials tested would depend in any way on their fracture toughness. This is confirmed by the plot of erosion resistance against fracture toughness shown in Figure 7.7, in which no correlation between these two parameters is observed. However, although the fracture toughness is incidental to the erosion process, it remains a highly relevant parameter, since components must always be sufficiently tough to ensure in-service reliability.

8.3 Cavitation erosion

8.3.1 Scaling effects

In this study, the cavitation erosion of a range of WC-Co composites has been investigated. The data obtained for erosion resistance indicate that a sharp transition in the erosion response of these materials occurs at a WC grain size of about $1\mu\text{m}$. Below this grain size, the erosion resistance decreases with increasing cobalt content of the material, and increases with increasing hardness and microstructural refinement. Above this grain size, the opposite trends are observed with respect to the cobalt content and the hardness, although the erosion resistance continues to decrease with increasing grain size.

This transition in the trends for erosion resistance coincides with a change in the material removal mechanism: in sub-micron grades, material removal occurs predominantly in bulk, leading to the formation of deep erosion craters. These craters expand laterally and eventually coalesce, leading to a steady state erosion surface which is highly undulating and contains small islands of uneroded material. In standard and coarse materials, material removal occurs predominantly on the scale of the microstructure, through the preferential removal of the cobalt phase and the consequent loss of unsupported WC grains. Some tendency is observed, particularly in standard grades, to the formation of shallow pits no more than one WC grain size deep. This is likely to be due to the fact that WC grains adjacent to eroded areas are more vulnerable to removal.

These observations contain strong parallels to those made during the slurry erosion of the same set of materials, and thus it is likely that the cavitation erosion response can be explained in terms of scaling effects in a mechanism similar to that proposed by Anand and Conrad for the particle erosion of composite materials.

In materials with fine microstructures, the damage zone caused by cavity collapse is appreciably larger than the microstructural dimensions and thus the material responds in bulk to erosive attack. The measured erosion resistance is highly sensitive to bulk deformation parameters, such as hardness, which are ultimately largely controlled by the binder mean free

path. In materials with coarse microstructures, the damage zone caused by cavity collapse is similar in size, or smaller than the microstructural dimensions, and the constituent phases of the composite respond individually to erosive attack. The measured erosion resistance therefore shows no meaningful relationship with bulk material properties.

8.3.2 Relationship to mechanical and microstructural properties

8.3.2.1 Sub-micron grades

The response of ultrafine grades to cavitation erosion is similar to that displayed under slurry erosion conditions: the material responds in bulk to erosive attack. Hence the erosion resistance of these materials is strongly dependent on bulk material deformation properties, such as hardness. The bulk deformation behaviour is largely characterised by the binder mean free path, as discussed in Section 2.2.2, and thus this parameter exerts a strong influence on the erosion resistance.

The behaviour of the fine grades is consistent with the trends observed in ultrafine materials, although the erosion response is less sensitive to the bulk deformation parameters. In fact the erosion resistance of these materials varies over a very narrow range and does not display a strong dependence on either the bulk deformation parameters or the microstructural characteristics: this indicates that the response of these materials may represent the transition between the two erosion regimes.

8.3.2.2 Standard and coarse grades

This study has shown the cavitation erosion resistance of standard and coarse WC-Co grades to increase with increasing cobalt, and also to exhibit a slight grain size dependency: the erosion resistance increases with decreasing grain size. These results are in good agreement with those obtained by Heathcock in his work on a series of hardmetals of similar grain sizes and binder contents [41]. Hankey's work has also shown that the cavitation erosion resistance of WC-Co may increase with increasing binder content over a particular range of binder content [142].

Scanning electron micrographs show standard and coarse materials to exhibit a localised response to cavitation erosion, which is therefore governed by the individual behaviour of the WC and cobalt phases. In contrast to their behaviour during slurry erosion, the WC grains appear to be largely unaffected by cavitation erosion attack. This is confirmed by X-ray diffraction analysis, which shows the WC(111) peak on the eroded surface to be significantly narrower than the corresponding peak on the as-ground surface, and to be of a similar size to that from the polished surface: this indicates the low level of deformation present in WC grains exposed to erosive attack.

The response of the material is therefore entirely dependent on the behaviour of the cobalt binder phase, which is usually largely characterised by the magnitude of the binder mean free path. However, the results obtained in this study demonstrate a conflicting influence of this parameter on the erosion resistance: when the binder mean free path is manipulated by changing the grain size, the erosion resistance is seen to increase with decreasing binder mean free path. However, when the binder mean free path is manipulated by changing the cobalt content, the opposite trend is observed: the erosion resistance increases with increasing binder mean free path. The influence of the cobalt content on the erosion response of the material is far greater than that of the grain size.

From the above, it is clear that under these conditions, the binder mean free path cannot be the most important parameter determining the behaviour of the cobalt binder phase. Other factors, such as the composition of the binder phase or the role of the WC/Co interface must therefore be taken into account.

It is interesting in this respect to consider Heathcock's study of the cavitation erosion of a range of WC-Co and WC-Ni composites (discussed in Section 4.2). The results of this study show the erosion resistance of WC-Ni materials with $2\mu\text{m}$ grain size to be considerably higher than that of WC-Co composites with the same microstructural parameters. Furthermore, the dependence of erosion resistance on binder content in WC-Ni grades appears to be the opposite to that observed in WC-Co grades, and is thus consistent with the generally observed relationship between the deformation behaviour of the binder phase and the binder mean free path [41]. This implies that the parameters governing the behaviour observed in WC-Co composites must be unique properties of the cobalt binder phase.

The two main differences between cobalt and nickel binder materials are that nickel is considerably more corrosion resistant and that it does not undergo a phase transformation, being a stable f.c.c. structure [139,141,155-158].

Thus four parameters have been identified which might affect the behaviour of the cobalt phase, namely its corrosion properties, its crystal structure, its composition and the role of the WC/Co interface. These will be discussed in detail in the following sections.

Erosion-corrosion and the role of the WC/Co interface

It is well known that initial cavitation erosion attack occurs preferentially at defect sites such as grain boundaries and interfaces [41,159]. Furthermore, the corrosion of WC-Co has been observed to occur preferentially at the WC/Co interface [137] and thus it is possible that the synergistic interaction of these two material removal mechanisms will produce enhanced attack in materials with a high WC/Co interfacial area. This mechanism explains why materials with low cobalt contents exhibit high erosion rates, but fails to account for the observed grain size dependence of the erosion response.

Binder phase composition

The level of retained tungsten in the binder phase is known to increase with increasing binder content due to the increased diffusion distance [30], while small WC grains are considered to promote the solubility of tungsten in the binder phase [66]. Thus, like the cavitation erosion resistance, the tungsten content of the binder increases with increasing binder content and decreasing grain size. No explanation can currently be advanced for this observation, and the relationship between these two parameters may indeed be entirely fortuitous. However, further investigation of the binder phase composition of samples subjected to cavitation erosion would be beneficial.

Phase transformation aspects

The results of this study confirm the generally accepted finding that the cavitation erosion of materials containing a cobalt phase is accompanied by a transformation of this phase from a

f.c.c. to a h.c.p structure [41,142,161]. This transformation has also been observed during the fatigue of WC-Co [40] and cobalt-based materials [158,160]. Schleinkofer and co-workers [40], in their study of the fatigue properties of WC-Co, showed this transformation to be a particular feature of cyclic loading, since it occurs only to a much smaller extent under static or monotonically increasing loads.

The f.c.c.→h.c.p. transformation is considered to improve the fatigue properties of Co-Ni alloys [158] and to account for the exceptionally good cavitation erosion resistance of Stellites [41]. This is thought to be due to the combination of two effects. Firstly, the transformation is associated with a decreased stacking fault energy, which promotes a planar deformation mechanism. Secondly, under erosive conditions, the phase transformation provides a means whereby energy may be absorbed without the usual increase in strain-hardening.

However, the phase transformation is considered to impact adversely on the fatigue and cavitation erosion performance of WC-Co. Schleinkofer and co-workers [40] have shown it to inhibit plastic deformation of the binder ligaments behind the crack tip, thus leading to premature failure of the ligaments and reduced crack tip shielding. Heathcock [41] considers it to account for the low erosion resistance of WC-Co relative to other materials, particularly WC-Ni. He proposed that the decrease in volume of the binder phase associated with the phase transformation results in increased stress at the WC/Co interface, and hence increased susceptibility to erosive attack.

Hankey's data [142], illustrated in Figures 4.7 and 4.8, shows a strong correlation to exist between the extent of the phase transformation and the cavitation erosion rate. This appears to indicate that the phase transformation is directly responsible for the poor erosion performance of WC-Co and for the observed trends in erosion response.

An attempt was made during the present study to duplicate Hankey's results. However, the data obtained appears to demonstrate the opposite trend, namely that the erosion rate is inversely related to the level of phase transformation occurring.

It is possible, therefore, that the phase transformation is merely incidental to the erosion process. This result is in agreement with the findings of Woodford [161] in his study of

cavitation-induced phase transformations in cobalt and iron-based alloys. It is also possible that a more sophisticated method for monitoring the extent of the phase transformation (such as transmission electron microscopy) is required.

In conclusion, it appears that insufficient data exists for the formulation of a satisfactory explanation for the observed cavitation erosion behaviour of standard and coarse grades. It is recommended that any further work be focussed on the role of the following parameters: the binder composition, the f.c.c. \rightarrow h.c.p. phase transformation, the WC/Co interface, and erosion-corrosion interactions.

8.4 Ultrafine grades

In this study, ultrafine grades have been shown to exhibit potentially very high erosion resistance in response to both slurry erosion and cavitation erosion, under the test conditions employed. However, the erosion resistance of these grades spans a very wide range, depending on the cobalt content of the material, and overlaps substantially with that of the fine grades. Furthermore, the erosion resistance of the worst-performing material is not substantially higher than that of the standard and coarse grades tested. These findings indicate that the small grain size of these materials does not in itself impart high erosion resistance, but instead has a less direct influence on the erosion performance.

The small grain size of ultrafine materials has two specific consequences, which combine to give the observed potential for high erosion resistance. The test conditions employed in this study are such that materials with a grain size below about $1\mu\text{m}$ exhibit a bulk ductile erosion response, which is characterised by a high sensitivity to bulk deformation parameters such as hardness. The small grain size of ultrafine materials imparts the capacity for very high hardness, which, in combination with the ductile deformation mechanism, results in high levels of erosion resistance.

It must be noted that the erosion data obtained in this study are strongly dependent on the parameters of the erosive system employed for testing. This is a particularly important consideration in relation to the transition point between the two erosion regimes. If any of the system parameters are changed, particularly the size and velocity of the erodent (in the case of slurry erosion), the transition point between the two erosion mechanisms will also be changed: for example, if the erodent size is decreased, the transition between a bulk ductile and a localised erosion regime will occur at lower grain sizes. It is not possible, from data obtained in this study, to predict the erosion response of ultrafine materials under conditions of localised erosion, or to predict the relative erosion resistances of all the grades tested, should the test parameters be such that they all exhibit the same mode of erosion. However, it may be said that under all conditions, ultrafine materials will always display the strongest tendency to bulk ductile erosion and hence are most likely to exploit the benefits of this erosion mechanism.

Further aspects of ultrafine materials which may enhance their suitability for erosive applications are their sintering and fracture toughness performance. As discussed in Section 2.3.2.2, a strong driving force exists for densification during sintering and this allows fully dense materials to be produced with lower cobalt contents than would be possible for materials with coarser microstructures. Thus the capacity exists for the production of materials with even higher hardnesses than those tested, and, consequently, improved erosion resistance. The fracture toughness behaviour of ultrafine materials is discussed in Sections 2.3.2.1 and 5.3.2.1, in which it is shown to be largely independent of the cobalt content. The hardness and erosion resistance of the material may therefore be increased by reducing the cobalt content without compromising the reliability of the component produced.

In conclusion, therefore, the microstructure/property trends observed in WC-Co as the grain size is lowered to ultrafine levels are such that materials may be produced with high hardnesses and a tendency to a bulk ductile erosion response. The combination of these two properties provides the potential for high erosion resistance. The sintering performance of ultrafine grades allows them to be produced with binder contents which might be considered insufficient in coarser grades, and thus the potential exists for further improvements in hardness and erosion resistance. The fracture toughness of ultrafine grades does not vary with the cobalt content, which may thus be reduced without compromising the integrity of the components.

8.5 Comparison of the two erosion systems

The cavitation and slurry erosion responses of the materials tested exhibit strong contrasts, both in the behaviour of the bulk material, but also in the role of defects. This serves to emphasise that erosion resistance is not a material property, but instead represents a specific material response to the parameters of the erosive system.

The clearest difference between the cavitation and slurry erosion responses of WC-Co is evident in the behaviour of the standard and coarse grades, which exhibit a localised mode of erosion under both the erosive systems tested. Under slurry erosion conditions, the erosion resistance of these materials decreases with increasing cobalt content; under cavitation erosion conditions, the opposite trend is observed. This indicates that the slurry erosion response of these grades is dictated purely by the deformation behaviour of the binder phase, and is not sensitive to the as yet unidentified parameters which dictate the cavitation erosion response. It is interesting to note that in contrast to Heathcock's findings in cavitation erosion, discussed earlier, no significant difference has been observed between the slurry erosion of cobalt- and nickel-based hardmetals [139].

The role of the WC grains in standard and coarse materials also differs strongly between the two erosive systems: WC grains exhibit no particular response to cavitation erosion, but display substantial chipping, cracking and plastic deformation in a slurry erosion environment. This implies that hardmetals with an alternative carbide phase such as TaC or TiC are likely to exhibit a similar cavitation erosion response to that observed in this study, whereas significant differences in the slurry erosion behaviour might be recorded.

The principal defects observed in this study are discontinuous grain growth and cobalt pools. Under cavitation erosion conditions, the former acts as a stress raiser and hence is subject to concentrated erosive attack, which undermines the erosion resistance of the material. Under slurry erosion conditions, however, it appears that discontinuous grains are retained by the microstructure, not being as vulnerable to loss as other WC grains. In this situation, the discontinuous grains remain at the surface of the microstructure until they are chipped away by the impacting erodent. During this time they tend to afford protection to the material beneath them, and hence a non-uniform grain size may be beneficial under these conditions.

The initial rate of attack of materials containing cobalt pools appears to be relatively high under both cavitation and slurry erosion conditions. However, while the steady state erosion rate under cavitation erosion conditions is comparable to that of defect-free materials, under slurry erosion conditions the performance of this material is significantly worse than that of other materials of the same grain size. This indicates that cobalt pools act as a damage initiation site under cavitation erosion, but do not undermine the entire structure of the material as is the case in slurry erosion.

Chapter 9

CONCLUSIONS AND RECOMMENDATIONS

In this study, a series of four ultrafine WC-Co alloys sintered from powder produced through the spray conversion process have been subjected to two significantly different forms of erosive attack, namely slurry erosion and cavitation erosion. A further twelve WC-Co alloys of varying cobalt contents and grain sizes, produced through conventional processes, have also been tested, in order to provide data for comparison. The following conclusions may be drawn from the results obtained:

1. The erosion resistance of all the grades tested increases with decreasing grain size, both under cavitation erosion and slurry erosion conditions.
2. Under both slurry and cavitation erosion conditions, the response of WC-Co undergoes a transition from a localised material removal mechanism to a bulk material removal mechanism as the grain size decreases below about $1\mu\text{m}$.
3. Sub-micron materials respond to slurry erosion conditions through the smearing of the material in bulk across the specimen surface. Erosion occurs preferentially at low angles of impact.
4. Sub-micron materials respond to cavitation erosion conditions through the formation of deep craters, which expand laterally and eventually coalesce.
5. Under both slurry erosion and cavitation erosion conditions, the erosion resistance of sub-micron materials is highly sensitive to bulk deformation parameters.
6. Materials with a grain size greater than $1\mu\text{m}$ respond to slurry erosion conditions through the deformation, chipping, cracking and displacement of WC grains, combined with the extrusion and preferential removal of the cobalt phase, which is followed by the loss of single unsupported WC grains. The erosion resistance of these materials is influenced more strongly by the binder mean free path than by the WC grain size, and increases with decreasing binder mean free path. Erosion occurs preferentially at high angles of impact.

7. Materials with a grain size greater than $1\mu\text{m}$ respond to cavitation erosion conditions through the preferential removal of the cobalt phase, which is followed by the loss of single unsupported WC grains. No response of the WC phase to erosive attack is observed. The erosion resistance of these materials increases with increasing binder content and decreasing grain size, and shows no dependence on bulk deformation parameters.
8. As a result of their small WC grain size and their bulk ductile response to erosive attack, ultrafine grades subjected to slurry erosion or cavitation erosion exhibit lifetimes which may be up to seven times greater than those of the best-performing materials with grain sizes above $1\mu\text{m}$. This increase in erosion resistance is achieved without any sacrifice in fracture toughness.
9. WC-Co alloys respond to slurry erosion and cavitation erosion conditions in significantly different ways. As a result, the ranking of the materials is specific to the erosive system, as is the role of material defects.

Recommendations

Two aspects of this study would benefit particularly from further investigation. Firstly, as discussed in Section 8.4, the transition point between bulk and localised modes of material removal is undoubtedly a function of system parameters. It would be useful to investigate this relationship, for example by subjecting materials to slurry erosion using erodents of differing hardnesses and sizes, and different impact velocities.

Secondly, a further investigation of the anomalous cavitation erosion response of standard and coarse WC-Co is required. Suggested approaches are:

1. Addition of corrosion inhibitors to the test bath, to evaluate material response in the absence of erosion-corrosion interactions
2. Detailed analysis of the composition of the binder phase as a function of the microstructure, particularly at the WC/Co interface.

3. Examination of eroded specimens under transmission electron microscopy, to evaluate the dislocation structure of the binder phase and to examine the influence of the phase transformation.
4. Further testing of WC-Ni alloys, to evaluate material response in the absence of phase transformation and corrosion effects.

REFERENCES

1. H.C.Lee and J.Gurland: *Hardness and deformation of cemented tungsten carbide*, Materials Science and Engineering, **33** (1978) 125-133
2. D.F.G.O'Quigley, S.Luyckx, and M.N.James: *New results on the relationship between hardness and fracture toughness of WC-Co hardmetals*, Materials Science and Engineering, **A209** (1996) 228-230
3. N.Sacks, I.Northrop, and C.Allen: *Fracture toughness of nanocrystalline WC-Co hardmetals*, in: G.Knerringer, P.Rödhammer, and P.Wilhartitz (eds.) Proc 14th International Plansee Seminar (Volume 2), Plansee AG, Reutte, 1997, 680-688
4. G.E.Spriggs: *A history of fine-grained hardmetal*, Int. J. of Refractory Metals and Hard Materials, **13** (1995) 241-255
5. L.E.McCandlish, B.H.Kear, and J.Bhatia: *Spray conversion process for the production of nanophase composite powders*, United States Patent no. 5 352 269, October 4, 1994
6. K.Jia and T.E.Fischer: *Abrasion resistance of nanostructured and conventional cemented carbides*, Wear, **200** (1996) 206-214
7. *Properties of sintered hardmetals*, customer information, Boart Longyear Research Centre, Krugersdorp, South Africa, 1990
8. F.V.Lenel: *Powder Metallurgy: Principles and Applications*, Metal Powder Industries Federation, Princeton, New Jersey, 1980, 383-400
9. A.Y.Liu, R.M.Wentzcovitch, and M.L.Cohen: *Structural and electronic properties of WC*, Physical Review B, **38** (1988) 9483-9489
10. D.N.French and D.A.Thomas: *Hardness anisotropy and slip in WC crystals*, Transactions of the AIME, **233** (1965) 950-952
11. S.B.Luyckx: *Slip systems of tungsten carbide crystals at room temperature*, Acta Metallurgica, **18** (1970) 233-236
12. M.K.Hibbs, R.Sinclair, and D.J.Rowcliffe: *Defect structure of WC deformed at room and high temperature*, in: R.K.Vishanadham, D.F.Rowcliffe and J.Gurland (eds.), Proceedings of the 1st International Conference on 'Science of hardmetals' (Jackson, WY, 1981) Plenum, New York, 1983, 121-135
13. D.J.Rowcliffe, V.Jarayam, M.K.Hibbs, and R.Sinclair: *Compressive deformation and fracture in WC materials*, Materials Science and Technology, **A105/106** (1988) 299-303
14. V.Jarayam: *Plastic incompatibility and crack nucleation during deformation on four independent slip systems in tungsten carbide-cobalt*, Acta Metallurgica, **35** No.6 (1987) 1307-1315
15. I.T.Northrop: *Developments in corrosion resistant hardmetals*, Mechanical Technology (South Africa), September 1995, 9-14
16. A.A.Ogwu and T.J.Davies: *Proposed selection rules for suitable binders in cemented hard metals with possible applications for improving ductility in intermetallics*, J. of Materials Science, **27** (1992) 5382-5388

17. L.F.Bates: *Modern Magnetism*, Cambridge University Press, 1963, 316
18. K.J.A.Brookes: *World directory and handbook of hardmetals and hard materials* (Fifth edition), International Carbide Data, East Barnet, United Kingdom, 1992
19. Z.Fang and J.W.Eason: *Non-destructive evaluation of WC-Co composites using magnetic properties*, Int. J. Powder Metallurgy, **29** (1993) 259-265
20. H.Winterhager and J.Krüger: *Pure cobalt and its properties*, Cobalt, **29** (1965) 185-195
21. H.E.Exner and J.Gurland: *A review of parameters influencing some mechanical properties of tungsten carbide-cobalt alloys*, Powder Metallurgy, **13** No.25 (1970) 13-31
22. J.R.Pickens and J.Gurland: *The fracture toughness of WC-Co alloys measured on single-edge notched beam specimens precracked by electron discharge machining*, Materials Science and Engineering, **33** (1978) 135-142
23. S.Bartolucci and H.H.Schlösin: *Plastic deformation preceding fracture in tungsten carbide-cobalt alloys*, Acta.Metallurgica, **8** (1966) 337-339
24. A.Henjered, M.Hellsing, H.-O.Andrén and H.Nordén: *The presence of cobalt at WC/WC interfaces*, in: E.A.Almond, C.A.Brookes, and R.Warren (eds.), Proceedings of the 2nd International Conference on 'Science of hard materials' (Rhodes, September 1984), Adam Hilger, Boston, 1986, 303-309
25. A.Laptev: *Intercarbide surface is the main obstacle to increase fracture toughness and strength of hardmetals*, in: PM'94: Powder Metallurgy World Congress (Paris, 6-9 June 1994), Les Editions de Physique, Les Ulis, France, 1994, 103-106
26. A.V.Laptev: *Influence of porosity on transverse rupture strength and fracture toughness of two-phase alloy*, in: Proceedings of EuroPM96: European conference on 'Advances in hard materials' (Stockholm 1996), European Powder Metallurgy Association, Shrewsbury, 1996, 313-320
27. B.Roebuck: *Terminology, testing, properties, imaging and models for fine grained hardmetals*, Int. J. of Refractory Metals and Hard Materials, **13** (1995) 265-279
28. R.Porat and J.Malek: *Binder mean free path determination in cemented carbides by coercive force and material composition*, Materials Science and Engineering, **A105/106** (1988) 289-292
29. B.Roebuck and E.A.Almond: *Deformation and fracture processes and the physical metallurgy of WC-Co hardmetals*, International Materials Reviews, **33** (1988) 90-110
30. M.Hellsing: *High resolution microanalysis of binder phase in as sintered WC-Co cemented carbides*, Materials Science and Technology, **4** (1988) 824-829
31. T.W.Penrice: *Some characteristics of the binder phase in cemented carbides*, Int. J. of Refractory Metals and Hard Materials, **15** (1997) 113-121
32. O.Rüdiger, D.Hirschfeld, A.Hoffman, J.Kolaska, G.Ostermann, and J.Willbrand: *Composition and properties of the binder metal in cobalt bonded tungsten-carbide*, Int. J. of Powder Metallurgy, **7** (1971) 29-38
33. B.Roebuck, E.A.Almond, and A.M.Cottenden: *The influence of composition, phase transformation and varying the relative f.c.c. and h.c.p. phase contents on the*

- properties of dilute Co-W-C alloys*, Materials Science and Engineering, **66** (1984) 179-194
34. A.M.Human, B.Roebuck, and H.E.Exner: *Electrochemical polarisation and corrosion behaviour of cobalt and Co(W,C) alloys in 1N sulphuric acid*, Materials Science and Engineering, **A241** (1998) 202-210
 35. J.Gurland: *A study of the effect of carbon content on the structure and properties of sintered WC-Co alloys*, Transactions AIME: J. of Metals, **200** (1954) 285-290
 36. A.Haerian: *Nondestructive evaluation of mechanical properties of WC-Co alloys*, in: R.K.Vishanadham, D.F.Rowcliffe and J.Gurland (eds.), Proceedings of the 1st International Conference on 'Science of hardmetals' (Jackson, WY, 1981) Plenum, New York, 1983, 43-52
 37. S.B.Luyckx: *Some features of the eta phase in substoichiometric WC-Co alloys*, in: H.M.Ortner (ed.), Proc. 10th Plansee Seminar (Volume 1), Metallwerk Plansee, Reutte, 1981, 629-634
 38. H.E.Exner: *The influence of sample preparation on Palmqvist's method for toughness testing of cemented carbides*, Transactions of the metallurgical society of AIME, **245** (1969) 677-683
 39. G.Wirrmann and G.L.Dunlop: *Phase transformations in the binder phase of Co-W-C cemented carbides*, in: R.K.Vishanadham, D.F.Rowcliffe and J.Gurland (eds.), Proceedings of the 1st International Conference on 'Science of hardmetals' (Jackson, WY, 1981), Plenum, New York, 1983, 311-328
 40. U.Schleinkofer, H.-G.Sockel, K.Görting, and W.Heinrich: *Microstructural process during subcritical crack growth in hard metals under cyclic loads*, Materials Science and Engineering, **A209** (1996) 103-110
 41. C.J.Heathcock: *Cavitation erosion of materials*, PhD thesis, University of Cape Town (1980)
 42. M.H.Poehch and H.F.Fischmeister: *Deformation of two-phase materials: a model based on strain compatibility*, Acta Metall. Mater., **40** No.3 (1992) 487-494
 43. M.H.Poehch, H.F.Fischmeister and R.Spiegler: *Assessment of the in situ flow properties of the cobalt phase in WC-Co hard metals*, J. of Hard Materials, **2** (1991) 197-205
 44. B.Roebuck: *Notched bend tests on WC-Co hardmetals*, J. of Materials Science, **23** (1988) 281-287
 45. B.Roebuck: *The tensile strength of hardmetals*, J. of Materials Science, **14** (1979) 2837-2844
 46. W.D.Schubert, A.Bock, and B.Lux: *General aspects and limits of conventional ultrafine WC powder manufacture and hard metal production*, Int. J. of Refractory Metals and Hard Materials, **13** (1995) 281-296
 47. T.Konig: *Production of nanosized powders by a recently developed gas-phase technology*, Int. J. of Refractory Metals and Hard Materials (News), **13** (1995) 232-234
 48. Y.Yamamoto, A.Matsumoto, and Y.Do: *Properties of ultrafine tungsten carbide and cemented carbide by direct carburisation*, in: G.Knerringer, P.Rödhammer, and

- P.Wilhartitz (eds.), Proc 14th International Plansee Seminar (Volume 2), Plansee AG, Reutte, 1997, 596-608
49. M.Xueming, Z.Ling, J.Gang, and D.Yuanda: *Preparation and structure of bulk nanostructured WC-Co alloy by high energy ball-milling*, J. of Materials Science Letters, **16** (1997) 968-970
 50. M.Willet and S.Porada: *Microwave sintering of hardmetals and ceramics*, in: Proceedings of EuroPM96: European conference on 'Advances in hard materials' (Stockholm 1996), European Powder Metallurgy Association, Shrewsbury, 1996, 69-75
 51. A.V.Ragulya and V.V.Skokohod: *Validity of rate-controlled sintering method for consolidation of dense nanocrystalline materials*, in: G.Knerringer, P.Rödhammer, and P.Wilhartitz (eds.) Proc 14th International Plansee Seminar (Volume 2), Plansee AG, Reutte, 1997, 634-643
 52. P.Seegopaul, L.E.McCandlish, and F.M.Shinneman: *Production capability and powder processing methods for nanostructured WC-Co powder*, Int. J. of Refractory Metals and Hard Materials, **15** (1997) 133-138
 53. Z.Fang and J.W.Eason: *Study of nanostructured WC-Co composites*, Int. J. of Refractory Metals and Hard Materials, **13** (1995) 297-303
 54. M.K.Keshavan and N.Jee, *Abrasion and erosion of WC-Co alloys*, Met. Powder Rep., **42** (1987) 866-869
 55. R.Porat, S.Berger, and A.Rosen: *Dilatometric study of the sintering mechanism of nanocrystalline cemented carbides*, NanoStructured Materials, **7** No.4 (1996) 429-436
 56. R.Porat, S.Berger, and A.Rosen: *Sintering behaviour and mechanical properties of nanocrystalline WC-Co*, Science Forum, **225-227** (1996) 629-634
 57. R.Porat, S.Berger, and A.Rosen: *Cemented carbide from micron grain size to nano size*, in: G.Knerringer, P.Rödhammer, and P.Wilhartitz (eds.) Proc 14th International Plansee Seminar (Volume 2), Plansee AG, Reutte, 1997, 183-196
 58. R.Porat, S.Berger, and A.Rosen: *Synthesis and processing of nanocrystalline WC/Co powders*, in: G.Knerringer, P.Rödhammer, and P.Wilhartitz (eds.) Proc 14th International Plansee Seminar (Volume 2), Plansee AG, Reutte, 1997, 582-595
 59. T.Taniuchi, K.Okada, and T.Tanase: *Sintering behaviour of WC-doped micro-grained cemented carbide*, in: G.Knerringer, P.Rödhammer, and P.Wilhartitz (eds.) Proc 14th International Plansee Seminar (Volume 2), Plansee AG, Reutte, 1997, 644-657
 60. G.Gille, B.Szesny, G.Leitner: *A new 0.4µm WC powder as well as powder-related properties and sintering behaviour of 0.6 to 30µm WC-Co hardmetals*, in: G.Knerringer, P.Rödhammer, and P.Wilhartitz (eds.) Proc 14th International Plansee Seminar (Volume 2), Plansee AG, Reutte, 1997, 139-167
 61. A.Egami, M.Ehira, and M.Machida: *Morphology of vanadium carbide in submicron hardmetals*, in: H.Bildstein and R.Eck (eds.) Proceedings of the 13th International Plansee Seminar (Volume 3), Metallwerk Plansee, Reute, 1993, 639-648
 62. D.F.Carroll: *Processing and properties of ultrafine WC/Co hard materials*, in: G.Knerringer, P.Rödhammer, and P.Wilhartitz (eds.) Proc 14th International Plansee Seminar (Volume 2), Plansee AG, Reutte, 1997, 168-182

63. A.Egami, T.Kusaka, M.Machida, K.Kobayashi: *Ultra submicron hardmetals for miniature drills*, in: H.Bildstein and H.M.Ortner (eds.), Proceedings of the 12th International Plansee Seminar (Volume 2), Metallwerk Plansee, Reutte, Austria, 1989, 53-70
64. G.S.Upadhyaya and D.Banerjee: *Role of Cr₃C₂ on tungsten carbide based hard composites*, in: G.Knerringer, P.Rödhammer, and P.Wilhartitz (eds.) Proc 14th International Plansee Seminar (Volume 2), Plansee AG, Reutte, 1997, 463-476
65. S.Inada and H.Yoshimura: *Material properties and end-milling performance of WC-10%Co-0.75%Cr₂C₃ micrograin cemented carbide*, in: H.Bildstein and R.Eck (eds.) Proceedings of the 13th International Plansee Seminar (Volume 2), Metallwerk Plansee, Reute, 1993, 67-79
66. K.Jia and T.E.Fischer: Microstructure, hardness and toughness of nanostructured and conventional WC-Co composites, *Nanostructured materials*, 10 No.5 (1998) 875-891
67. D.R.Moyle and E.R.Kimmel: *Effect of coarse grain WC grains on transverse rupture strength of fine grain hardmetals*, in: H.Bildstein and H.M.Ortner (eds.), Proceedings of the 12th International Plansee Seminar (Volume 2), Metallwerk Plansee, Reutte, Austria, 1989, 311-320
68. K.Mohan and P.R.Strutt: *Observation of Co nanoparticle dispersion in WC nanograins in WC-Co cermets consolidated from chemically synthesized powders*, *Nanostructured Materials*, 7 (1996) 547-555
69. L.J.Prakash: *Applications of fine grained tungsten carbide based cemented carbides*, *Int. J. of Refractory Metals and Hard Materials*, 13 (1995) 257-264
70. L.Nøkleberg and T.Søntvedt: *Erosion in choke valves – oil and gas industry applications*, *Wear*, 186-187 (1995) 401-412
71. R.J.K.Wood, B.G.Mellor and M.L.Binfield: *Sand erosion performance of detonation gun applied tungsten carbide/cobalt-chromium coatings*, *Wear*, 211 (1997) 70-83
72. A.W.Ruff and S.M.Wiederhorn: *Erosion by solid particle impact*, in: C.M.Preece (ed.), *Treatise on materials science and technology*, Volume 16: Erosion, Academic Press, New York, 1979, 69-126
73. I.M.Hutchings: *Friction and wear of engineering materials*, Edward Arnold, London, 1992
74. I.Finnie: *Erosion of surfaces by solid particles*, *Wear*, 3 (1960) 87-103
75. G.P.Tilly: *A two stage mechanism of ductile erosion*, *Wear*, 23 (1973) 87-96
76. J.G.A.Bitter: *A study of erosion phenomena: Part I*, *Wear*, 6 (1963) 5-21
77. J.G.A.Bitter: *A study of erosion phenomena: Part II*, *Wear*, 6 (1963) 169-190
78. I.M.Hutchings, R.E.Winter and J.E.Field: *Solid particle erosion of metals: the removal of surface material by spherical projectiles*, *Proc. R. Soc. Lond. A.*, 348 (1976) 379-392
79. I.M.Hutchings and R.E.Winter: *Particle erosion of ductile metals: a mechanism of material removal*, *Wear*, 27 (1974) 121-128

80. A.V.Levy: *The platelet mechanism of erosion of ductile metals*, *Wear*, **108** (1986) 1-21
81. B.R.Lawn, S.M.Wiederhorn and H.H.Johnson: *Strength degradation of brittle surfaces: blunt indenters*, *J. of the American Ceramic Society*, **58** No.9-10 (1975) 428-432
82. B.R.Lawn and M.V.Swain: *Microfracture beneath point indentations in brittle solids*, *J. of Materials Science*, **10** (1975) 113-122
83. B.R.Lawn and D.B.Marshall: *Indentation fracture and strength degradation in ceramics*, in: R.C.Bradt, D.P.H.Hasselmann, and F.F.Lange, *Fracture mechanics of ceramics (Volume 3: Flaws and testing)*, Plenum Press, New York, 1978, 205-229
84. I.Finnie, J.Wolak and Y.Kabil: *Erosion of metals by solid particles*, *J. of Materials*, **2** No.3 (1967) 682-700
85. A.Ninham: *The effect of mechanical properties on erosion*, *Wear*, **121** (1988) 307-324
86. A.Ball: *On the importance of work hardening in the design of wear-resistant materials*, *Wear*, **91** (1983) 201-207
87. K-H Zum Gahr: *Wear by hard particles*, in: I.M.Hutchings (ed.), *New directions in tribology: Plenary and invited papers from the First World Tribology Congress*, Mechanical Engineering Publications, Bury St. Edmunds, 1997, 483-494
88. S.Srinivasan and R.O.Scattergood: *Effect of erodent hardness on erosion of brittle materials*, *Wear*, **128** (1988) 139-152
89. A.V.Levy and P.Chik: *The effects of erodent composition and shape on the erosion of steel*, *Wear*, **89** (1983) 151-162
90. A.Misra and I.Finnie: *On the size effect in abrasive and erosive wear*, *Wear*, **65** (1981) 359-373
91. J.L.Routbort and A.P.L.Turner: *The erosion of reaction-bonded SiC containing various amounts of free silicon*, *Wear* **84** (1983) 381-385
92. S.Bahadur and R.Badruddin: *Erodent particle characterisation and the effect of particle size and shape on erosion*, *Wear*, **138** (1990) 189-208
93. M.A.Verspui, P.J.Slikkerveer, G.J.E.Skerka, I.Oomen and G.de With: *Validation of the erosion map for spherical impacts on glass*, in: *Abstracts of papers from the World Tribology Congress (London, September 1997)*, Mechanical Engineering Publications, Bury St Edmunds, 1997, p.212
94. M.Buijs and J.M.M.Pasmans: *Erosion of glass by alumina particles: transitions and exponents*, *Wear*, **184** (1995) 61-65
95. B.J.Hockey, S.M.Wiederhorn and H.Johnson: *Erosion of brittle materials by solid particle impact*, in: R.C.Bradt, D.P.H.Hasselmann and F.F.Lange, *Fracture mechanics of ceramics (Volume 3: Flaws and testing)*, Plenum, New York, 1978, 379-402
96. S.Turenne, M.Fiset and J.Masounave: *The effect of sand concentration on the erosion of materials by a slurry jet*, *Wear*, **133** (1989) 95-106
97. R.S.Lyon, K.K.Wong and H.McI.Clark: *On the particle size effect in slurry erosion*, *Wear*, **149** (1991) 55-71
98. J.A.Laitone: *Aerodynamic effects in the erosion process*, *Wear*, **56** (1979) 239-246

99. A.V.Levy, N.Jee, and P.Yau: *Erosion of steels in coal-solvent slurries*, *Wear*, **117** (1987) 115-127
100. K.K.Wong and H.McI.Clark: *A model of particle velocities and trajectories in a slurry pot erosion tester*, *Wear*, **160** (1993) 95-104
101. R.J.K.Wood: *Erosion-corrosion synergism for multiphase materials*, in: *Cavitation: International Conference* (Cambridge, December 1992) Mechanical Engineering Publications, Bury St. Edmunds, 1992, 151-158
102. R.J.K.Wood and S.P.Hutton: *The synergistic effect of erosion and corrosion: trends in published results*, *Wear*, **140** (1990) 387-394
103. G.M.C.Lee and D.C.McWhannell: *The effect of inhibitors on the mechanism of cavitation erosion*, in: *Proceedings of the second International Conference on 'Cavitation'*, (Edinburgh, September 1983), Mechanical Engineering Publications, Bury St. Edmunds, 1983, 259-268
104. J.H.Gummer and M.T.Thew: *A critical review of cavitation in ethylene glycol/water cooling systems*, in: *Cavitation: International Conference* (Cambridge, December 1992) Mechanical Engineering Publications, Bury St. Edmunds, 1992, 293-302
105. N.K.Bourne and J.E.Field: *A high-speed photographic study of cavitation damage*, *J. of Applied Physics*, **78** No.7 (1995) 4423-4427
106. B.Vyas and C.M.Preece: *Stress produced in a solid by cavitation*, *J. of Applied Physics*, **47** No.12 (1976) 5133-5138
107. S.M.Ahmed, K.Hokkirigawa, and R.Oba: *Fatigue failure of SUS 304 caused by vibratory cavitation erosion*, *Wear*, **177** (1994) 129-137
108. S.Fujikawa and T.Akamatsu: *Some recent aspects of bubble dynamics*, in: *Proceedings of the Second International Conference on 'Cavitation'* (Edinburgh, September 1993) Mechanical Engineering Publications, Bury St. Edmunds, 1983, 31-40
109. C.M.Preece: *Erosion of metals and alloys*, in: R.M.Latanision and J.T.Fourie (eds.), *Proceedings of the NATO Advanced Study Institute on 'Surface effects in crystal plasticity'* (Hohegeiss, Germany, September 1975) Noordhoff International Publishing, Leyden, 1977, 889-909
110. D.Gardellin: *Minimize valve cavitation by proper system design*, *Chemical Engineering Progress*, August 1996, 52-57
111. R.E.A.Arndt, C.R.Ellis, S.Paul: *Preliminary investigation of the use of air injection to mitigate cavitation erosion*, *Transactions of the ASME*, **117** (1995) 498-504
112. S.P.Hutton and W.A.Al-Meshhedani: *The effects of air injection upon cavitation erosion*, in: *Cavitation: International Conference* (Cambridge, December 1992), Mechanical Engineering Publications, Bury St Edmunds, 1992, 65-72
113. C.J.Heathcock, B.J.Protheroe, and A.Ball: *The influence of external variables and microstructure on the cavitation erosion of materials*, in: J.E.Field (ed.) *Proceedings of the 5th International Conference on erosion by liquid and solid impact*, (Cambridge September 1979) Cavendish laboratory, University of Cambridge, 1979, 63-1 – 63-8

114. C.J.Heathcock, B.E.Protheroe, and A.Ball: *Cavitation erosion of stainless steels*, *Wear*, **81** (1982) 311-327
115. R.L.Howard and A.Ball: *The solid particle erosion and cavitation erosion of titanium aluminide intermetallic alloys*, *Wear*, **186-187** (1995) 123-128
116. M.Johnson, D.E.Mikkola, P.A.March and R.N.Wright: *The resistance of nickel and iron aluminides to cavitation erosion and abrasive wear*, *Wear*, **140** (1990) 279-289
117. T.Okada, Y.Iwai, and A Yamamoto: *A study of the cavitation erosion of cast iron*, *Wear*, **84** (1983) 297-312
118. R.Howard and A.Ball: *Cavitation erosion of intermetallics*, *Acta Materialia*, **44** No.8 (1996) 3157-3168
119. W.J.Tomlinson and S.J.Matthews: *Cavitation erosion of aluminium alloys*, *J. of Materials Science*, **29** (1994) 1101-1108
120. S.Vaidya and C.M.Preece: *Cavitation erosion of age-hardenable aluminium alloys*, *Metallurgical Transactions A*, **9A** (1978) 299-307
121. R.H.Richman and W.P.McNaughton: *Correlation of cavitation erosion behaviour with mechanical properties of metals*, *Wear*, **140** (1990) 63-82
122. R.H.Richman, W.P.McNaughton, and A.S.Rao: *Cyclic deformation and phase transformation in cavitation erosion of alloys*, in: *Cavitation: International Conference (Cambridge, December 1992)* Mechanical Engineering Publications, Bury St Edmunds, 1992, 87-94
123. D.G.Graham: *Particle erosion of potential hydraulic valve materials*, MSc thesis, University of Cape Town (1985)
124. D.K.Shetty, I.G.Wright and J.T.Stropki: *Slurry erosion of WC-Co cermets and ceramics*, *ASLE Transactions*, **28** No. 1 (1985) 123-133
125. H.Reshetnyak and J.Kübarsepp: *Structure sensitivity of wear resistance of hardmetals*, *Int. J. of Refractory Metals and Hard Materials*, **15** (1997) 89-98
126. S.Wayne, J.G.Baldoni, S.-T.Buljan: *Abrasion and erosion of WC-Co with controlled microstructures*, *Tribology Transactions*, **33** No.4 (1990) 611-617
127. H.Conrad, D.McCabe, and G.A.Sargent: *Effects of microstructure on the erosion of WC-Co alloys*, in: R.K.Vishanadham, D.F.Rowcliffe and J.Gurland (eds.), *Proceedings of the 1st International Conference on 'Science of Hard Materials'* (Jackson, WY, 1981) Plenum, New York, 1983, 775-795
128. H.Conrad, Y.Shin and G.A.Sargent: *Erosion of sintered WC-Co alloys*, in: N.R.Comins and J.B.Clark (eds.), *Proceedings of the International Conference on recent developments in 'Speciality steels and hard materials'* (Pretoria, South Africa, November 1982) Pergamon Press, Oxford, 1983, 423-429
129. I.G.Wright, D.K.Shetty, and A.H.Clauer: *Slurry erosion of WC-Co cermets and its relationship to materials properties*, in: J.E.Field and N.S.Corney (eds.), *Proceedings of the 6th Conference on erosion by liquid and solid impact*, Cavendish Laboratory, Cambridge, 1983, 63-1 – 63-8

130. R.C.Pennefather, S.E.Hankey, R.Hutchings and A.Ball: *Recent observations of the erosion of hardmetals*, Materials Science and Engineering, **A105/106** (1988) 389-394
131. R.Pennefather: *The solid particle erosion of WC-Co alloys*, MSc thesis, University of Cape Town (1986)
132. A.Ball and A.W.Paterson: *Microstructural design of erosion resistant hard materials*, in: H.Bildstein and H.M.Ortner (eds.), Proceedings of the 11th International Plansee Seminar (Volume 2), Metallwerk Plansee, Reutte, Austria, 1985, 377-391
133. K.Anand and H.Conrad: *Microstructure effects in the erosion of cemented carbides*, in: K.C.Ludema (ed.), Proceedings of the International Conference on 'Wear of Materials' (Volume 1), The American Society of Mechanical Engineers, New York, 1989, 135-142
134. R.G.Wellman and C.Allen: *The effects of angle of impact and material properties on the erosion rates of ceramics*, Wear, **186-187** (1995) 117-122
135. K.Anand and H.Conrad: *Local impact damage and erosion mechanisms in WC-6wt%Co alloys*, Materials Science and Engineering, **A105/106** (1988) 411-421
136. K.Anand and H.Conrad: *Microstructure and scaling effects in the damage of WC-Co alloys by single impacts of hard particles*, J. of Materials Science, **23** (1988) 2931-2942
137. A.M.Human and H.E.Exner: *The relationship between electrochemical behaviour and in-service corrosion of WC based cemented carbides*, Int. J. of refractory metals and hard materials, **15** (1997) 65-71
138. P.J.L.Fernandez, S.B.Luyckx, A.M.Human and F.P.A.Robinson: *Does the cobalt mean free path affect the corrosion behaviour of WC-Co?*, J. of Hard Materials, **3** No.2 (1992) 185-194
139. E.J.Wentzel and C.Allen: *The erosion-corrosion resistance of tungsten carbide hardmetals*, Int. J. of Refractory metals and hard materials, **15** (1997) 81-87
140. E.J.Wentzel and C.Allen: *Erosion-corrosion resistance of tungsten carbide hardmetals with different binder compositions*, Wear, **181-183** (1995) 63-69
141. E.J.Wentzel: *Erosion-corrosion resistance of tungsten carbide based hardmetals with different binder compositions*, MSc thesis, University of Cape Town (1995)
142. S.E.Hankey: *Cavitation erosion of WC-Co*, MSc thesis, University of Cape Town (1987)
143. ASTM Standard B 276-86: *Standard test method for apparent porosity in cemented carbides*
144. ASTM Standard B 665-85: *Practice for metallographic sample preparation of cemented carbides*
145. *SGS Metallurgical laboratory acceptance standards for micrograin carbide rod*, SGS Tool Company, Munroe Falls, Ohio, 1994
146. Mr.I. T.Northrop, Boart Longyear Research Centre, South Africa: personal communication
147. E.E.Underwood: *Quantitative Stereology*, Adison Wesley, Reading MA, 1970
148. H.Fischmeister and H.E.Exner: *The mechanical properties of cemented tungsten-carbide cobalt alloys as dependent on structure*, Archiv. Eisenhüttenwesen, **37** (1966) 499-508

149. J.B.Zu, I.M.Hutchings, G.T.Burstein: *Design of a slurry erosion test rig*, *Wear*, **140** (1990) 331-334
150. A.J.Sparks and I.M.Hutchings: *Effects of erodent recycling in solid particle erosion testing*, *Wear*, **162-164** (1993) 139-147
151. S.Turenne, M.Fiset and J.Masounave: *The effect of sand concentration on the erosion of materials by a slurry jet*, *Wear*, **133** (1989) 95-106
152. D.Cooper, F.A.Davis, and R.J.K.Wood: *Selection of wear-resistant materials for the petrochemical industry*, *J. Phys. D: Appl. Phys.* **25** (1992) A195-A204
153. C.M.Preece: *Cavitation erosion*, in: C.M.Preece (ed.), *Treatise on Materials Science and Technology* (Volume 16: Erosion), Macmillan, Indianapolis, 1979, 72-89
154. D.K.Shetty, I.G.Wright, P.N.Mincer and A.H.Clauer: *Indentation fracture of WC-Co cermets*, *J. of Materials Science*, **20** (1985) 1873-1882
155. A.M.Human, I.T.Northrop, S.B.Luyckx, and M.N.James: *A comparison between cemented carbides containing cobalt and nickel-based binders*, *J. of Hard Materials*, **2** No.3-4 (1991) 245-255
156. W.J.Tomlinson and C.R.Linzell: *Anodic polarisation and corrosion of cemented carbides with cobalt and nickel binders*, *J. of Materials Science*, **23** (1988) 914-918
157. S.M.Brabyn, R.Cooper and C.T.Peters: *Effects of the substitution of nickel for cobalt in WC based hardmetal*, in: H.M.Ortner (ed.), *Proc. 10th Plansee Seminar* (Volume 2), Metallwerk Plansee, Reutte, 1981, 675-692
158. G.Chaland and L.Remy: *The slip character and low cycle fatigue behaviour of f.c.c. twinning and strain-induced f.c.c. \rightarrow h.c.p. transformation*, *Acta Metallurgica*, **28** (1980) 75-88
159. D.J.Mills: *The tribological properties of a high nitrogen manganese austenitic stainless steel*, MSc thesis, University of Cape Town (1995)
160. H.Farangi, R.W.Armstrong, and W.F.Regnault: *Transmission electron microscopy detection of cyclic-deformation-induced f.c.c.-to-h.c.p. transformation in a cobalt-based prosthetic device material*, *Materials Science and Engineering*, **A114** (1989) L25-L28
161. D.A.Woodford: *Cavitation-erosion-induced phase transformations in alloys*, *Metallurgical Transactions*, **3** (1972) 1137-1145